

72-30,378

PESKIN, Charles Samuel, 1946-  
FLOW PATTERNS AROUND HEART VALVES: A DIGITAL  
COMPUTER METHOD FOR SOLVING THE  
EQUATIONS OF MOTION.

Yeshiva University, Ph.D., 1972  
Physiology

University Microfilms, A XEROX Company, Ann Arbor, Michigan

© Copyright by  
CHARLES SAMUEL PESKIN  
1972

FLOW PATTERNS AROUND HEART VALVES:

A Digital Computer Method for  
Solving the Equations of Motion

by

Charles S. Peskin

Submitted in partial fulfillment of the requirements for the degree of  
Doctor of Philosophy  
in the Sue Golding Graduate Division of Medical Sciences  
Albert Einstein College of Medicine  
Yeshiva University

1972

TO LUCY AND ERIC

### ACKNOWLEDGMENTS

This work has been jointly supervised by Edward Yellin of the Albert Einstein College of Medicine and by Alexander Chorin of the Courant Institute of Mathematical Sciences (NYU).

Edward L. Yellin has been my adviser throughout this research. I am extremely grateful for his advice, criticism, encouragement and support. Our many conversations on the subject of heart valves have had a tremendous influence on my thinking.

Alexander J. Chorin introduced me to fluid mechanics and also to numerical methods. His own research in these areas has made the present work possible. In addition, he has supervised the mathematical aspects of this work, made valuable suggestions, and helped me to put my ideas in mathematical form.

Discussions with the following people have contributed to the present work: R. W. M. Frater, Berle Bass, Nancy Buckley, Ted Feit, Olof Widlund, Peter Lax, C. Leiva, D. Fischer, T. MacMahon, Edward Peskin, John Gersh.

Erika Epstein bravely mediated my disputes with the computer. Marion Peskin pointed out many references of interest. Preparation of the manuscript would not have been possible without the assistance and hard work of Ethol S. Koelle, Lucille Ingenito, Joanne Marchetta and Kathleen Mulqueen.

This investigation has been supported in part by Grant 5T5-GM-1674 from the Institute of General Medical Sciences, National Institutes of Health. Computer time and office space were generously made available by the Courant Institute of Mathematical Sciences (NYU) under U. S. A. E. C. Contract AT(11-1)-3077.

## FLOW PATTERNS AROUND HEART VALVES:

### A Digital Computer Method for Solving the Equations of Motion

#### ABSTRACT

The flow pattern of blood in the heart is intimately connected with the performance of the heart valves. The motions of blood and valve leaflet interact strongly. Points of the valve leaflet are carried along at the local fluid velocity. At the same time these points exert forces on the fluid which significantly alter the fluid motion.

A mathematical method for studying these phenomena is introduced. Its basis is an idealization of the cardiac tissue as a neutrally buoyant, force-generating structure, immersed in a viscous incompressible fluid. A unified mode of representation has been found for such structures which encompasses natural valves, prosthetic valves, and heart muscle. In this "link formalism", specified pairs of points of the structure are connected by links which fix its topology and embody its physical properties. The length-tension relation for each link is fixed for the passive valve leaflet and time-varying for the active heart muscle.

A numerical method is introduced which incorporates a previously existing algorithm for solving the Navier-Stokes equations on a rectangular mesh. Points of the link structure (cardiac tissue) need not coincide with fluid mesh points. We introduce an analog of the  $\delta$ -function which is used to interpolate the fluid velocity field to points of the cardiac tissue and also to spread the cardiac forces onto the fluid mesh. Numerical stability is secured by using at each time step a system of forces which are approximately the final forces for that time step. In solving for these forces we exploit the special mathematical structure of the link formalism to introduce a version of Newton's method which is efficient despite the large number of unknowns.

We use this technique to study the physiology of mitral valve closure. Four distinct streamline types are identified, together with a universal sequence of their appearance in time during a single diastole and a hierarchy of their effects on valve performance. This classification is also applicable to prosthetic valves. These streamline types are:

- A. Fills the ventricle; does not move the valve.
- B. Circulates and closes valve; no effect on ventricular volume.
- C. Closes the valve and reduces the ventricular volume.
- D. Reduces ventricular volume; does not move the valve.

The type B circulating streamlines are of special interest in that they move the valve toward closure without reducing the ventricular volume. In our work the valve leaflets themselves participate in the formation of the circulating streamlines, which are only formed when the open valve is restrained by the chordae. This contrasts with the views of some workers that the chordae are slack during diastole. Thus our mathematical method gives the physiologist the freedom to postulate the properties of the heart, to create a corresponding cardiac structure in the computer, and to observe its performance. In this way he refines his understanding of cardiac physiology.

Projected uses of this technique include the design and computer testing of prosthetic valves. As shown in this work the details of the flow pattern significantly influence valve performance. The flow pattern is not accessible in vivo, however, and in vitro testing chambers usually have rigid walls, unlike the chambers of the heart. The present method can provide an appropriate setting for the systematic variation of the parameters of prosthetic valve design.

## CONTENTS

### ACKNOWLEDGMENTS

### ABSTRACT

I.	INTRODUCTION	1
II.	BRIEF STATEMENT OF THE PROBLEM AND METHOD OF SOLUTION	4
III.	HISTORY	9
	Early Ideas	9
	Interpretation; Unification of the Foregoing Theories	14
	Recent Confirmation of the Early Ideas	16
	Flow Patterns and Artificial Valves	22
	Pressure-Flow Relations for Heart Valves	28
	Numerical Integration of the Navier-Stokes Equations for Incompressible Fluid Flow	34
IV.	THE COMPARATIVE FLUID DYNAMICS OF MAMMALIAN HEARTS	38
V.	EQUATIONS OF MOTION	43
	Description	43
	Navier-Stokes Equations	48
	Representation of the Heart Apparatus	49
	Boundary Conditions	53
VI.	NUMERICAL SOLUTION OF THE NAVIER-STOKES EQUATIONS FOR A VISCOUS INCOMPRESSIBLE FLUID	57
	Rectangular Mesh	57
	Discrete Time Steps	57
	Discrete Operators Corresponding to $\underline{u} \cdot \nabla - \nabla^2$	58
	Discrete Projection Operator P	58
	Difference Equations	59
	Solution of the Local Difference Equations on a Periodic Domain	60
	Solution of the Discrete Poisson Equation	64

VII.	REPRESENTATION OF VALVE AND MUSCLE: THE LINK FORMALISM	67
	Natural Valve Leaflet	68
	Rigid Occluders for Artificial Valves	69
	Muscle	69
VIII.	NUMERICAL STABILITY	71
IX.	THE CONNECTION BETWEEN VALVE AND FLUID	84
X.	SUMMARY OF THE NUMERICAL METHOD	92
XI.	COMPUTER EXPERIMENTS ON THE PHYSIOLOGY OF THE NATURAL MITRAL VALVE	94
XII.	CONCLUSIONS	102
	The Physiology of Mitral Valve Closure	102
	Future Applications	110
	Further Development of the Methods	112
	Concluding Remarks	113
	LITERATURE CITED	114



## I. INTRODUCTION

The aim of this work is the prediction of the flow pattern of blood in the heart from Newton's laws. Newton's laws have been known for several centuries. There has been interest in the flow patterns around heart valves for even longer, beginning with the work of Leonardo da Vinci. The questions that we seek to answer in this work are old questions, and the physical principles that we shall use have been known for a long time. It was not known until recently how to use the principles to answer the questions. In other words, the equations could be written down, but they could not be solved.

In this work, the aim of solving the equations is to explore the interaction of heart valves with the flow of blood in the heart. This interaction is strong in both directions. The movements of the flexible valve leaflets are completely determined by the motion of the fluid, but the valve leaflets strongly influence that motion. For example, when the valve is closed, it completely prevents backward flow. More subtle aspects of the interaction are illustrated by the hypothesis of Leonardo da Vinci that frictional drag on the thin layer of fluid adjacent to the valve leads to the production of a vortex and that this vortex is responsible for the early closure of the valve and for the lack of any observed backflow associated with closure. Such mechanisms are interesting in their own right, and it is reasonable to assume that understanding them will lead to improved design of artificial heart valves.

The main result of this thesis is the introduction of a method for investigating such phenomena. The method consists of a computer technique or numerical scheme for constructing approximate solutions

of the equations of motion of the blood-valve-heart system. Some of the main strengths and weaknesses of the method will be mentioned here with more detailed discussion in subsequent sections.

The method is not limited to any particular geometry of heart or valve. The correct geometry can be specified to any desired degree of accuracy -- the only limitation being the endurance of the programmer who is supplying the data to the computer.

The physical properties of the heart, in particular, the active muscular properties of the heart wall can be included in the scheme, again with any desired degree of accuracy.

A unified mode of representation has been found that includes both flexible structures (natural valves) and almost rigid structures (artificial valves).

In principle, the method can be used in three dimensions without making any assumptions about axial symmetry. (However, this potential cannot yet be realized, see below).

With the present generation of computers, the method is very expensive in computer time and space. As a practical matter, this limits what one can do as follows: First, one can only study two dimensional heart-like structures. Second, one can only study small hearts. As to the former limitation, it will be seen by the results that much can be learned (especially about the mitral valve) from a two dimensional representation. As to the latter, it is likely that the flow patterns and valves of small mammals are roughly scale models of the human. (See Section IV on Comparative Fluid Dynamics of Mammalian Hearts). The limitations will be gradually removed as computer technology advances, and perhaps more rapidly removed by the

further development of the present methods.

The method assumes that all structures of the heart are neutrally buoyant in blood. Studies with artificial valve occluders of varying mass confirm the idea that the inertia of the blood itself completely dominates any other inertial effects in the heart. [1]

The method assumes that all structures are immersed in fluid. Strictly speaking then, we are studying a heart beating in an aquarium of fluid, rather than in situ.

## II. BRIEF STATEMENT OF THE PROBLEM AND METHOD OF SOLUTION

We are concerned in this work with the flow patterns of blood in the neighborhood of heart valves. The valves themselves have a strong influence on this flow pattern, and the flow pattern has a strong influence on the performance of the valves. The aim of this work is to study the interaction.

As a starting point, we take the laws of fluid mechanics for a <sup>s</sup> viscous incompressible fluid. From these laws it is possible in principle, given the state of the fluid at one time, to predict its state at all subsequent times. Of course, to do this one needs to know the forces acting on the fluid. An important example is the force applied to the fluid along a material boundary, such as the heart valve leaflet. This force is central to the function of heart valves: when the valve is closed it is the force that stops the flow. Similarly, the force applied by heart muscle to the fluid constitutes the function of that muscle. In the present work, material boundaries are represented in terms of the forces they exert on the fluid. This is to be contrasted with the more classical approach in which boundaries are regarded as constraints on the fluid motion. It is simplest to calculate the influence of such forces if they are applied to the interior of the fluid rather than at its edges. In the case of the heart valve leaflet, which is immersed in fluid, the forces really are applied in the interior. It is convenient, however, to regard the whole heart as immersed in fluid so that the muscular forces also are applied to interior points. When the material boundaries are thus immersed, and represented as forces, they disappear as boundaries in a mathematical sense. Instead, they are simply specialized regions of the fluid where extra forces are

applied. The next step is the calculation of such forces. An essential principle here is the following.

If the material boundaries do not introduce any additional mass into the fluid (i.e. if they are either infinitely thin or neutrally buoyant) then the forces they exert on the fluid can be calculated entirely from the state of the boundaries, without regard to the state of the fluid.

The proof of this requires only Newton's laws. Let  $B'$  be a chunk of the material boundary  $B$ . The forces on  $B'$  are of two types. There are forces  $\underline{f}_1$  exerted by the fluid on  $B'$  and forces  $\underline{f}_2$  exerted by the rest of the material boundary  $B$  on  $B'$ . The force  $\underline{f}_1$  depends on the state of the fluid and  $\underline{f}_2$  depends on the state of the material boundary. If the mass of  $B'$  is zero, we must have  $\underline{f}_1 + \underline{f}_2 = 0$  to avoid infinite acceleration of  $B'$ . Consequently,  $-\underline{f}_1 = \underline{f}_2$ . But  $-\underline{f}_1$  is the force exerted by  $B'$  on the fluid. Since it is completely determined by  $\underline{f}_2$  the theorem is proved. One way to summarize this theorem is to state that in the case of massless material boundaries all forces applied to one part of the boundary by another are transmitted directly to the fluid.

Consequently, we restrict attention to material boundaries which do not add mass to the fluid. For example, we approximate the heart muscle as a bag of neutrally buoyant fluid in which additional forces (the muscular forces) act, over and above the usual fluid forces. This point of view guarantees automatically the constant volume feature of muscular contraction, since the fluid in the muscle is incompressible, like the rest of the fluid. The forces due to the boundary will be calculated purely from the state of the boundary. This avoids the

necessity of evaluating the fluid stress tensor in the neighborhood of the boundary.

The next step is the specification of the state of the boundaries in such a manner that the forces can be evaluated at each instant of time. For elastic structures the state of stress (i.e. the set of forces exerted by one part of the structure on another) is completely determined by the configuration of the material points of the structure in space. One can take a structure which is formally elastic in this sense and make it active (like a muscle) by having the relation between its configuration and its state of stress change with time. Consequently, we have adopted the point of view that the configuration in space of the material boundary is the central determinant of the boundary forces, whether the boundary be active or passive.

Moreover, we have found that an especially simple type of elastic structure is sufficiently general for our purposes. Thus, we restrict consideration to structures in which all forces act along straight line segments joining pairs of points of the structure. Such segments are called links. The topology of the structure is determined by giving a list of all of the links together with the names of their endpoints. The physical properties of the structure are determined by stating how the tension in each link depends on the length of that link. In Section VII it is shown that this type of structure may be used to represent natural valves, artificial valves, or heart muscle.

Toward the beginning of this section, it was said that the state of the fluid could be determined in principle at all subsequent times if it was given at some initial time. When this is actually done in a computer the state of the fluid at every point in space cannot be

stated, as there are an infinite number of such points. Instead, only a finite number of points are used: points arranged like intersections of a piece of graph paper. These are called mesh points. However, the points of the immersed boundaries are moving about the domain, and they cannot be required to coincide with mesh points at all times without introducing excessive distortion that will interfere with the accurate computation of the boundary forces. Consequently, it is necessary to allow the boundary points to lie anywhere in the domain, and this raises, at once, the following difficulties:

How to interpolate the fluid velocity field from the fluid mesh points to the points of the immersed boundaries.

How to distribute the forces associated with these boundary points to the nearby mesh points of the fluid.

Both of these problems are solved simultaneously by the introduction of an analog of Dirac's  $\delta$ -function, which is essentially a pulse of zero width and area 1. Here we use instead a pulse which is 4 mesh widths wide and has area 1. This pulse, centered on the boundary point, determines the coupling coefficient between that boundary point and the mesh points of the fluid. As the resolution of the fluid mesh becomes finer and finer, our pulse approaches a Dirac  $\delta$ -function. The particular shape of the pulse that we use is that of a single cycle of  $\cos^2 \theta$ . This shape is optimal in the sense discussed in Section IX.

A further difficulty is the question of numerical stability. Briefly, the problem is that the act of introducing finite time steps, which is essential for a computer solution, has the tendency to introduce oscillations which grow with time and which have nothing to do with the physical solution of the problem. This can be avoided by using in each time step a system of boundary forces which are approximately the forces

for the end of the time step, not those known at the beginning. The final forces are unknown at the beginning of the time step. Moreover, they depend on the forces that are applied to the fluid during the time step. If we want the final forces to equal the applied forces, then we have to solve what is known mathematically as a fixed point problem for the boundary forces. Unfortunately, in this case the problem has roughly a thousand unknowns and an equal number of equations; moreover, it is non-linear. Fortunately, the associated matrix is mostly full of zeros, because each boundary point is connected by links to only a few other boundary points. How to take advantage of all of these zeros is not a trivial problem. The solution is given in Section VIII.

With these techniques established the construction of the solution proceeds step by step as follows:

1. Solve for a set of boundary forces which will be approximately the final forces for the current time step.
2. Distribute these forces on the fluid mesh using the  $\delta$ -function.
3. With these forces given, allow the fluid velocity field to move forward in time one step under their influence and also under the influence of the fluid forces.<sup>†</sup>
4. Interpolate the new velocity field to the boundary points using again the  $\delta$ -function, and move the boundary one time step ahead.

This completes the time step. Return to 1.

<sup>†</sup>Step 3 is a complicated one, the details of which are not emphasized in this section because the techniques were known when the present author began this work. The numerical techniques used in the present work for step 3 were invented by A. J. Chorin. They are discussed in more detail, with references, in Section VI.



### III. HISTORY

#### Early Ideas

Two crucial hypotheses have dominated the thinking of many of the present workers in the field of heart valves. They are the hypotheses of Leonardo da Vinci [2] and of Henderson and Johnson [3]. Both are concerned with the question of the efficiency of valve closure, that is with the phenomenon of zero backflow.

Leonardo's views can only be understood when it is realized that the circulation of the blood was not known in his day. To him, the function of the aortic valve was the same as it is to us: namely, to allow blood to pass away from the heart and not to return. But his view of the mitral valve was that blood passed it in both directions and in this manner became heated, thinned and ready for use. Therefore, in the case of the aortic valve he devised a mechanism that would account for zero backflow during closure. In the case of the mitral valve he proposed that the blood lying between the cusps at the instant that closure begins is the blood that constitutes the reflux into the atrium. It is Leonardo's aortic valve, then, that is of interest to us; for we know now that reflux into the atrium through the mitral valve can only be harmful and ought to be minimized in valve design.

For the aortic valve, Leonardo proposed that as the blood flowed over the opened valve a thin layer of fluid adjacent to the valve leaflet is retarded by frictional forces, and that thin layer of fluid in some way generates a vortex which lies behind the valve leaflet and holds the cusp away from the wall of the aorta. The tendency of the vortex is always to close the cusp. During maximal forward flow, it is prevented from doing so by the blood rushing out of the ventricle,

but as the flow decreases, the cusps move toward each other. At the instant of zero forward flow they are already closed and no backflow occurs across the valve.

These ideas ought to be remarkable to fluid dynamicists, because they contain the essence of what is now known as boundary layer theory, which was discovered in 1901 by Prandtl. It is now an accepted principle of fluid dynamics that vorticity in a fluid is often generated by frictional forces in the thin retarded layer of fluid adjacent to material boundaries. Leonardo says he got his ideas by watching fluid pour out of the end of a pipe. He noted that the fluid from the center of the pipe went higher (if the pipe was vertical) or further (if the pipe was horizontal) than fluid from near the sides. The fact that Leonardo observed a thin layer of retarded fluid in this experiment shows that the velocity profile he was observing was like that shown in Fig. (3-1a) rather than in (3-1b). The profile of Fig. (3-1b) is the one we associate with an infinite pipe or with a finite pipe at a large distance from its inlet. Since Leonardo observed a profile like that shown in a, he must have used a pipe which was short compared to the inlet length: It would have been difficult for him to do otherwise since inlet lengths are long under conditions that approximate human physiology. In the case of the aorta for example, inlet length is on the order of 2000 radii. (See Landau, Lifshitz [4], p. 150 for a discussion of inlet length).

The ideas of Henderson and Johnson are best described by a discussion of two simple experiments of theirs. In the first a U-shaped section is attached to a straight tube near the middle as in Fig. (3-2). Initially, there is flow directly through the straight tube with very

Fig. (3-1)      Velocity profile in a pipe (a)  
near the entrance, and (b) far from the entrance.

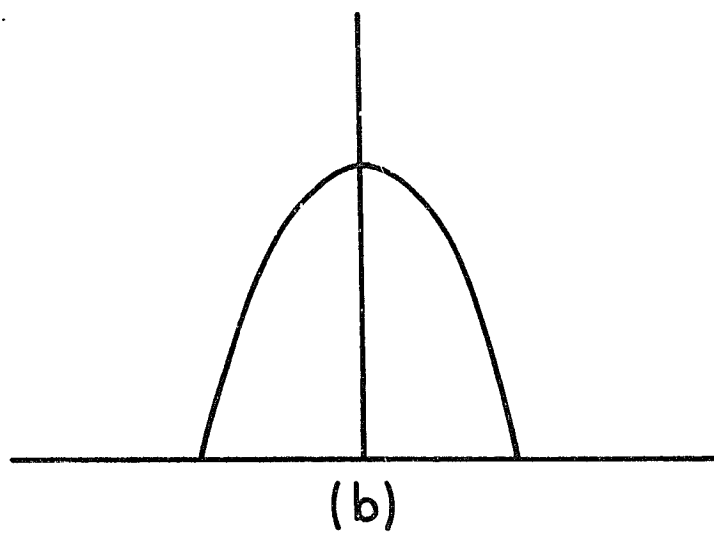
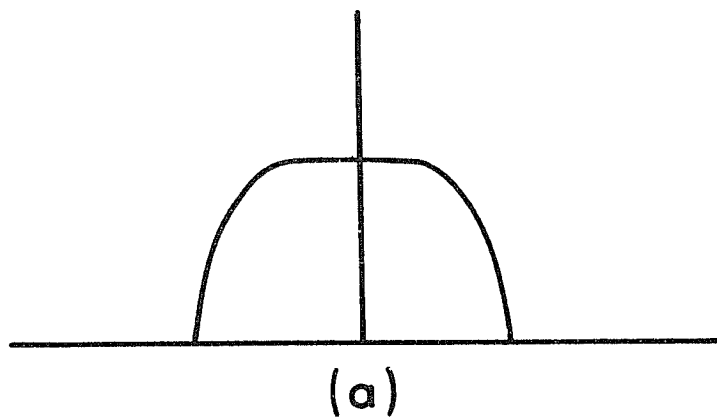
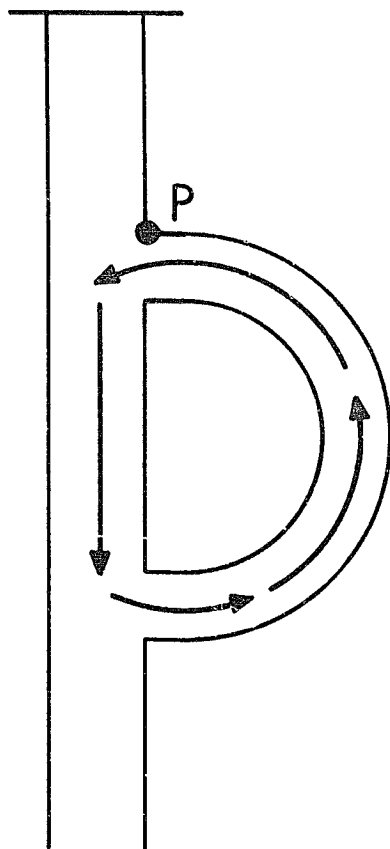
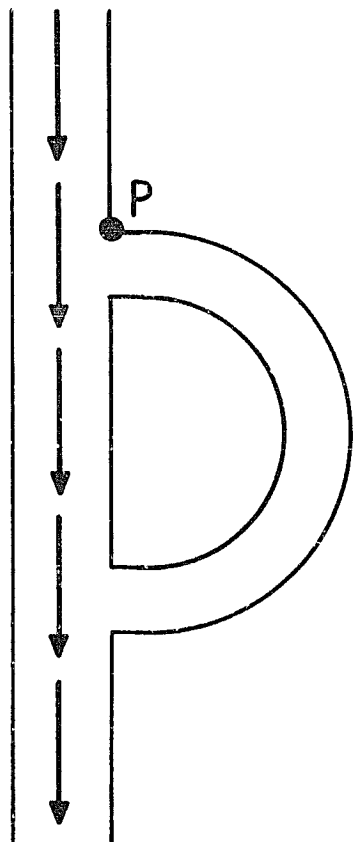


Fig. (3-2)      Initially the bulk of the flow is through the straight tube. When this path is suddenly cut off, fluid begins to circulate through the U-shaped segment.



little diverted into the U. Then the straight-through flow is stopped suddenly by occluding the tube either above or below the U. The result is that fluid begins to circulate around the circuit formed by the U and the section of the straight tube that closes it.

It is instructive to analyze this experiment in more detail than Henderson and Johnson did in their paper. The fluid is imagined to be ideal (zero viscosity) and to flow in all cases parallel to the walls of the tubes with uniform distribution of flow over the cross sections. Let the straight tube be designated by the subscript 1 and the U shaped segment by the subscript 2, <sup>so</sup> ~~that~~ <sub>A</sub> that their cross sectional areas will be  $A_1$  and  $A_2$ ; their velocities  $v_1$  and  $v_2$  and their lengths  $\ell_1$  and  $\ell_2$ . Actually, we let  $\ell_1$  equal the length of that portion of the straight tube that closes the U. The positive direction of velocity is down in the straight tube and up in the U. The notation is illustrated in Fig. (3-2b).

Let  $C$  be a closed D-shaped curve of length  $\ell_1 + \ell_2$  that goes around the loop formed by the straight tube and the U. Then let

$$K = \int_C \underline{v} \cdot d\underline{\ell} = v_1 \ell_1 + v_2 \ell_2 \quad (3-1)$$

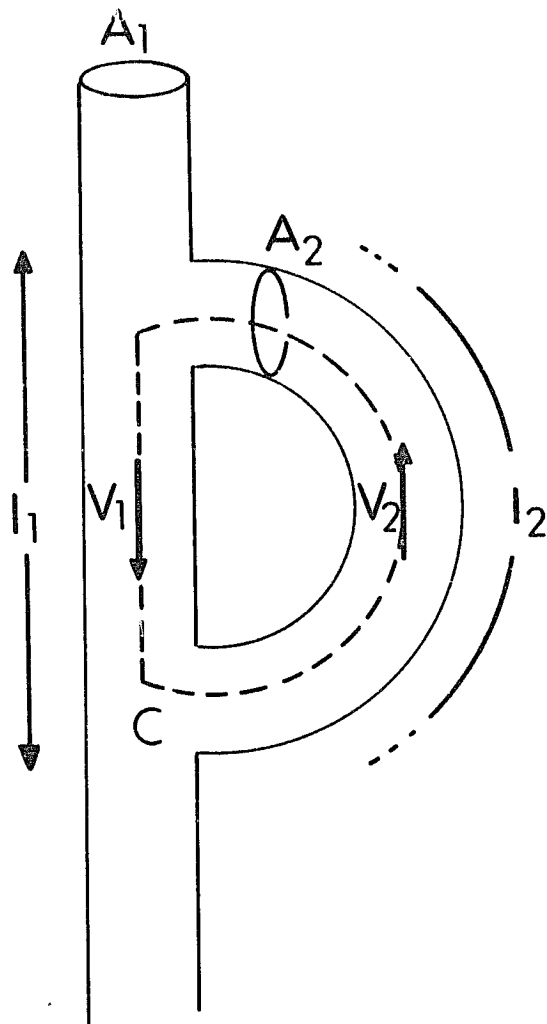
$K$  is called the circulation around  $C$ . During the sudden occlusion of the straight tube at either end,  $K$  is conserved. The total flux in the straight tube is  $v_1 A_1$  and that in the U is  $v_2 A_2$ . After the occlusion these must be equal. Thus the quantities  $v_1$  and  $v_2$  after the occlusion are given by

$$\ell_1 v_1 + \ell_2 v_2 = \ell_1 v_1^0 \quad (3-2)$$

$$A_1 v_1 = A_2 v_2 \quad (3-3)$$

Fig. (3-2b)      Notation for the analysis of  
Henderson and Johnson's experiment.





with the solution

$$v_1 = \frac{A_2 \ell_1 v_1^0}{A_1 \ell_2 + A_2 \ell_1} \quad (3-4)$$

$$v_2 = \frac{A_1 \ell_1 v_1^0}{A_1 \ell_2 + A_2 \ell_1} \quad (3-5)$$

In the simplest case  $A_1 = A_2$ , we get

$$v_1 = v_2 = \frac{\ell_1 v_1^0}{\ell_1 + \ell_2} \quad (3-6)$$

The essential point is that the circulation  $K$  is conserved during the occlusion and that this condition permits a determination of the final velocities. A more subtle question is: how did the circulation become established in the first place. One might expect, for example, that the initial flow condition was like that shown in Fig. (3-3), with  $v_1 \ell_1 + v_2 \ell_2 = 0$ , initially.

For this initial condition, occlusion of the straight tube will completely stop the flow everywhere at once. The reason why Henderson and Johnson did not observe this kind of flow initially was that separation had occurred at the corner indicated in Fig. (3-4).

Thus, the initial circulation was created by fluid flow separating from the wall. The detailed analysis of this phenomenon inevitably involves consideration of the wall region, or boundary layer, and the frictional forces operating there. Once this point is understood a relationship begins to emerge between the considerations of Henderson

Fig. (3-3)      If  $K = v_1 l_1 + v_2 l_2 = 0$  initially,  
sudden occlusion would stop the flow everywhere  
at once.

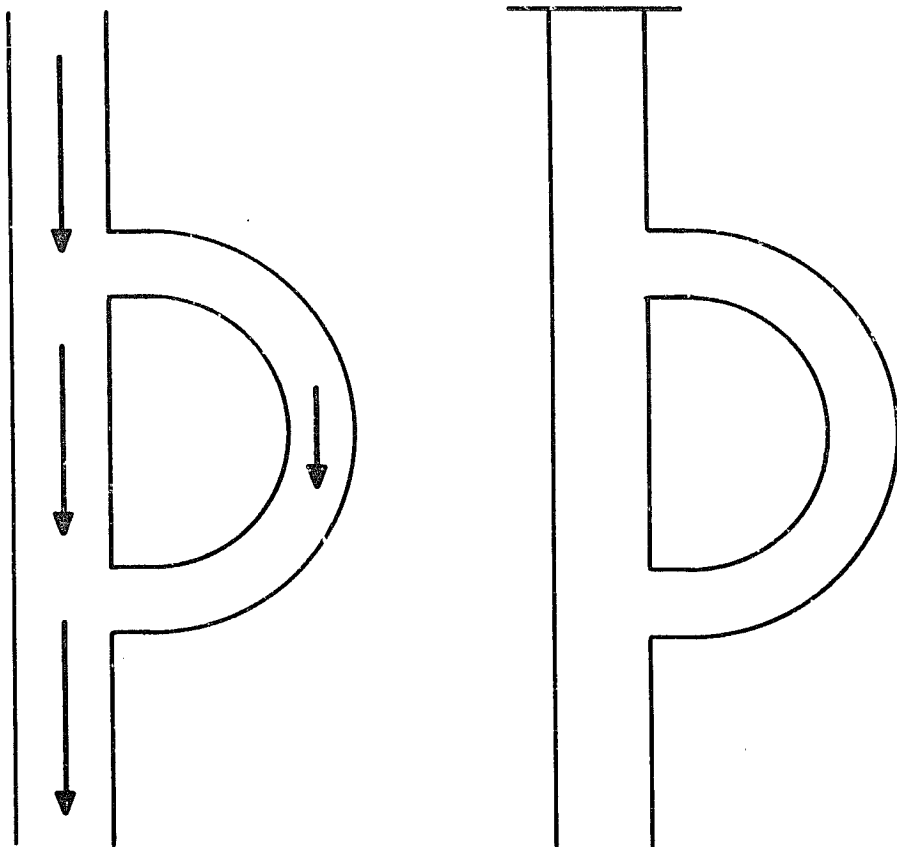
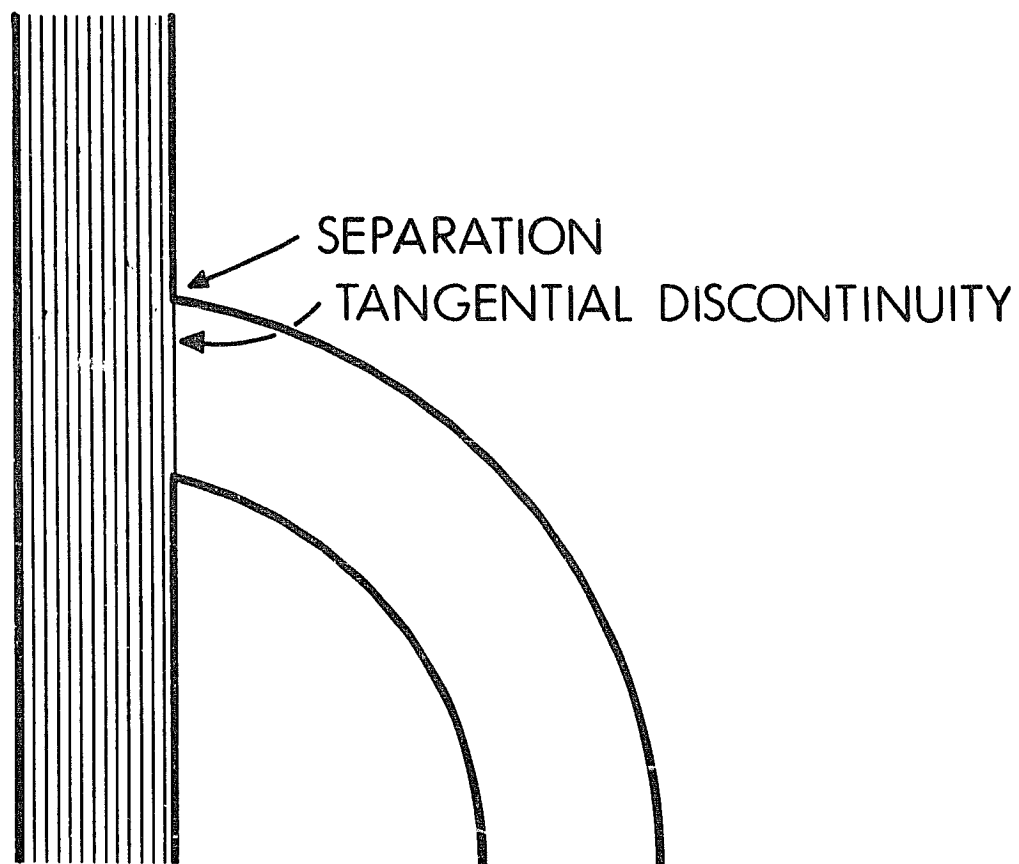


Fig. (3-4)      How non-zero circulation  $K$  is  
established in the experiment of Henderson and  
Johnson. The flow is unable to follow the sharp  
angle and separates from the wall.



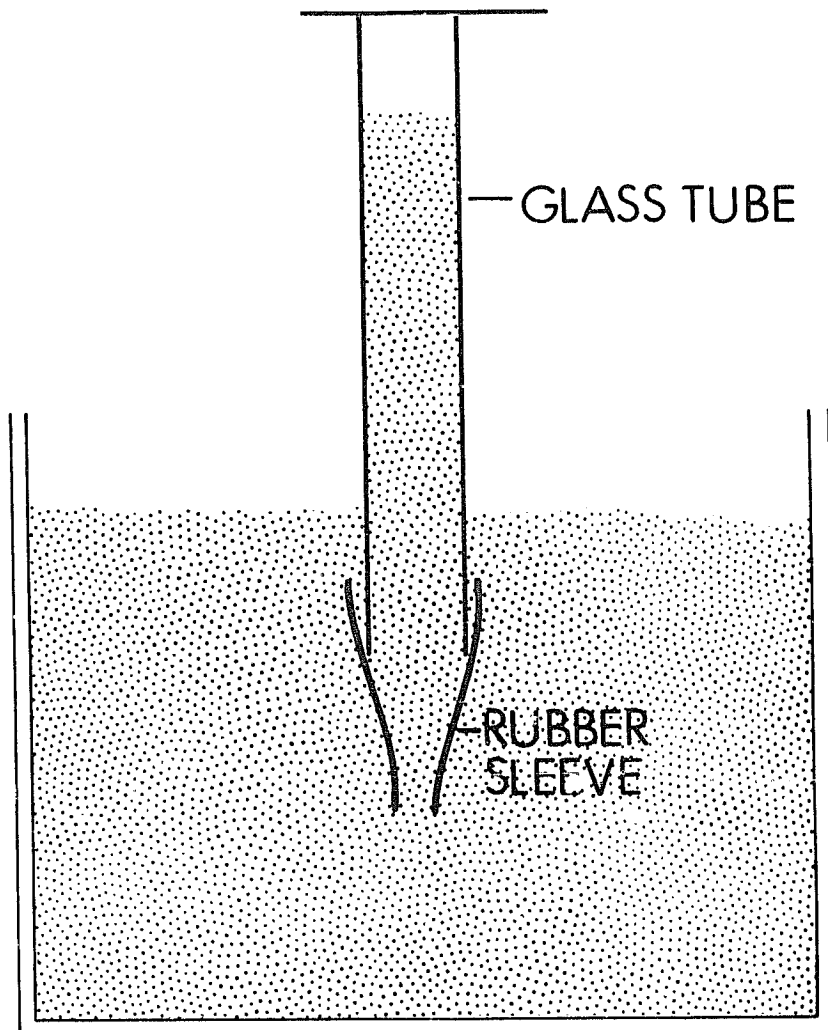
and Johnson and those of Leonardo.

The second experiment of Henderson and Johnson is illustrated in Fig. (3-5). A flexible rubber sleeve is fitted to the end of a glass tube which is initially filled with water. The tube is held vertically above an aquarium with the end of the tube and rubber sleeve below the surface. The fluid is held in the tube by the finger of the experimenter covering the top. The column of fluid is released and falls in the tube. When the level in the tube becomes below that in the aquarium, fluid rushes in from the sides and collapses the rubber sleeve. The closure is so effective that by the end of the experiment the fluid level in the tube is at rest below the fluid level of the aquarium. Henderson and Johnson explain this result by noting that the column of fluid actually continues down into the aquarium in the form of a jet. When the pressure head in the glass tube becomes too low, however, the jet is broken. The submerged part continues to move ahead leaving a negative pressure region behind which draws fluid rushing in from the sides.

To Henderson and Johnson this experiment demonstrated the importance of atrial systole to mitral valve closure. They concluded that atrial systole establishes a jet, which, when broken, leads to valve closure.

Fig. (3-5)        A second experiment of Henderson and Johnson. The column of water in the tube is released; it falls suddenly. When the level in the column is below that in the aquarium the sleeve collapses and holds the level low.





### Interpretation: Unification of the Foregoing Theories

We begin by noting that the experiment of Henderson and Johnson with the U-shaped tube can actually be made the basis for construction of an extremely efficient valve (see Fig. 3-6).

When the valve is open it blocks the U-shaped channel so that flow goes straight through. When a reverse pressure difference is applied flow begins to circulate round the tube and this slams the valve shut from the side with no backflow. This valve is hereby proposed for use with artificial hearts, as shown in Fig. (3-7).

Next we note that Fig. (3-6) looks a lot like an aortic sinus, the main difference being that the aortic sinus doesn't have a D-shaped segment cut out of it but instead is filled with fluid. Consequently, we replace this cut out segment by a vortex as shown in Fig. (3-8).

We emphasize again that the ultimate source of the vorticity is, as stated by Leonardo, the thin layer of retarded fluid adjacent to the valve leaflet.

The connection between Leonardo's ideas and those of Henderson and Johnson is now complete. It remains, however, to show how the foregoing considerations can be applied to the mitral valve. To do this one simply throws away the downstream straight tube and makes the U deformable, like the ventricular wall in diastole. One has then the configuration of Fig. (3-9).

One final remark of a mathematical nature:

In Fig. (3-6) one can draw two types of simple closed curves lying entirely in the fluid or possibly crossing the valve. One type encircles the cut out section, the other does not. These two types are topologically distinct; they cannot be deformed into each other without

Fig. (3-6)      Plan for an efficient valve based on the principles of Henderson and Johnson's experiment. Open, the valve offers little resistance to flow. Sudden application of a reverse pressure difference during forward flow causes circular flow which closes the valve.

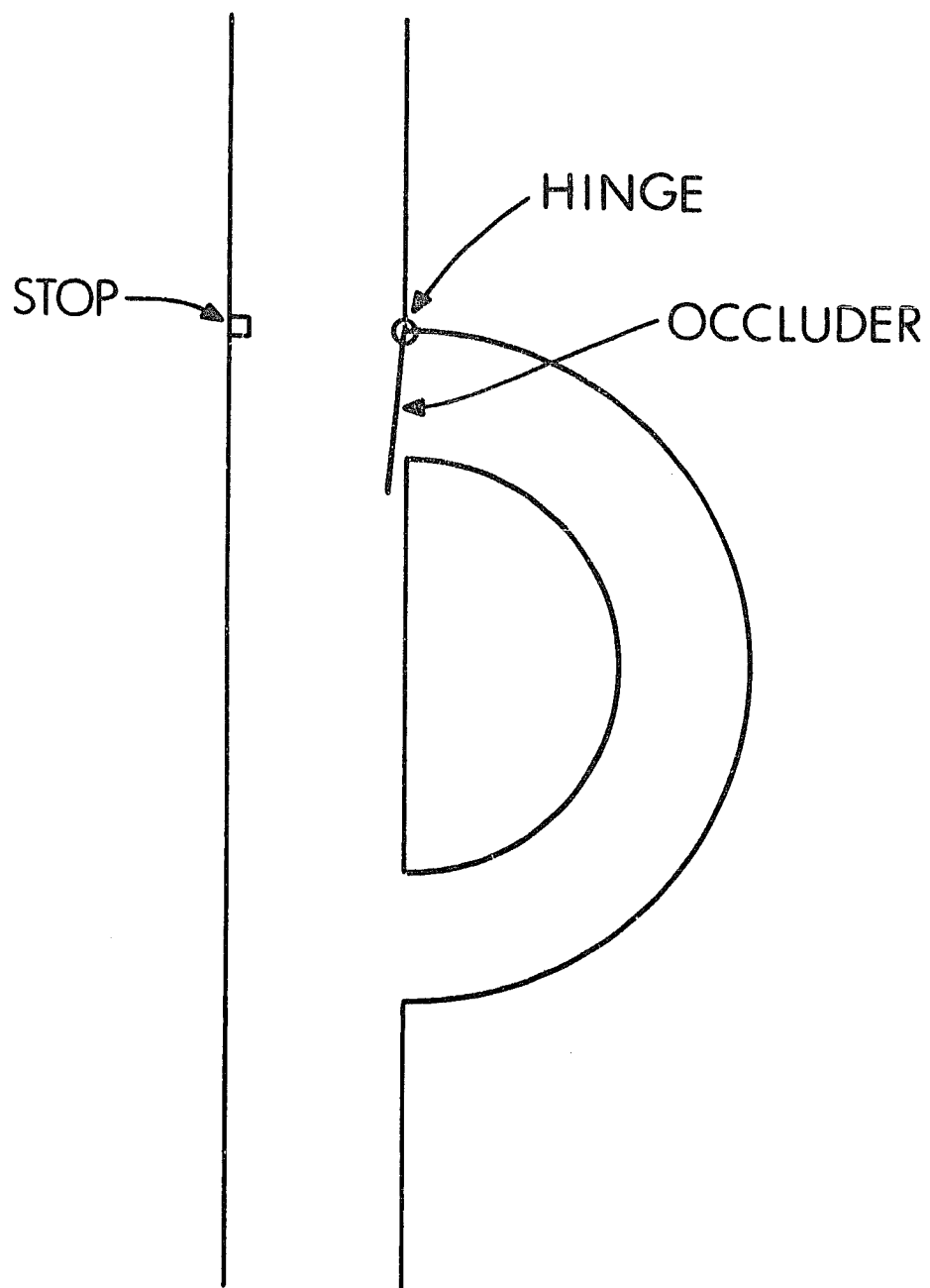


Fig. (3-7)      Plan for an artificial ventricle  
using the valve of Fig. (3-6) in both the inflow  
and outflow positions. The ventricle is shown  
in diastole.

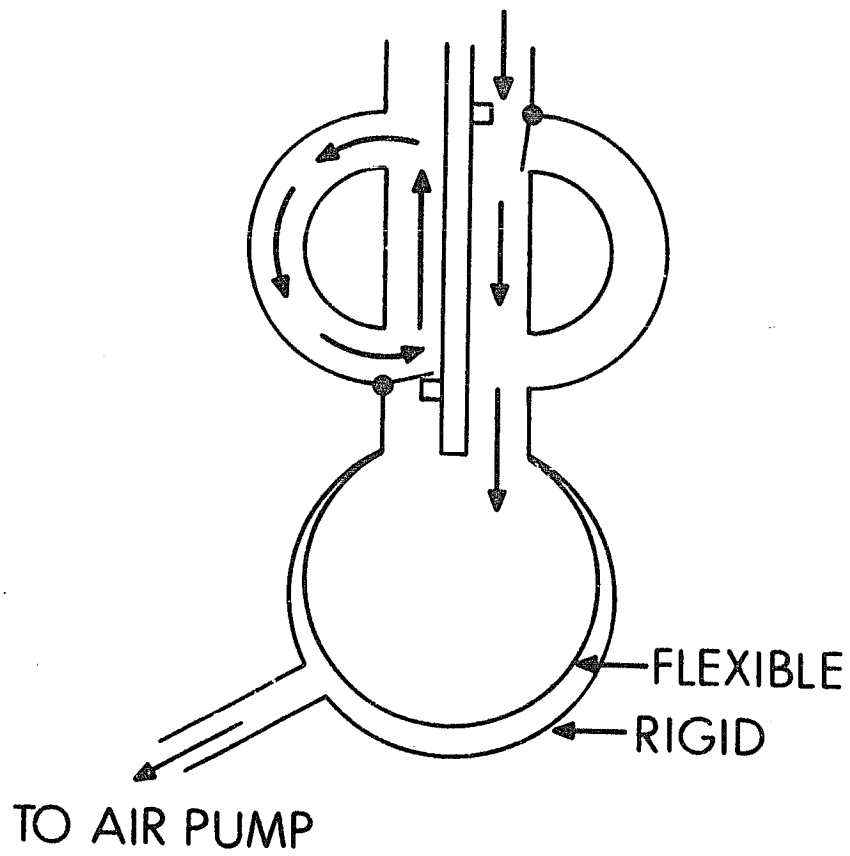


Fig. (3-8)      A vortex replacing the cut out  
section of Fig. (3-6). The configuration is  
now that of an aortic sinus.

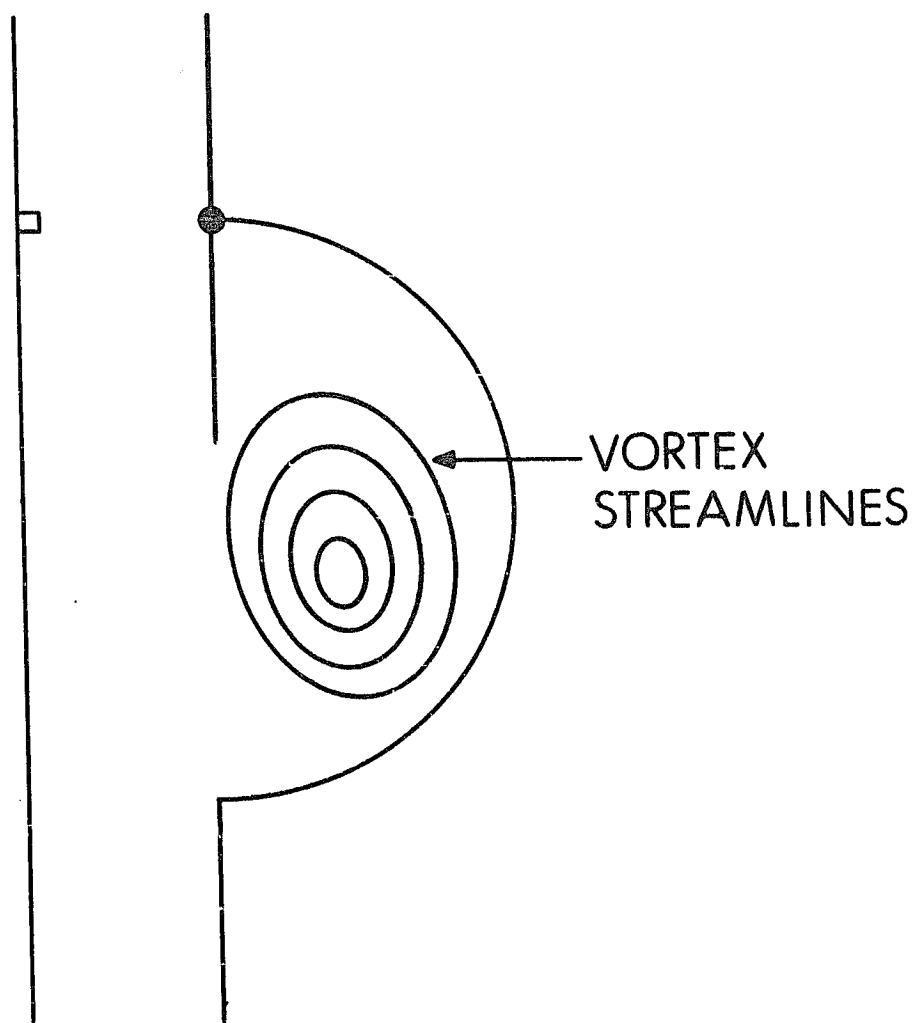
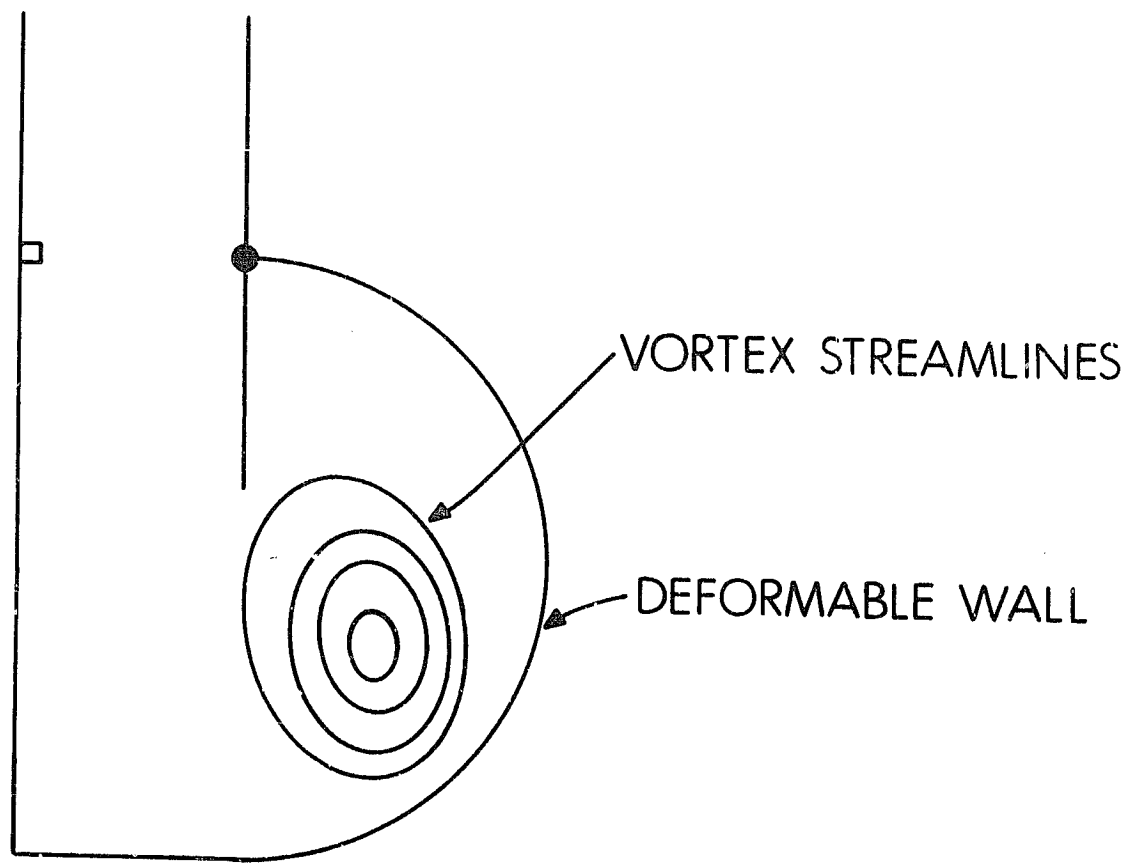




Fig. (3-9)      The outflow path has been  
replaced by a deformable wall. The configuration  
is now that of half a ventricle in diastole.



crossing walls. In Fig. (3-8) there are similarly two types of simple closed curves, those that encircle the center of the vortex and those that do not. Thus, the vortex not only plays the same role as the cut out section physically, but also topologically. In both instances, a potential function can be introduced to describe the flow (approximately), but because of the topology this function must be multivalued.

### Recent Confirmation of the Early Ideas

Taylor and Wade [5,6] have observed the flow patterns directly in mammalian hearts by taking ciné films using x-ray with radiopaque dye as a fluid marker and also using endoscopic techniques with bubbles as a fluid marker. In a different study, the same workers actually measured the fluid velocity at different points across the mitral valve orifice. Their results are so striking and important that they will be quoted here at length:

"The basic flow patterns observed were identical in the two species, and of a similar nature round both mitral and tricuspid valves. They were characterized by stability of flow with no gross turbulence with only a slow tendency to lateral dispersion of streams. Fluid entering the atria during ventricular systole collected as an expanding bolus. The only site where swirling and dispersion was observed was in the right atrium adjacent to the entrance of the coronary sinus. In ventricular diastole when the atrio-ventricular valves opened stable streams were drawn into the ventricle through the valve canal. On reaching the valve outlet at the cusp margins these streams diverged to flow around the lateral and septal walls of the ventricle and then down the ventricular aspect of the atrio-ventricular valve cusps. At this stage they flowed adjacent and parallel to the entering stream and formed stable expanding vortex systems behind the cusps, which were fed and maintained by the flow from the atrium. In late ventricular diastole, and with atrial systole, the streams became transiently less stable, with waviness appearing as flow decelerated. There was also some lateral swirling which was most marked at the time of atrioventricular valve closure. Despite this terminal instability there was no evidence of flow reversal at the time of valve closure."

"Records at different distances across the mitral valve orifice under steady state conditions showed no significant change in the flow velocity curve. It was not possible to record within 2 mm of the wall."

The main conclusions on the character of mitral valve flow may be summarized:

- (1) Flow is not turbulent.
- (2) Vortices are formed and are stable.
- (3) Boundary layers are thin.
- (4) There is no backflow during closure.

(5) The flow pattern is species independent (on the two species observed - sheep and dogs).

Remark: The conclusion that the flow is not turbulent is surprising to many fluid dynamicists who point out that turbulent flow would result if the peak flow rate through the mitral orifice were maintained steadily in a pipe of the same diameter. However, as Taylor and Wade point out, the character of the flow is completely different from that of steady flow in a pipe. In particular, the velocity profile is flat so that to a first approximation the bulk of the fluid is simply being transported as a rigid body.

Further confirmation and extension of the early ideas comes from the work of Bellhouse and Talbot [7] on the aortic valve and of Bellhouse and Bellhouse [8] on the mitral valve. These workers constructed realistic models of the natural aortic and mitral valves and mounted them in a transparent elastic heart-like chamber which was activated by air pressure. They were able to measure the flow pattern with hot-film probes and to observe it by watching suspended particles and dye.

Their main conclusions are similar to those listed above but with many additions and refinements, some of which will be discussed here.

In the case of the aortic valve, Bellhouse and Talbot [7] found that during the time of forward flow, vortices filled the aortic sinuses and "locked" the valve leaflets into a fixed open position, the same position as in steady flow. The stream of fluid just adjacent to the valve leaflet was split into two parts at the sinus ridge (as demonstrated by watching dye): part was diverted into the sinus and

the rest flowed down the aorta. When the main flow decelerated, the vortices pushed the valve leaflets together, so that closure was essentially complete by the time of flow reversal. The results were identical whether the sinuses were flexible or rigid, and the position of the valve cusps at maximum opening was the same in steady flow as in pulsatile flow. With a stenotic valve streamlines leaving the ventricle met the aortic wall further downstream than the sinus ridge and there was little circulation in the sinuses.

It is emphasized by Bellhouse and Talbot that the sinus vortex would not have time to form during a single systole if it were formed by the viscous shearing action of the main aortic flow across the initially still fluid in the aortic sinus. Instead, they claim that there is a continuing exchange of fluid with a complex flow pattern in and out of the sinuses. Indeed, such an exchange is demonstrated even in steady flow by their dye experiments. The authors do not comment on what is the nature of the flow pattern that produces this exchange, but it is evidently not turbulent, for the valve leaflets were not observed to flutter.

If the sinuses are rigid and the valve leaflet at rest, then flux into the sinus must equal flux out (Neglecting coronary flow, which was absent in the model system). Consequently, one has to imagine a streamline from the ventricle passing near the valve leaflet, looping one or more times round the sinus, and proceeding on down the aorta. But streamlines do not cross themselves, and such a streamline would have to cross itself if it lay in a single plane. It follows that the flow cannot be axisymmetric, not even if the valve and aorta were axisymmetric, if these phenomena are to occur. Indeed, it appears from the photographs of the leaflets that flow enters the sinuses primarily at the three

are occupied by the centers of the cusps and leaves primarily at the three commissures.

In their model mitral valve studies, Bellhouse and Bellhouse [8] again demonstrated vortices forming behind the valve cusps which aided in valve closure. The strength of the vortex was found to be dependent on the size of the ventricle, it was stronger in smaller ventricles. As expected, then, closure of the valve occurred later in the larger ventricle and there was more regurgitation. It should be emphasized that the absolute size of the ventricle was not the experimental variable here, but, rather, the ratio of stroke volume to end systolic (i.e. residual) volume. When that ratio was 1.62 the authors found an intense vortex and a valve that was 88% closed by the end of diastole. When the ratio was 0.14 the vortex was weak and the valve was only 28% closed at the end of diastole.

A crucial result of the studies that Bellhouse and Bellhouse performed with their model mitral valve is the demonstration of a diastolic closure movement of the anterior leaflet of the mitral valve that occurs long before atrial systole; in fact, it begins even before peak forward flow. Atrial systole first interrupts the progress of closure and then accelerates it. With or without atrial systole the closure is nearly complete by the end of diastole in small ventricles (small in the sense discussed above). As the authors point out, however, at low heart rates one may have a long period of slow filling during which the valve remains open because viscous action has time to degrade any vortices that are formed.

In such a situation, atrial systole can reestablish the vortex and promote diastolic closure of the valve. Conversely, if atrial systole

present the valve will be open at the beginning of ventricular systole and regurgitation will result.

The gradual diastolic movement of the anterior leaflet toward closure has also been demonstrated by echocardiography [9]; in fact, it is such a characteristic feature that it identifies the mitral valve to the cardiologist.

The conclusions of Bellhouse and Talbot, and of Bellhouse and Bellhouse are particularly satisfying because they are confirmed by a mathematical model. The nature of that model will be indicated here, mainly to contrast it with the present work. The starting point for the models of both the mitral and aortic valves is to assume the geometry of the flow pattern. That is, a vortex of a particular form is assumed to exist in the sinus or ventricle, the valve is assumed to form the curved surface of a truncated cone, and the flow in the main stream is assumed to be in the axial direction and uniform across each cross-section. When these geometric assumptions are made only a small number of variables remain to completely characterize the flow. For example, one has the vortex strength, the vertex angle of the valve cone, the velocities at the valve ring and valve tips. The evolution of these variables in time is then determined by applying conditions such as conservation of energy and momentum, and by matching the flow through the valve with the flow in the vortex. The conservation laws lead to a system of ordinary differential equations in which the time derivatives of the above parameters appear. The distribution of the flow in space, or the flow pattern, is assumed.

A major strength (or weakness, depending on one's point of view) of this approach is the insensitivity of the results to the assumed flow



pattern. In the theory used by Bellhouse and Talbot, the center of vorticity lies in the center of the aortic sinus, while in their measurements it lies just behind the tip of the open valve cusp.

In valve design, one wants the capability of predicting the flow-pattern for different valves. Consequently, a more refined mathematical technique is called for, in which the starting point is not some assumed geometry for the flow path, but simply the physics of the fluid. The equations that must be used contain derivatives with respect to both space and time: they are partial differential equations. The unknowns are not single variables but functions, giving, for example, the distribution of velocity in space instead of the velocity at a single point. In the present work we have adopted this approach, which is extraordinarily less efficient than that of the Bellhouse group but which hopefully will lead to a technique applicable to a wider range of problems and capable of answering more refined questions about the physiology and design of valves. This much has been said only to show how the present work is different and why the difference may be useful. The work of the Bellhouse group, both mathematical and experimental, is without any doubt the most important contribution to the physiology of heart valves since Leonardo.

### Flow Patterns and Artificial Valves

Wieting's apparatus:

The question may be asked: for the different types of valves in use, are the flow patterns significantly different? Do the differences suggest that knowledge of the flow pattern is crucial to understanding valve performance? These questions have been answered affirmatively by the thesis research of David Wieting. [10]

Wieting's technique consisted of mounting valves in a transparent test chamber, and of illuminating the chamber with a plane of light formed by a narrow slit. Particles suspended in the transparent fluid (a glycerol-water mixture) could be photographed. With still photography, the exposure time was chosen in such a way that the streaks left by the particles on the film were essentially instantaneous velocity vectors for the fluid at the time of the photograph. With ciné photography it was possible to follow the trajectories of individual fluid particles.

Six valve types were compared by Wieting, including a natural aortic valve obtained at autopsy. Striking differences in the flow pattern appeared even in cases where the general shape of the paths available for flow were quite similar: for example, both the caged ball and the caged disc present obstacles in midstream and force the flow to go around them. Nevertheless, when Wieting plotted the velocity profile during systole 51 mm downstream from these valves, he found that the ball valve velocity profile showed a strong dip in midstream (reaching zero flow) with strong positive peaks near the sides. The profile for the disc valve at the same location showed a strong positive peak in midstream. From the photographs it appears that the intense

vortices at the edges of the disc guide the flow back toward the center more rapidly than in the case of the ball where the vortices are larger and more diffuse. The natural valve showed an essentially flat profile at 51 mm downstream. Thus Wieting demonstrated that the disc and ball, despite a superficial similarity to each other deviated from the natural valve in opposite ways when their downstream flow patterns were compared. This kind of result illustrates the importance of studying the flow pattern in detail.

Wieting's conclusions on valve design will not be repeated here, but it is worthwhile to mention the aspects of the flow pattern that he considered important. These are the mean pressure drop across the valve, the amount of backflow, the amount of turbulence and eddy formation, the presence of regions of stasis, the distance around the valve that the flow pattern was noticeably disturbed by the presence of the valve, and the maximum shear stress. It is an open question how to rank these factors with regard to their importance to the patient, but significant differences did appear among the valve types. If the natural aortic valve is taken as a standard, Wieting reports, it has low pressure drops, no turbulence, no stasis, little backflow (probably none: but a certain amount of flow is required to balloon the compliant cusps and this gives the appearance of backflow), and a remarkably undisturbed flow pattern.

One important limitation of Wieting's technique is its inability to measure flows which do not lie in a plane. This limitation is inherent in the use of slit lighting. If a particle suspended in the fluid has a significant component of velocity perpendicular to the plane of light, its trace on the film is not its velocity vector. In fact, it is not even the component of velocity parallel to the plane

of light. This point is illustrated in Fig. (3-10).

Consider a particle which has a component of velocity  $v_1$  perpendicular to the plane of the slit. If the particle is in the slit at any time during the exposure it will appear on the film. Call the left-hand edge of the slit  $x=0$  and the right-hand edge  $x=d$ . Let the exposure time be  $\delta t$ . The particle appears on the film if its initial position is anywhere in the interval  $(-v_1 \delta t, d)$ . This interval has length  $d+v_1 \delta t$ . On the other hand, the particle crosses an edge of the slit (and therefore gives an incorrect result) if its initial position is in either of the intervals  $(-v_1 \delta t, 0)$  or  $(d-v_1 \delta t, d)$ . The combined length of these two intervals is  $2v_1 \delta t$ . Thus, the chance that a particle on the film is giving an incorrect result is

$$\frac{2 v_1 \delta t}{d + v_1 \delta t} \quad (3-7)$$

Note that the probability is 1 when  $v_1 \delta t = d$ . For  $v_1 \delta t > d$  the above arguments break down but the probability remains 1. Thus, the requirement for the reliability of the method is

$$v_1 \delta t \ll d \quad (3-8)$$

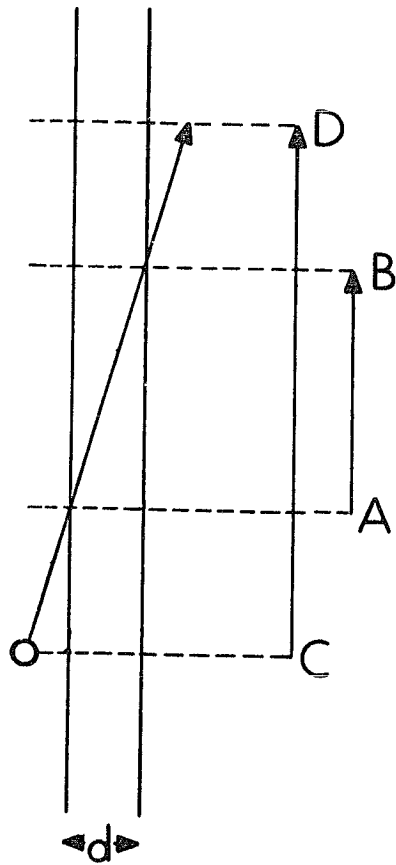
Another way to state this is to let

$$\theta = \frac{v_1}{v} \quad (3-9)$$

Where  $v$  is the velocity of the particle parallel to the slit. Then the reliability requirement becomes

$$\theta \ll \frac{d}{v \delta t} \quad (3-10)$$

Fig. (3-10)      When a particle crosses the slit during a single exposure, it appears to have a velocity component parallel to the slit given by AB. But this is actually too small; the correct velocity component parallel to the slit is CD.



In short, the flow must be very nearly parallel to the plane of the light if reliable observations are to be made by Wieting's method.

### Three-Dimensional Generalization of Wieting's Apparatus

To overcome the limitations described above, the present author began this thesis research by designing an apparatus<sup>A</sup> which may be thought of as a three-dimensional generalization of Wieting's. The valve is mounted in a test chamber much like Wieting's, but the chamber is illuminated from the ends, and all of the chamber is illuminated. Two mutually perpendicular views of this chamber are then photographed from the sides simultaneously by a single ciné camera. This is made possible by the arrangement of mirrors shown in cross-section in Fig. (3-11), which bring the two views side by side on a single piece of film. The resulting image on the film has the configuration shown in Fig. (3-12).

Each particle suspended in the fluid appears as a pair of white dots. The members of the pair have the same z-coordinate, and this is how they are identified as belonging to the same physical particle. If two physical particles have exactly the same z-coordinate four points of light appear on the film at that z-coordinate and ambiguity results as to how to identify them into pairs. However, the ambiguity might be removable by looking at the next frame in time or the previous frame where the particles may well have had different z-coordinates. The analysis is easiest when the density of particles is low. In any case, each pair of image points that share a z-coordinate determines the x, y, and z coordinates of one particle suspended in the fluid. By following such coordinates from frame to frame one builds up a list of trajectories of fluid particles. Of course, such a list only gives

Fig. (3-11)      Optical system that brings two perpendicular views of the test chamber side by side on a single piece of film. The Z axis is perpendicular to the plane of this figure.



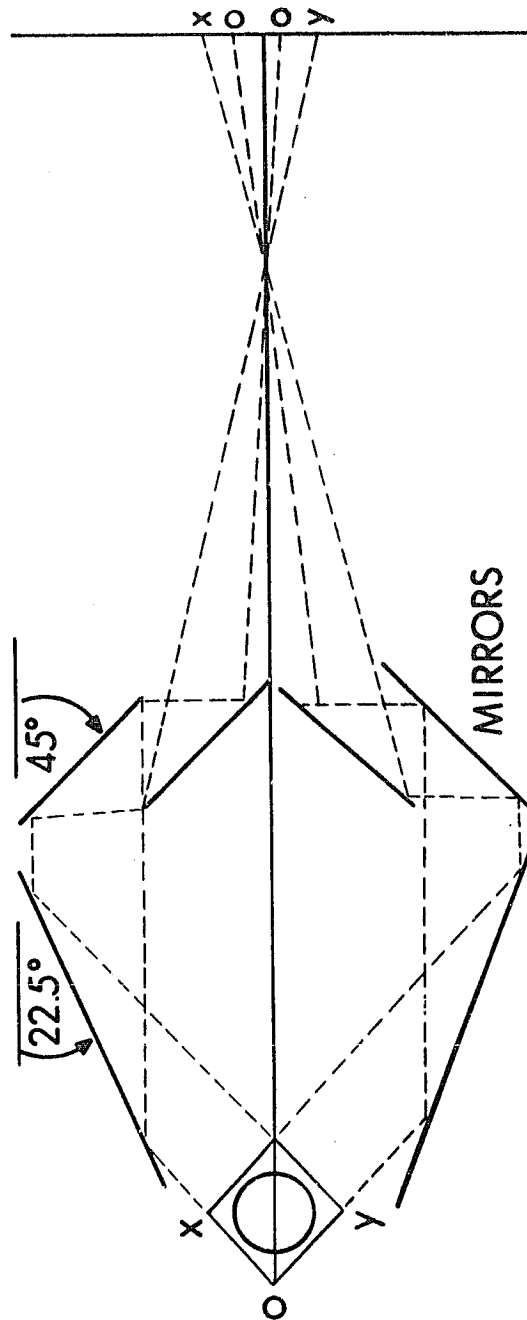
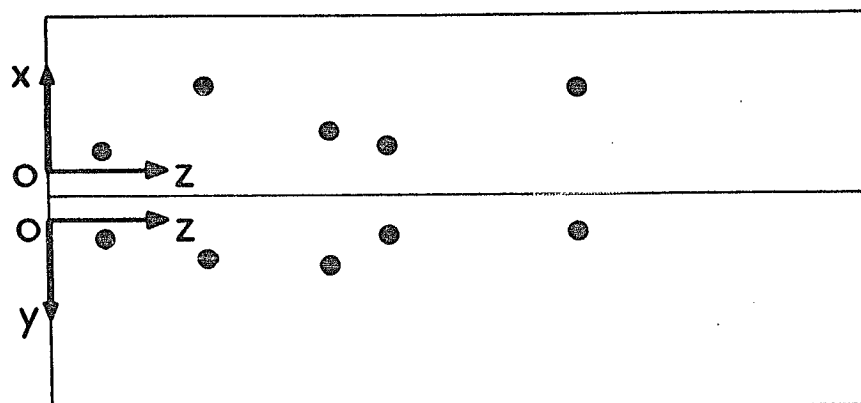


Fig. (3-12)       Images of suspended particles  
produced by the optical system of Fig. (3-11).  
Each particle appears as two dots which have a  
Z-coordinate in common.



information about the flow pattern at those points of space and time where a suspended particle happened to be. The resolution can be made arbitrarily fine, however, by looking at the flow over many cycles. In fact, if the flow has some statistical character, the distribution of velocity at each point  $x, y, z, t$  can be measured.

This apparatus has actually been constructed from the author's plans and successful high quality ciné films of an eccentric monocusp valve have been taken at 64 frames/sec. To avoid parallax effects, a telephoto lens was used, enabling the ciné camera to be further away from the test chamber.

Remark: One might make the mistake of thinking that the enlargement due to the telephoto exactly cancels the greater distance so that nothing is gained, but this is not the case. To see what is involved here, consider Fig. (3-13). With the notation indicated in Fig. (3-13), we have:

$$\frac{D}{R} = \frac{D'}{f} \quad (3-11)$$

So that

$$\frac{D'}{D} = \frac{f}{R} \quad (3-12)$$

Similarly

$$\frac{e'}{e} = \frac{f}{R} \quad (3-13)$$

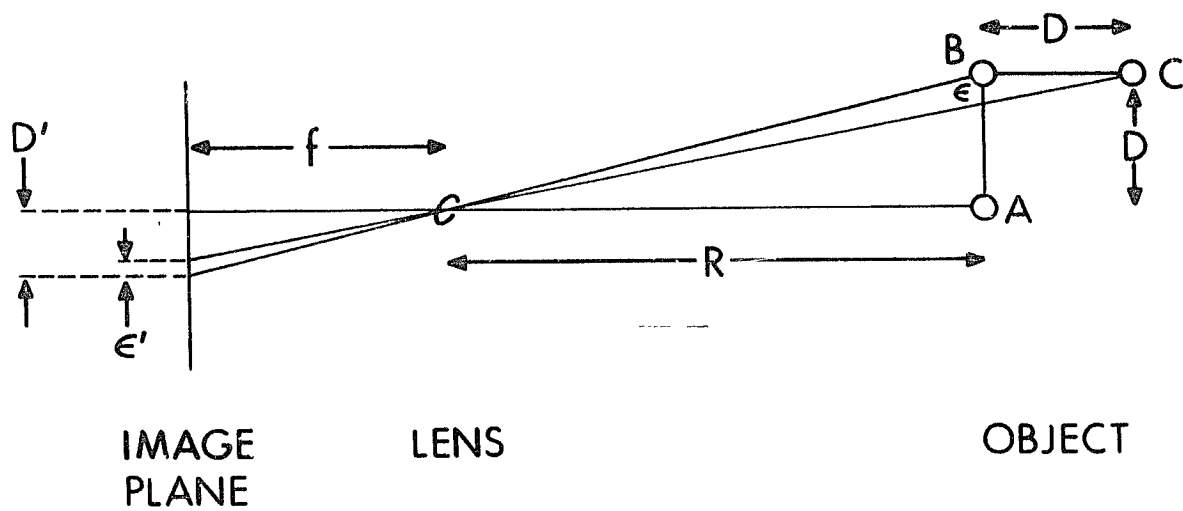
But

$$\frac{e}{D} = \frac{D}{R} \quad (3-14)$$

So that

$$e' = f \frac{D^2}{R^2} = \left(\frac{f}{R}\right) D \left(\frac{D}{R}\right) \quad (3-15)$$

Fig. (3-13)      Notation for the analysis of parallax effects. Points B and C lie behind each other and their images ought to be at the same point on the film. In fact, the images are separated by distance  $e'$ .



Thus, if  $f/R$  is held constant the images of two points which are side by side in space remain a constant distance apart on the film. But two points which are behind each other have images on the film which approach each other as  $R$  is increased, even though  $f/R$  remains constant. Thus long focal length lenses at large distances give the same size image with less parallax, a fact well known to photographers.

The successful reconstruction of the flow pattern from such a film requires a fairly sophisticated data reduction technique which we have not yet developed. There are two difficulties: first, to physically read the frames of film into a computer memory in some form, and then to write a program that would reduce the frames of film to particle trajectories and reconstruct the flow pattern by differentiating these particle trajectories. Apparatus<sup>Q</sup> for performing the first task is available in at least one computer center [11], and programs to perform the latter could certainly be written, but this represents a major piece of work which is hereby bequeathed to anyone interested.

In summary, we have successfully developed the means of measuring three-dimensional flow patterns around heart valves in vitro, but we have not yet developed the means of putting the data in a useable form. This technique is a direct descendent of Wieting's, the only thing new being the optics, which is important because it makes three dimensional measurements possible. This technique should not be thought of as a main result of the present thesis, but, rather, as a promising but unfinished by-product.

### Pressure-Flow Relations for Heart Valves

This section reviews a different body of work on heart valves. This work is characterized by the prominent place given to two variables: the pressure difference across the valve and the net flow (volume per unit time) through the opening guarded by the valve. There is no doubt that these variables are important to the patient. The integral of the flow over a heart beat gives the stroke volume of the heart, which, multiplied by heart rate, gives the cardiac output. Pressure disturbances due to valve malfunction may cause chronic changes in the heart and lungs. Such considerations lead to a simple criterion for evaluating heart valves. Worse valves require more pressure difference to drive the same flow.

The typical experiment for evaluating a valve in this way is to insert a pressure catheter on each side of the valve and to measure the flow through the valve ring with an electromagnetic flow meter. Such measurements have been made by Spencer and Greiss [12] for the aortic valve, and for the mitral valve by Nolan, et al [13] and by Yellin, et al [14,15]. All of these workers recorded instantaneous pressures and flows. Their results demonstrated at once the importance of fluid inertia, since peak flow occurred after peak pressure difference and forward flow continued for a time even against an adverse pressure difference.

It is an important point that the inertia demonstrated in these experiments is that of the fluid and not that of the valve itself. In the case of the natural valve this is obvious, the leaflets being too thin to have any significant mass with respect to blood. In the case of artificial valves, Frater, et al [1] have ruled out the



mass of the occluder as a significant factor by systematically varying the mass and observing substantially unchanged pressure and flow records. In practice, the occluders of artificial valves are made neutrally buoyant.

On the other hand, inertia is not the only factor that limits forward flow. If it were, one would expect that under conditions of zero pressure difference the flow would remain constant. The observation is that the flow decreases when the pressure difference is zero. This indicates that a dissipative process is at work. Yellin [16] has studied the nature of this dissipation in vitro by driving a sinusoidal flow through a stenosis (a narrowing in a pipe) and noting that the observed pressure difference could be resolved into two components as shown in Fig. (3-14).

Thus Yellin found that the flow  $Q$  across a stenosis was related to the pressure drop  $\Delta P$  by an equation of the form

$$\Delta P = K_1 Q|Q| + K_2 \frac{dQ}{dt} \quad (3-16)$$

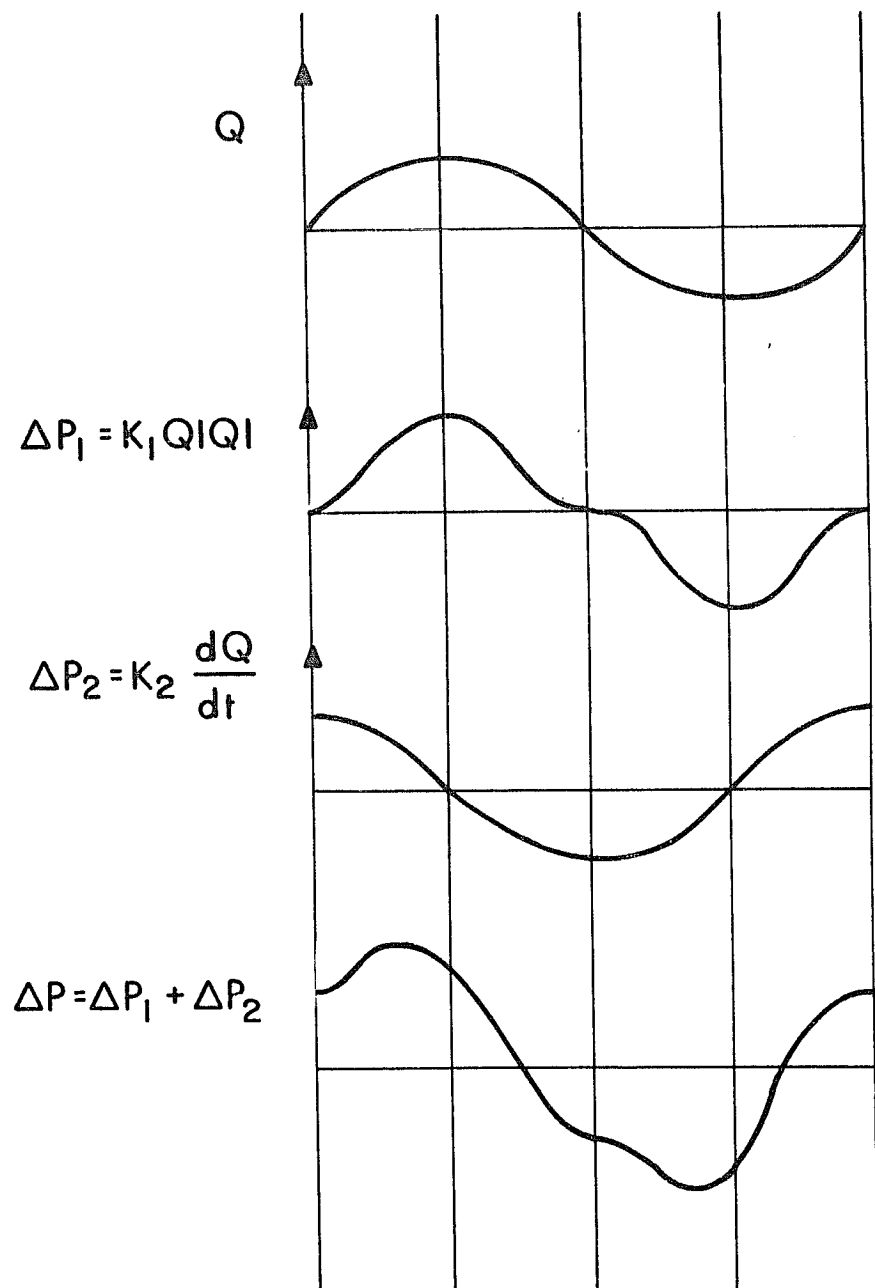
It is reasonable to assume that this equation also describes the pressure-flow relations for a valve, when the valve is open.

From the equation it is easy to predict analytically the form of  $Q$  when  $\Delta P = 0$ . For the mitral valve this condition holds at low heart rates in mid-diastole, after rapid filling, but before atrial systole. The solution is

$$Q = Q_0 \frac{1}{1 + (t/T)} \quad (3-17)$$

Where  $Q_0$  is the initial flow. To check this, and to evaluate  $T$ , substitute (3-17) in (3-16) with  $\Delta P = 0$  and  $Q > 0$  to obtain

Fig. (3-14)        Schematic of the pressure drop  $\Delta P$  obtained by Yellin when he forced a sinusoidal flow  $Q$  through a stenosis. The resolution of  $\Delta P$  into a dissipative term  $\Delta P_1$  and an inertial term  $\Delta P_2$  is shown.



$$0 = K_1 Q_0^2 \frac{1}{(1 + t/T)^2} - K_2 Q_0 \frac{1}{(1 + t/T)^2} - \frac{1}{T} \quad (3-18)$$

It follows that

$$Q_0 T = \frac{K_2}{K_1} \quad (3-19)$$

The interpretation of  $T$  is the time required for the flow to decay to  $\frac{1}{2}$  its initial value. This time depends on  $Q_0$  because of the non-linearity. To check the theory plot  $1/Q$  against time. The result should be a straight line. In practice it may be difficult to be sure that  $\Delta P = 0$  over a sufficiently long interval of time.

Equation (3-16) can also be applied to times when  $\Delta P \neq 0$  but an analytic solution is not so easy to obtain. In that case a simple analog computer becomes helpful, see below. The main features of the forward flow predicted by this equation and observed in practice are as follows.

For a competent valve the main forward flow begins at the same time as the pressure difference becomes positive, but for an incompetent valve which has backflow throughout the time when the valve ought to be closed, the onset of forward flow is delayed. In all cases peak pressure difference comes before peak flow, and zero pressure difference comes before zero flow.

Pressure-flow studies are also useful in determining the amount of backflow associated with any given valve. spurts of backflow are usually recorded around the time of valve closure by the flow meter, but these must be interpreted with care. In the case of most artificial valves such backflow is real; it represents the non-zero volume of fluid which must flow back to close the valve. This volume is reasonably constant as the heart rate varies. But the stroke volume decreases at

high heart rates. Consequently the backflow associated with the closure of an artificial valve is relatively more important at high heart rates. This point is illustrated in Fig. (3-15). In the case of natural valves the closure is almost complete by the end of forward flow, and the observed spurt of backward flow represents mostly the volume displaced by the closed leaflets as they balloon backward under the pressure load that holds them closed. In principle one can distinguish these two types of backflow from the pressure and flow records. The reason for this is that backflow due to the ballooning of a compliant valve will be returned in the forward direction as the adverse pressure difference dies away. This will result in a shoulder of forward flow that occurs before the pressure has become favorable for forward flow. True backflow will not produce this result. The point is illustrated in Fig. (3-16).

In practice it may be difficult to make such distinctions, because the flows involved are small.

Nevertheless the distinction can be made by observing the occluder or leaflet motion on a ciné film carefully timed with the pressure and flow records. This has been done by Yellin, Frater, et al. [14,15,17]

In summary, pressure-flow dynamics for the natural mitral valve can be understood in terms of the concepts of inertia, dissipation and compliance. In the case of artificial valves one has to consider also the true backflow associated with closure.

Analog simulation of pressure-flow dynamics.

That the concepts of inertia, dissipation and compliance are

Fig. (3-15)      The backflow associated with closure for an eccentric monocusp valve in the mitral position is relatively independent of heart rate. However, since the forward flow depends on heart rate, the backflow expressed as a % of forward flow is strongly rate dependent. (Data courtesy of E. Yellin)

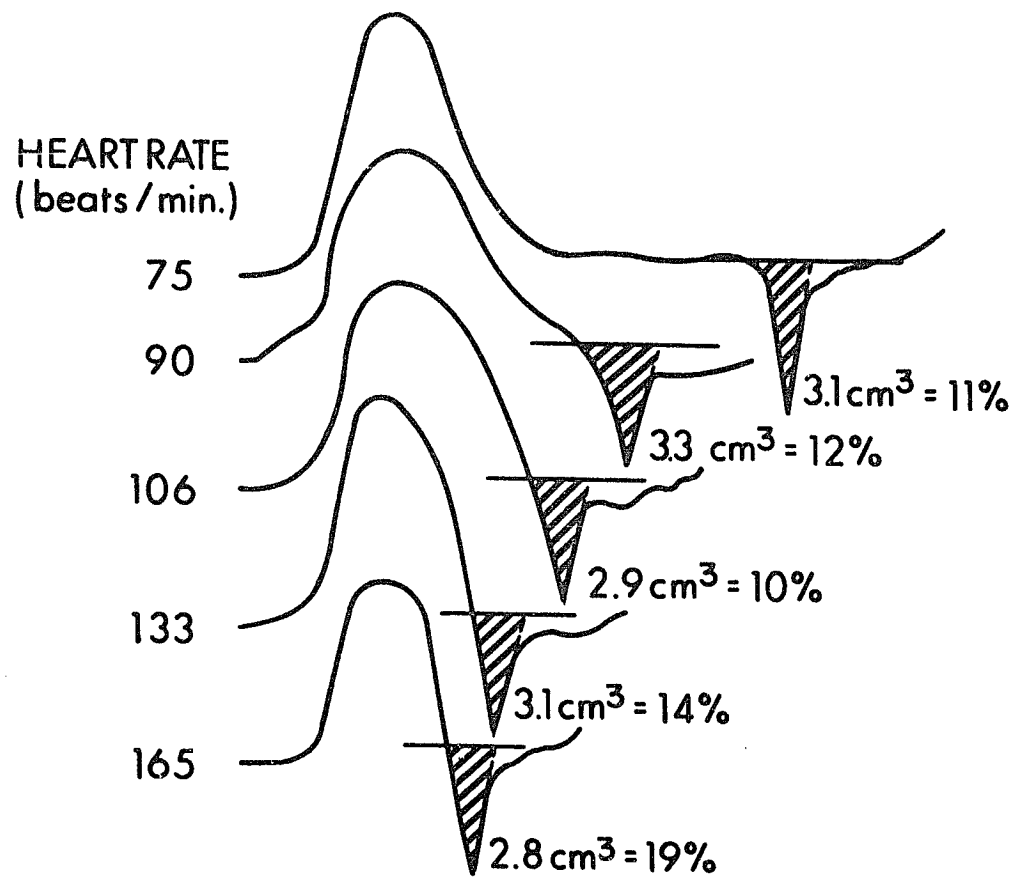
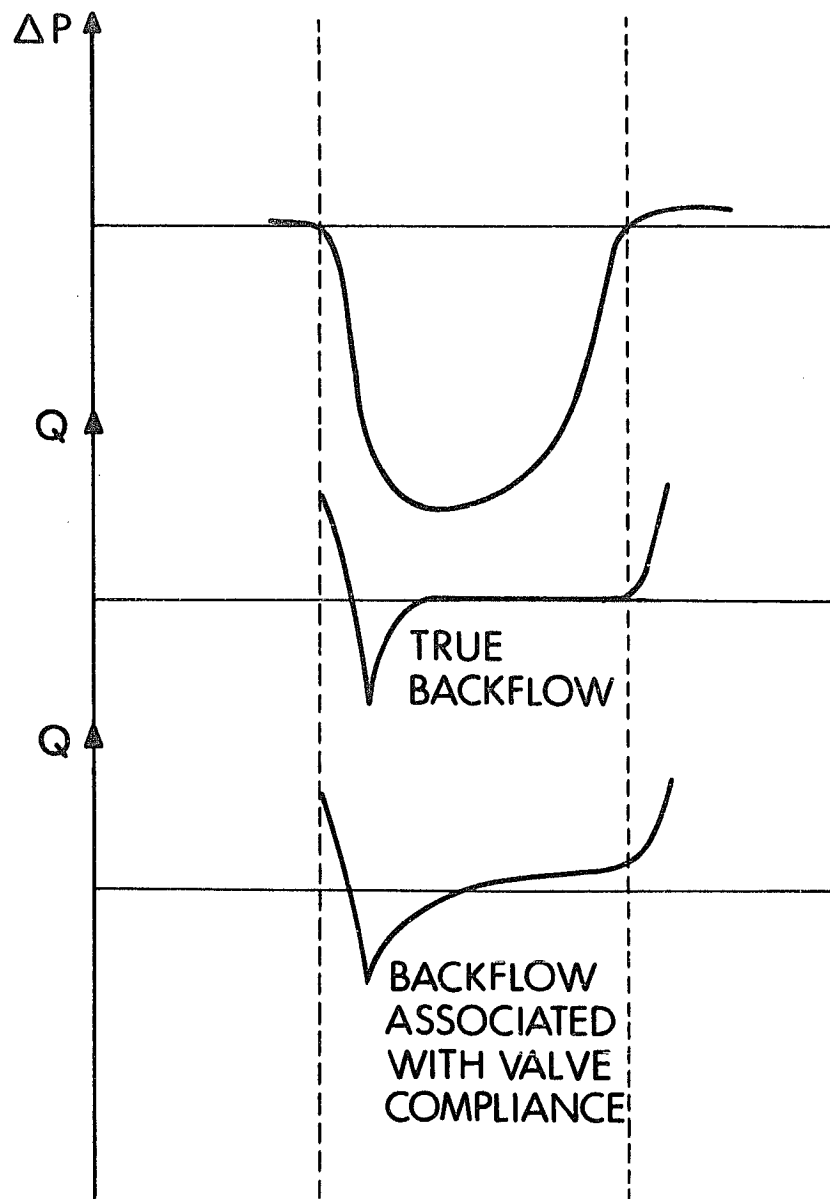


Fig. (3-16)        Schematic to indicate the difference in the flow records that one would expect between true backflow and the backflow associated with valve compliance. In the latter case the fluid is returned in the forward direction before the opening of the valve.





sufficient to account for the observed pressure-flow dynamics at the natural mitral valve has been confirmed by the present author, who constructed a simple analog circuit incorporating these principles. The aim of the circuit is to predict the flow at the mitral valve ring given the waveform of the pressure difference between atrium and ventricle.

In constructing this circuit the principle equation of motion is taken to be

$$\Delta P_T = K_1 Q \left| Q \right| + K_2 \frac{dQ}{dt} \quad (3-20)$$

where

$$\Delta P_T = \Delta P + \Delta P_V$$

$\Delta P$  = Pressure difference between atrium and ventricle

$\Delta P_V$  = Pressure exerted by the tensed valve leaflets on the fluid  
( $\Delta P_V = 0$  when the valve is open)

The term  $\Delta P_V$  is assumed proportional to the volume of fluid stored in the tensed valve leaflets. That is

$$\Delta P_V = K_3 \int_{t^*}^t (-Q) dt' \quad (3-21)$$

where  $t^*$  is the time when the flow becomes negative. Equation (3-21) holds only as long as  $\Delta P_V$  remains positive. When  $\Delta P_V$  returns to zero again the valve opens and  $\Delta P_V = 0$  until the next zero crossing of the flow. Therefore, the time  $t$  of valve opening is given by the condition

$$\int_{t^*}^t Q dt' = 0 \quad (3-22)$$

This means that the valve is assumed competent, since there is no net backflow while it is closed. On the other hand, there will be backflow at the beginning of the interval  $(t^*, t)$ , followed by forward flow at

the end. Both of these flows are small.

An equivalent circuit for these equations is shown in Fig. (3-17a). In Fig. (3-17b) a modification is shown which is more realistic in that it takes into account the visco-elastic (rather than purely elastic) nature of the papillary muscle supports of the valve.

While the circuits of Fig. (3-17) are simple, they have three drawbacks as actual devices: the need for a  $\sqrt{\quad}$  element, the difficulty of finding inductors large enough for real time operation, and the fact that the output  $Q$  appears as a current rather than a voltage. These are overcome by the operational amplifier network of Fig. (3-18), which corresponds to the more realistic circuit (3-17b). The first operational amplifier is used as an integrator to compute  $-Q$  from the forces tending to change  $Q$ . The second is used simply to invert  $-Q$  so that both  $-Q$  and  $Q$  will be available. The third represents the valve which can store fluid only when it is closed but not open. The inner feedback loop computes the dissipation, while the outer allows the tensed valve leaflet to push on the flow.

The signal  $\Delta P$  can be either a simulated waveform, or the actual pressure difference recorded from an animal experiment. To date only simulated waveforms have been used, but the qualitative features of mitral flow have been reproduced. One such qualitative feature is a low amplitude damped oscillation which appears in both the flow trace and in  $\Delta P_v$  following valve closure which, we feel, is related to the first heart sound.

In Fig. (3-19) pressure-flow records from the animal and from the analog are compared.

Fig. (3-17)      Electrical analog of a mitral valve.  $\Delta P$  is the pressure difference across the valve,  $\Delta P_V$  is the pressure exerted on the fluid by the tensed valve leaflets.  $\Delta P_T = \Delta P_V + \Delta P$ .  $Q$  is the flow. The  $\sqrt{2}$  element is defined by the current-voltage characteristic  $V = k|I|I$ . The losses in it represent losses due to eddy formation. The inductor represents fluid inertia and the capacitor represents valve compliance. (b) differs from (a) by the inclusion of viscous effects in the valve supports.

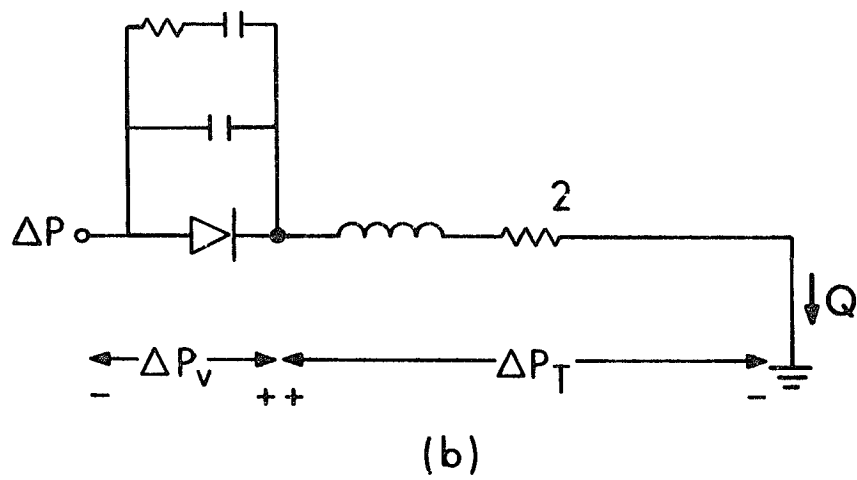
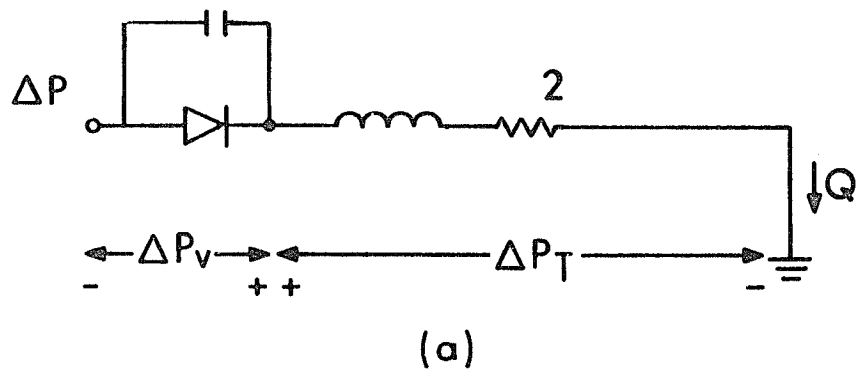


Fig. (3-18)      Operational amplifier  
realization of Fig. (3-17b).

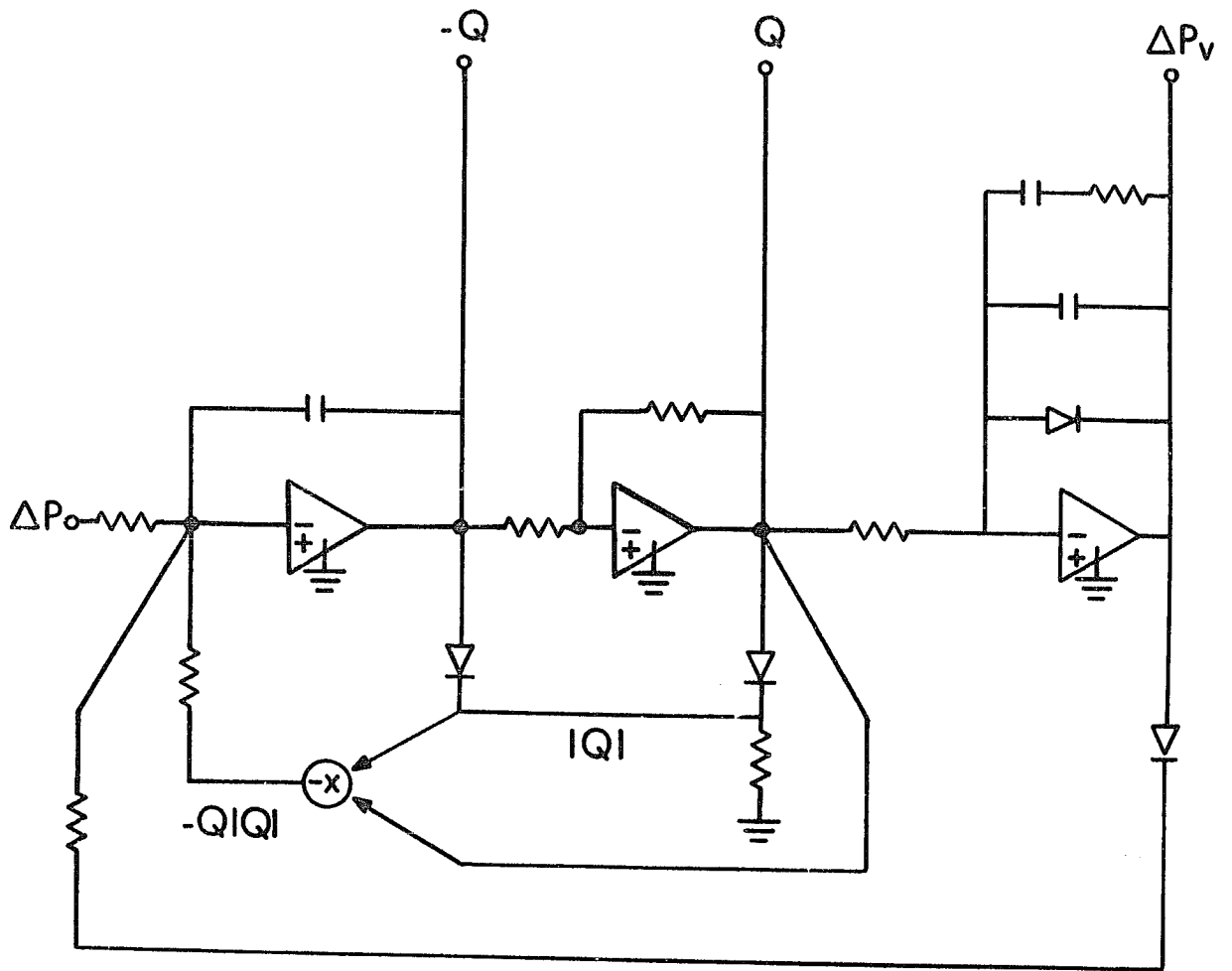
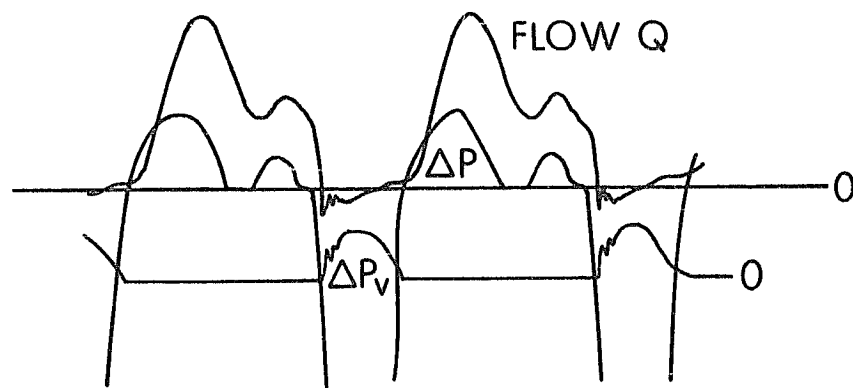
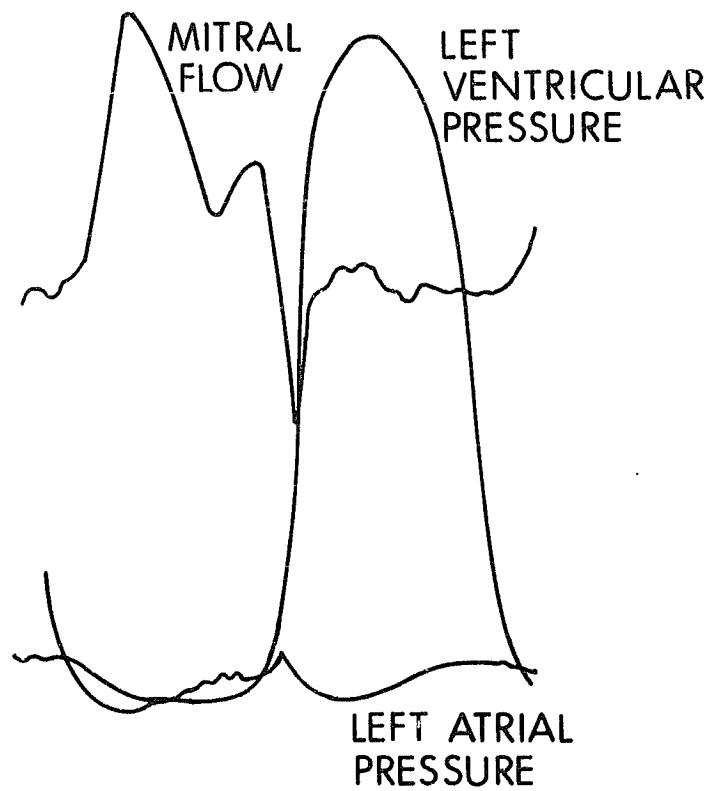


Fig. (3-19) Waveforms produced by (a) the analog circuit of Fig. (3-18) and (b) an animal experiment. In the analog we supply the waveform  $\Delta P$  which is meant to correspond to the difference between the atrial and ventricular pressures. In (a)  $\Delta P_v$  (plotted to a different scale than  $\Delta P$ ) represents the pressure exerted by the tensed valve leaflets on the fluid. This quantity was not accessible in the animal experiment.





(a)



(b)

## Numerical Integration of the Navier-Stokes Equations For Incompressible Fluid Flow

This is an enormous subject, which cannot be reviewed completely here. Only those items in the literature that have a direct relation to the present work will be considered. Some of the items discussed here are included because of their mathematical relation with the present work, while others are included because, despite the lack of a mathematical connection the authors were interested in heart valves.

At the outset it should be stated that incompressible fluid flow presents a distinctly different mathematical problem to the numerical analyst than compressible flow. The reason for this is that with compressible flow there is an upper limit to the speed at which interactions can propagate, the sound speed  $c$ . Hence if the time step taken is  $\delta t$ , the state of the fluid at the beginning of the time step influences that at the end only within a sphere of radius  $c\delta t$ . That is, all interactions are local. For an incompressible fluid the sound speed is infinite and this local character is lost.

One of the early successful approaches to the numerical solution of the Navier-Stokes equations for incompressible flow is the Marker and Cell (MAC) technique of Harlow and Welch [18]. In this technique marker particles representing points of the fluid move along a rectangular computational grid. At each time-step a pressure field is computed on the grid that is just sufficient to prevent compression of the particles.

Subsequently, A. J. Chorin [19,20] developed a method of solution in which the marker particles are not used and all of the fluid quantities are calculated on the computational grid. In Chorin's scheme each time step is divided into two main phases. In the first

phase all the fluid forces other than the pressure are allowed to act on the fluid. Because the pressure term is missing, compression of the fluid may occur. The rate of compression can be measured from the velocity field directly, so that marker particles are not needed. In the second phase a new pressure field is calculated which is just sufficient to cancel in one time step the rate of compression produced by the other forces in the first phase. This pressure field is applied and the time step is complete. An important advantage of Chorin's method is that convergence of the numerical scheme can be rigorously proved assuming only that the differential equations have a sufficiently smooth solution [20].

J. A. Vieceilli has generalized the MAC technique in such a way that the method may be applied to problems involving arbitrary external boundaries [21]. The basis of his scheme is that when marker particles attempt to cross the boundary, a pressure distribution is applied along the boundary which is just sufficient to drive the particles back. In a more recent paper [22], Vieceilli applied the same idea to problems involving moving boundaries whose motion was known in advance. In fact, he presented a calculation involving a collapsing heart-shaped bag of fluid; that is, a simulation of ventricular systole. The assumption that the motion of the boundary is known precludes the application of this technique to heart valves, however. One of the main points of the present work is to solve for the motion of the valve leaflet and thereby to gain greater understanding of the mechanisms that determine that motion.

The relation of the present work (The mathematical technique will appear in [23]) to those discussed above is the following. First,

we have used Chorin's scheme for solving the equations of motion of the fluid, but we have added an extra term that represents the influence of the immersed boundaries (like the heart valve leaflet) on the fluid. Second, we have represented such boundaries by marker particles like those of the MAC technique, so that these boundaries move with the fluid. However, these boundary markers are the only markers that we have used. (It is certainly possible in our technique to introduce marker particles into the fluid for display purposes, but they are not needed for the calculation.) Third, we have calculated the force exerted by these marker particles on the fluid from the configuration of the boundary in space. In other words we treat the boundary as an elastic structure, whose configuration determines its state of stress. Like Vieceilli, then, we represent the boundary in terms of the physical forces that it exerts on the fluid. Unlike Vieceilli, we calculate these forces from the configuration of the boundary and not from the extent to which fluid motion is violating a boundary ~~constraint~~ <sup>constraint</sup> ~~constant~~. Because of this difference we can solve problems in which the boundary motion is not known in advance. Moreover, because we use forces instead of pressures we are not limited to the case in which the force is normal to the boundary. This is important, since the tangential drag exerted by the valve leaflet on the flow is, at least in the hypothesis of Leonardo da Vinci, the source of the vorticity that helps close the valve. We could not study this hypothesis without the inclusion of tangential forces. Finally we remark that the dependence of the forces on the boundary configuration together with the fact that this configuration is not known in advance constitutes the major mathematical difficulty overcome by the present work. One cannot simply move the boundary, find the new forces, apply

them to the fluid, move the boundary again and so on ad infinitum. Instead one must solve for the motion and the forces simultaneously. This is the subject of Section VIII.

Incompressible flow calculations always involve the solution of Poisson's equation  $\nabla^2 \phi = f$  in one way or another. Until recently this has been the most time consuming part of such computations. Very fast stable direct methods are now available for solving such problems on rectangular domains. For an excellent review of the practical aspects of this subject with comparisons of the computer times and accuracy of various methods see Hockney [24]. In the present work all material boundaries are treated as immersed in fluid, and the overall domain is rectangular. Moreover, the immersed boundaries do not act as constraints but are simply the parts of the fluid where special forces are applied. Consequently, these methods are applicable and have been recently incorporated in the program with good effect. The particular method used is due to O. Widlund who has reviewed the mathematical aspects of numerical methods for Poisson-like equations [25].

To the author's knowledge there has been no previous calculation of the motion of a flexible leaflet of a natural heart valve, which takes as its starting point the full partial differential equations of fluid motion. However, different numerical techniques for these equations have been applied to various representations of artificial valves. Two workers in this field are Tin Kan Hung [26] and Greenfield, et al [27].

#### IV. THE COMPARATIVE FLUID DYNAMICS OF MAMMALIAN HEARTS †

Mammalian hearts are approximately scale models of each other [28]. That is, their geometries are roughly the same, except for scale, and it is reasonable to assume that the motions of their walls are about the same except for scale. The purpose of this section is to see what can be learned about the character of the flow patterns in different mammalian hearts from such considerations.

If the hearts are geometrically similar, all of their geometric aspects are functions of some typical length  $L$ , such as the length of the ventricular cavity. All lengths are proportional to  $L$ , all areas to  $L^2$ , and all volumes to  $L^3$ . Weights are also proportional to  $L^3$ , if the density is constant, which is a reasonable assumption. In Fig. (4-1) we plot heart weight vs. length of the ventricular cavity on a log-log scale, for various mammals. The data are taken from [28]. If the hearts are geometrically similar with constant density, the result should be a straight line with slope 3, and this is confirmed.

To set the scale of time for the motion we introduce the parameter  $T$ , the period of a heartbeat, which is the reciprocal of heart rate. In Fig. (4-2) we plot heart rate vs. heart weight on a log-log scale. The slope is approximately  $-1/3$ , which indicates that  $L \propto T$ . This result has several interesting consequences, any one of which may be thought of as the "reason" why  $L \propto T$ .

a. Velocity has dimensions of  $L/T$ . Therefore, the velocity

† This section grew out of a discussion with T. MacMahon of Harvard. One of his interests is the consideration of corresponding systems in different animals as scale models of each other. MacMahon pointed out one of the main results, that blood pressure is independent of the size of the cardiovascular system, and he said that this could be understood in terms of wall stress in the heart and blood vessels.

Fig. (4-1)      Log heart weight vs. log length  
of left ventricular cavity in various mammals.  
Data from [28]. If the hearts are geometrically  
similar and of the same density, we anticipate  
a slope of 3. This is confirmed.

2400

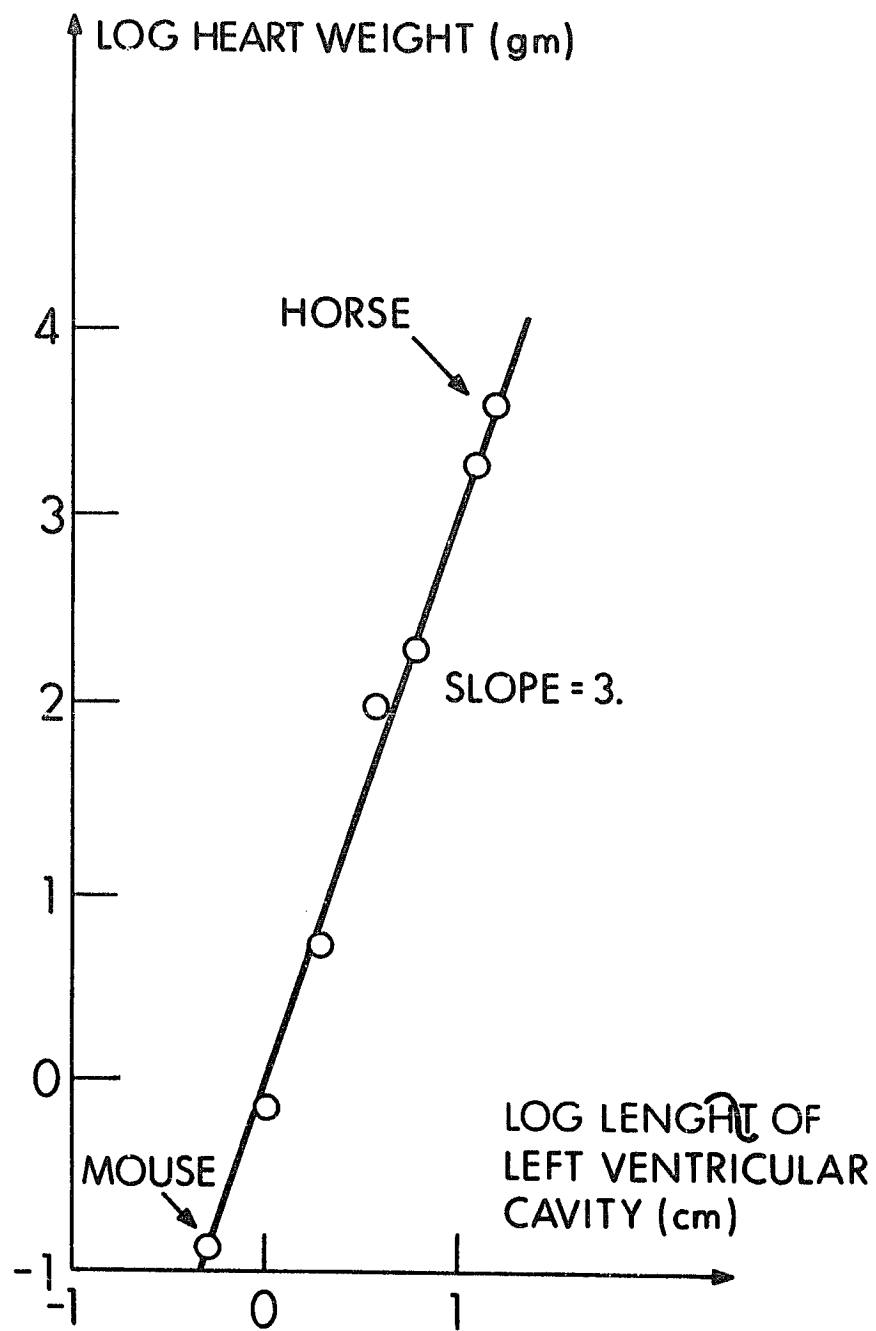
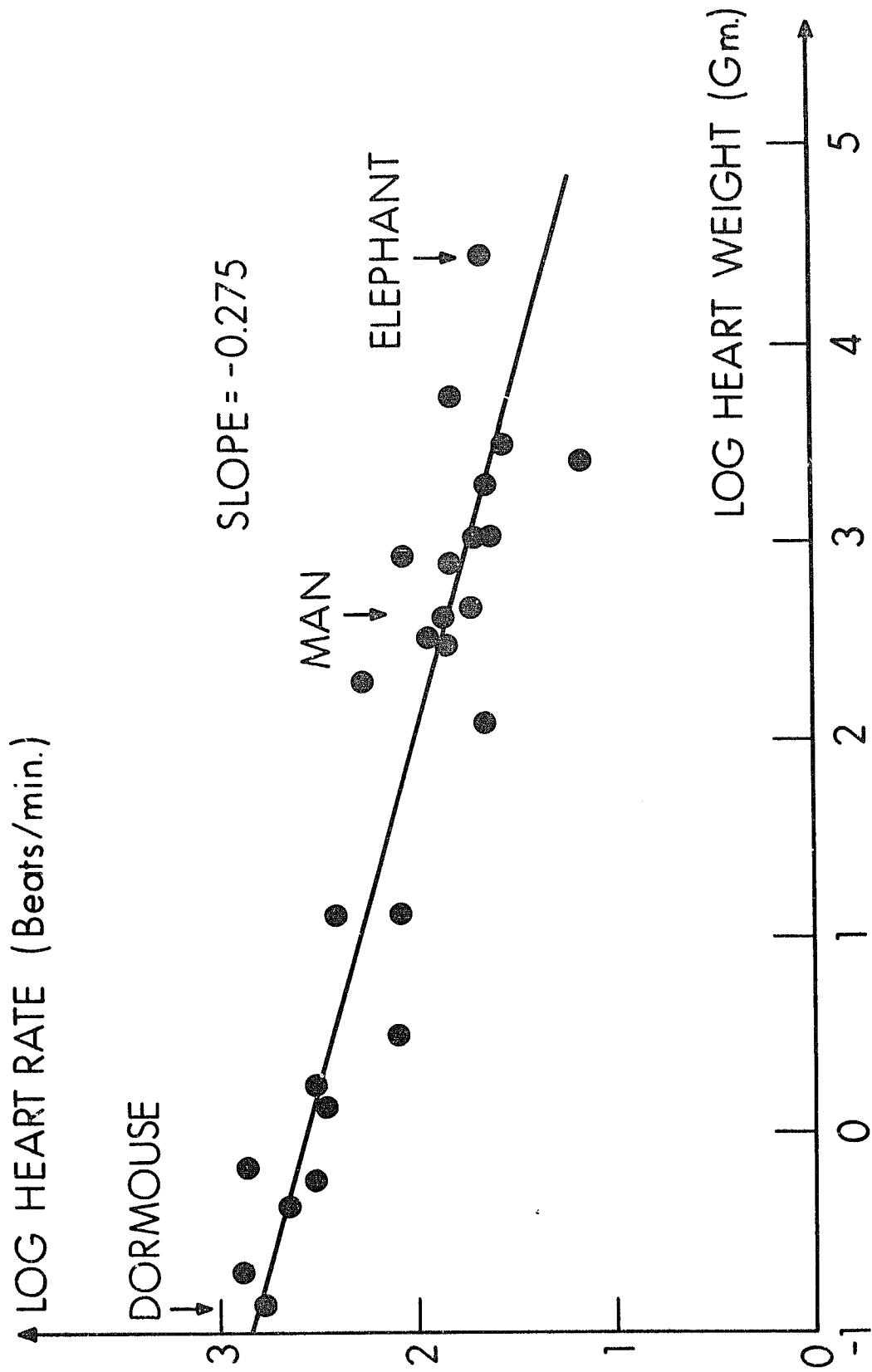




Fig. (4-2)      Log heart rate vs. log heart  
weight for various mammals. The slope is roughly  
 $-1/3$  which indicates that length is approximately  
proportional to the period of the heart beat.  
The data are from [ 29].



of blood at corresponding points in the hearts of different mammals should be independent of heart size. (Strictly speaking this holds only outside the boundary layer, see below.)

b. Pressure has dimensions of  $\rho L^2/T^2$ , where  $\rho$  is the density. Therefore, pressures at corresponding points will also be independent of heart size, as the density of blood is the same in all cases. Similarly, stress in the wall has the same dimensions as pressure and will also be independent of heart size.

c. Cardiac Output = Stroke Volume x Heart Rate  $\propto L^3/T \propto L^2$

Thus cardiac output should depend on  $L^2$  or on area. Now the ratio of heart weight to body weight shows no significant trend with heart size [28]. This suggests that area in the heart and body surface area also have a ratio which is independent of heart size. On the average, then, cardiac output is proportional to body surface area, an index of metabolic rate.

It is useful at this point to introduce the dimensionless quantity

$$R = \frac{L^2}{\nu T} \quad (4-1)$$

where  $\nu$  is the kinematic viscosity  $\nu = \eta/\rho$ . Since  $L \propto T$  and  $\nu$  is constant,  $R \propto L$ .

To see the importance of  $R$ , one can non-dimensionalize the Navier-Stokes equations (see Section V) by introducing variables

$$\underline{x}' = \underline{x}/L \quad t' = t/T \quad \underline{u}' = \underline{u}/(L/T) \quad p' = \underline{p}/(\rho(L^2/T^2)) \quad (4-2)$$

the resulting equations are

$$\frac{\partial \underline{u}'}{\partial t'} + (\underline{u}' \cdot \nabla) \underline{u}' = -\nabla p' + \frac{1}{R} \nabla^2 \underline{u}' \quad (4-3)$$

$$\nabla \cdot \underline{u}' = 0$$

Where the  $\nabla$  indicates derivatives with respect to  $x'$ ,  $y'$ ,  $z'$ .

With given dimensionless boundary conditions, there is a dimensionless solution of this problem for each  $R$ , and each such solution generates a whole family of physical solutions formed from the dimensionless solution by fixing  $L$  and  $T$  in such a way that  $R = L^2 / \nu T$ . All the physical solutions corresponding to a given  $R$  are the same except for scale.

Mammalian hearts, however, do not share the same  $R$  (as shown above, for mammalian hearts  $R \propto L$ ) and therefore their flow patterns are not strictly similar. The qualitative nature of the differences will be discussed below.

To study the physical meaning of  $R$  consider the following instructive example:

An infinite plane wall suddenly begins moving parallel to itself with velocity  $U_0$  at  $t=0$ . Let  $u(z, t)$  be the velocity of the fluid parallel to the motion of the plane at the distance  $z$  from the plane. For this case the Navier-Stokes equations reduce to

$$\frac{\partial u}{\partial t} = \frac{\partial^2 u}{\partial z^2} \quad (4-4)$$

$$u(0, t) = U_0$$

$$u(z, 0) = 0$$

This is equivalent to a one-dimensional heat conduction problem. It has a solution

$$u = U_0 \left( 1 - \left( \frac{2}{\pi} \right)^{1/2} \int_0^{\theta/\sqrt{2}} e^{-(1/2)x^2} dx \right) \quad (4-5)$$

where

$$\theta = (z^2 / \nu t)^{1/2}$$

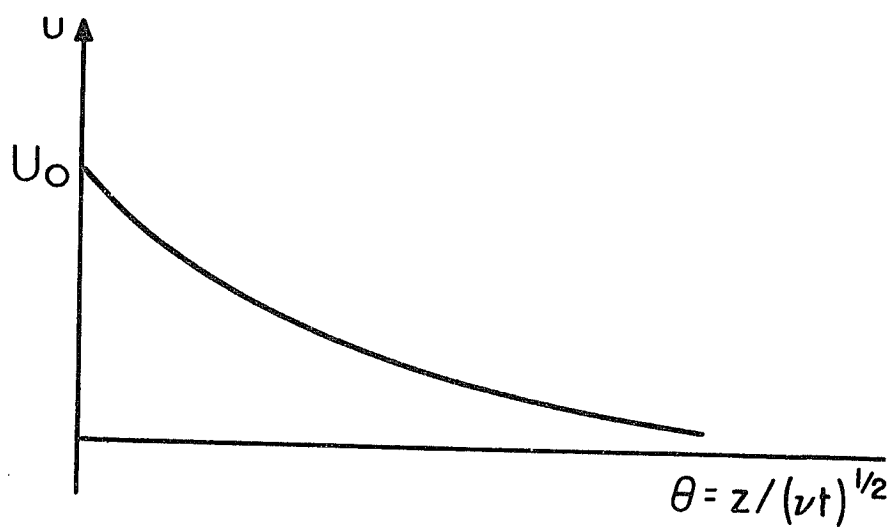
The important point is that  $u$  depends on  $z$  and  $t$  only through the combination  $z^2 / \nu t$ .

A plot of  $u$  vs.  $\theta$  is given in Fig. (4-3).

Thus, the shape of the velocity profile is the same for all  $t$ , only the scale changes with time. The influence of the moving wall is small for large  $\theta$  and it is reasonable to pick some particular value of  $\theta$  say  $\theta = 1$ , and call this the depth of penetration of the influence of the moving wall. That is, at time  $t$ ,  $z = (\nu t)^{1/2}$  gives the thickness of the layer of fluid that has been significantly affected by the shearing action <sup>of the</sup> moving wall. This layer is called the boundary layer. (The choice  $\theta = 1$  is clearly arbitrary, as the influence of the wall extends to infinity. At  $\theta = 1$ ,  $u/U_0 = 0.48$ ).

In the case of the heart, if  $T$  is the period of a heartbeat, we may say that the maximum thickness of the boundary layer is given by  $z$  where  $z^2 = \nu T$ . But we already have

Fig. (4-3)      Velocity profile near a plane wall which began moving with velocity  $U_0$  parallel to itself at  $t = 0$ . The distance from the wall is  $z$ . The shape of the velocity profile is independent of time, but the scale changes according to  $(\nu t)^{1/2}$ .



$$L^2 = \nu TR$$

so that  $(z/L) = R^{-1/2}$ . Thus, the relative depth of penetration of the influence of the shearing action of the walls is determined by  $R$ . At distances large compared to  $z$ , the flow pattern is not appreciably influenced by the shearing action of the walls and for such interior points we anticipate approximate similarity of the flow patterns for different mammalian hearts.

Since  $R \propto L$ ,  $(z/L) \propto L^{-1/2}$  and small mammals have relatively thick boundary layers. From Fig. (4-2) it is clear that the range of heart weights is nearly 6 log units from the dormouse to the elephant. Therefore, the range of heart lengths is nearly 2 log units and the relative thickness of the boundary layer spans a range of 1 log unit or 10:1.

To the extent that these different hearts appear to be designed according to the same plan, this suggests that the thickness of the boundary layer is not a crucial design parameter.



## V. EQUATIONS OF MOTION

### Description

There are two equivalent ways to describe the motion of a fluid. The first (Lagrangian) is to label the individual particles of fluid in some way, for example, by their position in space at  $t = 0$ , and then to give the motion of all of these particles. The second method (Eulerian) is to state a velocity field  $\underline{u}(\underline{x}, t)$  which gives at time  $t$  the velocity of the fluid particle which happens to lie at the point  $\underline{x}$  in space.

The acceleration of a fluid particle in the Lagrangian description is simply  $\frac{d^2 \underline{x}}{dt^2}$ , while in the Eulerian description it is a more complicated expression. To find it, note that

$$\delta \underline{u} = \frac{\partial \underline{u}}{\partial x} \delta x + \frac{\partial \underline{u}}{\partial y} \delta y + \frac{\partial \underline{u}}{\partial z} \delta z + \frac{\partial \underline{u}}{\partial t} \delta t \quad (5-1)$$

and hence

$$\frac{\delta \underline{u}}{\delta t} = \frac{\partial \underline{u}}{\partial x} \frac{\delta x}{\delta t} + \frac{\partial \underline{u}}{\partial y} \frac{\delta y}{\delta t} + \frac{\partial \underline{u}}{\partial z} \frac{\delta z}{\delta t} + \frac{\partial \underline{u}}{\partial t} \quad (5-2)$$

The foregoing holds for arbitrary increments  $\delta x$ ,  $\delta y$ ,  $\delta z$ ,  $\delta t$ . One can then specialize to the case where the increments are those of a fluid particle. That is

$$\frac{\delta x}{\delta t} = u_x \quad \frac{\delta y}{\delta t} = u_y \quad \frac{\delta z}{\delta t} = u_z \quad (5-3)$$

The notation for the derivative with respect to time computed following a fluid particle is  $\frac{D}{Dt}$ . Thus

$$\begin{aligned}
 \frac{Du}{Dt} &= u_x \frac{\partial u}{\partial x} + u_y \frac{\partial u}{\partial y} + u_z \frac{\partial u}{\partial z} + \frac{\partial u}{\partial t} \\
 &= (\underline{u} \cdot \nabla) \underline{u} + \frac{\partial \underline{u}}{\partial t}
 \end{aligned}
 \tag{5-4}$$

Because the description of the acceleration is so much simpler in the Lagrangian notation, one might think that the Lagrangian representation would be the preferred description for computational purposes. In fact, however, the reverse is true. To understand why, it is necessary to recall that in the Lagrangian representation fluid particles are labeled according to their positions at  $t = 0$ . However, as time evolves particles which were initially close together may become far apart. A rectangular mesh in the fluid becomes progressively distorted if it is allowed to move with the fluid, and spatial derivatives become more and more difficult to calculate. For this reason, the Lagrangian description is not often used. There are exceptions: suppose the fluid motion is periodic in the sense that the individual particles of fluid return after time  $T$  to their initial positions. Then the progressive distortion described above does not occur and a Lagrangian calculation becomes practical. Such is the case for a wave sloshing back and forth in a trough, and a Lagrangian calculation has been done for this problem [30]. It is not the case for the heart, where despite the periodicity of the motion of the walls, the trajectories of the particles of blood are certainly not closed. Indeed, the particles enter the ventricles through one set of valves and leave by another. On the other hand, the Eulerian velocity field for blood in the heart is periodic with the period of

a heartbeat. That is, at each fixed point in space the velocity vector returns after one heartbeat to the value it had at the beginning of that heartbeat, despite the fact that at the end of the heartbeat it is a different particle of blood which occupies the fixed point in space than at the beginning. By contrast, if we consider a point on a valve leaflet or on the heart wall it is in fact the same material point that returns to the same point in space after a heartbeat. Moreover in the case of valves or heart wall it is important to know where the material points are in space at any instant, since these data enter into the computation of the forces exerted by the wall or valve on the fluid. In the fluid itself it is of no importance which material particle is where; all that matters is the spatial distribution of the motion. For these reasons it is appropriate to describe the motion of the fluid in Eulerian form and the motion of heart apparatus in Lagrangian form.

Incompressibility is described as follows: over any closed surface, at any instant of time, the total flux out of the surface is zero. That is

$$\iint_S (\underline{u} \cdot \underline{\hat{n}}) da = 0 \quad (5-5)$$

Where  $\underline{\hat{n}}$  is the outward unit vector normal to the closed surface  $S$  with area element  $da$ . Applying this condition to a small cube one can conclude that

$$\nabla \cdot \underline{u} = 0 \quad (5-6)$$

where

$$\nabla \cdot \underline{u} = \frac{\partial u_x}{\partial x} + \frac{\partial u_y}{\partial y} + \frac{\partial u_z}{\partial z} \quad (5-7)$$

This condition plays a central role in determining the character of the motion. The following considerations are important in understanding that role.

Let  $\underline{w}$  be any vector field. Then it is possible to decompose  $\underline{w}$  as follows:

$$\begin{aligned}\underline{w} &= \underline{u} + \nabla\varphi \\ \text{where} \quad \nabla \cdot \underline{u} &= 0\end{aligned}\tag{5-8}$$

One need only let  $\varphi$  be a solution of Poisson's equation

$$\nabla^2\varphi = \nabla \cdot \underline{w}\tag{5-9}$$

and then set

$$\underline{u} = \underline{w} - \nabla\varphi\tag{5-10}$$

so that

$$\nabla \cdot \underline{u} = \nabla \cdot \underline{w} - \nabla^2\varphi = 0\tag{5-11}$$

as desired.

The decomposition (5-8) is unique if the scalar  $\varphi$  is uniquely determined by (5-9). To insure this we must apply some boundary condition, for example, that  $\underline{u}$ ,  $\underline{w}$ ,  $\varphi$  are periodic in space with period 1 in each coordinate direction.

When some boundary conditions have been supplied such that (5-8) uniquely determines  $\underline{u}$ , then one may write

$$\underline{u} = \mathcal{P}\underline{w}\tag{5-12}$$

where  $\mathcal{P}$  is a linear operator, which, we may say, extracts the divergence-free part of  $\underline{w}$ .

Two evident properties of  $\mathcal{P}$  are:

$$\begin{aligned}\text{If } \nabla \cdot \underline{u} &= 0, \quad \mathcal{P}\underline{u} = \underline{u} \\ \text{If } \underline{w} &= \nabla\varphi, \quad \mathcal{P}\underline{w} = 0\end{aligned}\tag{5-13}$$

The significance of this operator to the present work is as follows. Let a system of force density,  $\underline{F}$ , act in the fluid. Then the quantity that actually influences the fluid motion is

$$\rho \underline{F} = \underline{F} - \nabla \varphi \quad (5-14)$$

where

$$\nabla^2 \varphi = \nabla \cdot \underline{F} \quad (5-15)$$

Now  $\underline{F}$  may be non-zero in only a small region, but  $\varphi$  is non-zero throughout the fluid (other than at exceptional points). This expresses the fact that in an incompressible fluid even localized forces are felt throughout, instantaneously.

### Navier-Stokes Equations

The equations of motion of a viscous incompressible fluid are

$$\rho \frac{D\mathbf{u}}{Dt} = \rho \left[ \frac{\partial \mathbf{u}}{\partial t} + (\mathbf{u} \cdot \nabla) \mathbf{u} \right] = -\nabla p + \eta \nabla^2 \mathbf{u} + \mathbf{F} \quad (5-16)$$

$$\nabla \cdot \mathbf{u} = 0$$

In these equations  $\rho$  is the density of the fluid and  $\eta$  is the viscosity. The scalar  $p$  is the pressure, and  $\mathbf{u}$  is the velocity vector.  $\mathbf{F}$  is the density of external force applied to the fluid, that is, the external force per unit volume. By external force we mean any force acting on the fluid which does not arise in the fluid itself. In particular the heart wall and valves exert external forces on the fluid. The first equation in the pair (5-16) expresses Newton's law that mass times acceleration equals force. In (5-16) however, each term of Newton's law is divided by volume so that on the left hand side we have the density of mass times acceleration, while on the right hand side we have the densities of the various forces that may act on a fluid. These force densities are the pressure gradient,  $-\nabla p$ , the force density due to thermal diffusion of momentum  $\eta \nabla^2 \mathbf{u}$ , and the external force density  $\mathbf{F}$ . The second equation in the pair (5-16) expresses the fact that the fluid is incompressible; it acts as a constraint on the motion. It will appear in the following that this constraint is enforced by the pressure field  $p$ .

Equations (5-16) can be rewritten in the following way.

$$\rho \frac{\partial \underline{u}}{\partial t} + \nabla p = -\rho (\underline{u} \cdot \nabla) \underline{u} + \eta \nabla^2 \underline{u} + \underline{F}$$

$$\nabla \cdot \left( \rho \frac{\partial \underline{u}}{\partial t} \right) = 0$$
(5-17)

Comparison of (5-17) with (5-8) shows that we may write

$$\rho \frac{\partial \underline{u}}{\partial t} = \rho (-\rho (\underline{u} \cdot \nabla) \underline{u} + \eta \nabla^2 \underline{u} + \underline{F})$$
(5-18)

Note that the pressure  $p$  in (5-17) corresponds to the scalar  $\varphi$  in (5-8) which is introduced to remove the divergence of  $\underline{w}$ . Physically, any tendency toward a change in density of the fluid is cancelled out by the pressure gradient. That is how the fluid maintains its property of incompressibility. Equation (5-18) is the starting point for the construction of a numerical scheme, as discussed in Section VI.

#### Representation of the heart apparatus

By the heart apparatus we mean all the non-fluid parts of the heart, including the muscular walls, the valve leaflets, and any parts of artificial valves that may be present. Since these material structures bound the fluid we shall refer to them collectively as the boundary  $B$ .

In this work the heart apparatus or boundary will be regarded as a specialized region of the fluid in which extra forces, the "boundary

forces" are applied to the fluid. We do not assume any additional mass in these regions. That is, we regard the heart apparatus as neutrally buoyant.

As indicated above, the heart apparatus will be described in Lagrangian form. That is, the material points of the apparatus will be labeled, and the labels retained by the material points as they move about in space. Ordinarily, in a Lagrangian representation, the labels are the coordinates of the points at some fixed time, say  $t = 0$ . One has then, a system of coordinates embedded in the material. Here we use a different procedure, based on the selection of a dense sequence of sample points of  $B$ . An important advantage of our procedure is that the notation is the same whether the "boundary"  $B$  consists of a surface, a volume, or a curve in space.

Choose an infinite sequence of material points  $P_k \in B$  such that the set  $\{P_k\}$  is dense in  $B$ . Let  $\underline{x}_k$  be the location in space of the material point  $P_k$  at some instant. Then the set  $\{\underline{x}_k\}$  completely determines the configuration of  $B$ , since  $\{P_k\}$  is dense in  $B$  and the deformations of  $B$  are continuous.

Now a region  $R$  of the fluid feels a force  $\underline{f}(R)$  due to the boundary  $B$ . We assume that this force depends on the configuration of the boundary and hence on the sequence  $\{\underline{x}_k\}$ .

The function  $\underline{f}(R)$  can also be expressed as a limit in which the representation of the boundary is gradually made finer and finer. To do this we introduce the following definitions: Let  $\{P_1 \cdots P_N\}$  be the  $N$ -point representation of the boundary and let  $\{\underline{x}_1 \cdots \underline{x}_N\}$  be the  $N$ -point configuration. Then we can construct functions

$$\underline{f}_k(N, \underline{x}_1 \cdots \underline{x}_N) \quad k = 1, 2, \cdots, N$$



such that

$$\underline{f}(R) = \lim_{N \rightarrow \infty} \sum_{\substack{k \leq N \\ \underline{x}_k \in R}} \underline{f}_k(N, \underline{x}_1 \cdots \underline{x}_N) \quad (5-19)$$

The interpretation of  $\underline{f}_k(N, \underline{x}_1 \cdots \underline{x}_N)$  is that it is the force exerted on the fluid by point  $P_k$  in the  $N$ -point representation. Accordingly,  $\underline{f}_k$  contributes to  $\underline{f}(R)$  only if  $\underline{x}_k \in R$ .

Specifying the functions  $\underline{f}_k(N, \underline{x}_1 \cdots \underline{x}_N)$  is one way to state the physical properties of the heart apparatus. Since parts of this apparatus are active (the muscle) the functions may also depend on the time explicitly, or on some set of internal parameters which change with time. Actually, for the numerical scheme one does not need the whole family of functions  $\underline{f}_k(N, \underline{x}_1 \cdots \underline{x}_N)$  but only those functions for a particular  $N$ , large but finite. It is easier to describe the construction of the functions for a particular physiological structure of interest once  $N$  has been fixed; consequently, we defer this discussion until Section VII, where it is shown that an especially simple class of functions  $\underline{f}_k$  is general enough to be used in the representation of flexible valve leaflets, rigid valve occluders and cardiac muscle.

We now transform the right-hand side of (5-19) as follows: †

$$\begin{aligned}
 \underline{f}(R) &= \lim_{N \rightarrow \infty} \sum_{\substack{k \leq N \\ \underline{x}_k \in R}} \underline{f}_k(N, \underline{x}_1 \cdots \underline{x}_N) \\
 &= \lim_{N \rightarrow \infty} \sum_{k=1}^N \underline{f}_k(N, \underline{x}_1 \cdots \underline{x}_N) \left\{ \begin{array}{ll} 1 & \underline{x}_k \in R \\ 0 & \underline{x}_k \notin R \end{array} \right\} \\
 &= \lim_{N \rightarrow \infty} \sum_{k=1}^N \underline{f}_k(N, \underline{x}_1 \cdots \underline{x}_N) \int_R \delta(\underline{x} - \underline{x}_k) d\underline{x} \\
 &= \int_R \lim_{N \rightarrow \infty} \sum_{k=1}^N \underline{f}_k(N, \underline{x}_1 \cdots \underline{x}_N) \delta(\underline{x} - \underline{x}_k) d\underline{x}
 \end{aligned} \tag{5-20}$$

†At the point where the  $\delta$ -function is introduced in this development, the operations become purely formal. The subsequent interchange of integration with the limit is similarly to be regarded as a formal operation. The force density  $\underline{F}(\underline{x})$  derived in this way, Eq. (5-22), is singular and its use to calculate the force on a region  $R$  requires a reversal of the steps used to derive Eq. (5-22). In the numerical scheme we never actually pass to the limit  $N = \infty$  in any case.

But we also have

$$\underline{f}(R) = \int_R \underline{F}(\underline{x}) d\underline{x} \quad (5-21)$$

where  $\underline{F}$  is the force-density due to the boundary.

Since the foregoing hold for all regions  $R$

$$\underline{F}(\underline{x}) = \lim_{N \rightarrow \infty} \sum_{k=1}^N \underline{f}_k(N, \underline{x}_1 \cdots \underline{x}_N) \delta(\underline{x} - \underline{x}_k) \quad (5-22)$$

Since the fluid is viscous, the equation of motion of the point  $\underline{x}_k$  of the boundary is

$$\frac{d\underline{x}_k}{dt} = \underline{u}(\underline{x}_k) = \int_{\text{fluid}} \underline{u}(\underline{x}) \delta(\underline{x} - \underline{x}_k) d\underline{x} \quad (5-23)$$

To summarize: the physical properties of the heart apparatus are described by the functions  $\underline{f}_k(N, \underline{x}_1 \cdots \underline{x}_N)$  and the connection between the apparatus and the fluid is described by equations (5-22) and (5-23). Note the appearance of the functions  $\delta(\underline{x} - \underline{x}_k)$  in each of these equations. The  $\delta$  function is important when fluid quantities are transformed into boundary quantities and vice versa. In the numerical scheme we have to construct a function which plays a similar role; see Section IX.

### Boundary conditions

In the previous section it was shown how the heart apparatus

can be represented in terms of the forces which it exerts on the fluid.

We now take the additional step of regarding the apparatus as completely immersed in fluid, so that all of its parts have fluid on both sides. In fact, this assumption is correct for the valve leaflet, and it will not make much difference to the internal flow pattern if we put fluid outside the heart, provided that the external chamber is not so constricted as to impede the normal motion of the walls.

When the heart apparatus has been immersed in fluid and represented in terms of its force field  $\underline{F}$  it disappears as a boundary in the mathematical sense. While we still have the condition  $\frac{dx}{dt} = \underline{u}(\underline{x})$  at points of the heart apparatus, this is no longer a constraint on the velocity field  $\underline{u}$ , as it would be if  $\underline{x}(t)$  were known in advance. Instead, it is an equation of motion for  $\underline{x}$ .

It remains, however, to choose some external boundary conditions. That is, the heart apparatus will be immersed in fluid, but this fluid must be of finite extent so that a numerical computation is possible. The shape of this enlarged domain and the conditions at its edges are completely at our disposal, and are chosen for mathematical convenience.

The simplest shape to choose is rectangular, with the boundaries of the domain parallel to the coordinate planes. The problem of imposing special conditions at these boundaries can be avoided by making the domain periodic in each space direction. That is, if the domain is  $0 \leq x, y, z \leq L$  we regard the plane  $x = L$  as equivalent to the plane  $x = 0$ , as though the  $x$  axis were bent around in itself into a circle of length  $L$ . The same thing is done in each of the other coordinate directions. The result is impossible to visualize

in three dimensions though the process we have just described could be done to a three dimensional manifold in some higher dimensional space. In fact, it could be done while retaining the Euclidian geometry of the manifold just as a plane rectangle can be bent into a cylinder without stretching and hence without changing the intrinsic geometry of the surface. In a computer we can do without the higher dimensional space. Let the discrete points of the  $x$ -axis be  $i = 1, 2, \dots, N$ . Then we regard the point  $N$  as adjacent to the point  $1$ , so that arithmetic on points of the domain is done in a cyclic fashion with  $N + 1 = 1$ , for example. The advantage of using a periodic domain is that it makes all points of the domain equivalent in the same sense that all points of a circle are equivalent.

An alternate description of a heart immersed in a periodic domain is derived as follows: consider an infinite cubic lattice of hearts beating in unison in an infinite fluid. To describe the state of such an array, one need only say what is going on in one cube of the lattice, and this cube is our periodic domain.

### Summary

We have a periodic domain  $D$  on which the fluid velocity field  $\underline{u}$  and the force density  $\underline{F}(\underline{x})$  is defined. Contained in  $D$  is the immersed boundary  $B$ , represented by the dense subset of points  $\{P_k\}$  with coordinates  $\{\underline{x}_k\}$ . The physical properties of  $B$  are described by the functions  $\underline{f}_k(N, \underline{x}_1 \dots \underline{x}_N)$  each of which represents the force applied to the fluid by point  $k$  in the  $N$ -point representation of  $B$ . The equations to be solved are:

$$\rho \frac{\partial \underline{u}}{\partial t} = \rho (-\underline{u} \cdot \nabla) \underline{u} + \eta \nabla^2 \underline{u} + \underline{F}$$

$$\frac{\partial \underline{x}_k}{\partial t} = \underline{u}(\underline{x}_k) = \int_{\text{fluid}} \underline{u}(\underline{x}) \delta(\underline{x} - \underline{x}_k) d\underline{x}$$

$$\underline{F}(\underline{x}) = \lim_{N \rightarrow \infty} \sum_{k=1}^N \underline{f}_k(N, \underline{x}_1 \cdots \underline{x}_N) \delta(\underline{x} - \underline{x}_k) \quad (5-24)$$

## VI. NUMERICAL SOLUTION OF THE NAVIER-STOKES EQUATIONS FOR A VISCOUS INCOMPRESSIBLE FLUID

Most of the methods described in this section have been taken directly from the work of A. J. Chorin [19, 20] and incorporated into our numerical scheme. In subsequent sections (VII, VIII, IX) the contributions of the present author will be discussed. One way to describe the division of labor is to say that Chorin's methods can be used once the external force field  $\underline{F}$  is known, while the present work is concerned primarily with the method of calculating  $\underline{F}$  from the state of the heart apparatus.

Consider the non-dimensional equation

$$\frac{\partial \underline{u}}{\partial t} = \mathcal{P} ( -(\underline{u} \cdot \nabla) \underline{u} + \nabla^2 \underline{u} + \underline{F} ) \quad (6-1)$$

where  $\mathcal{P}$  is the projection operator defined in Section V, and  $\underline{F}$  is the external force which we take as given, for the purposes of this section. The equation is to be solved on a 1 x 1 periodic domain. The construction of the numerical scheme proceeds as follows:

### Rectangular Mesh

Cover the domain with an  $N \times N$  rectangular mesh. Let  $h = 1/N$  so that  $h$  is the mesh width, and let the subscripts  $ij$  denote the point  $x = ih$ ,  $y = jh$ .

### Discrete Time Steps

Let time proceed in discrete steps of length  $\delta t$  and let the superscript  $n$  denote the time  $t = n\delta t$ .

Thus

$$\underline{u}_{ij}^n = \underline{u}(ih, jh, n\delta t) \quad (6-2)$$

Discrete Operators Corresponding to  $\underline{u} \cdot \nabla - \nabla^2$

Introduce the spatial operators  $Q_x^n, Q_y^n$  defined by

$$(Q_x^n \varphi)_{ij} = \frac{1}{2h} u_{1,ij}^n (\varphi_{i+1,j} - \varphi_{i-1,j}) - \frac{1}{h^2} (\varphi_{i+1,j} + \varphi_{i-1,j} - 2\varphi_{ij}) \quad (6-3)$$

$$(Q_y^n \varphi)_{ij} = \frac{1}{2h} u_{2,ij}^n (\varphi_{i,j+1} - \varphi_{i,j-1}) - \frac{1}{h^2} (\varphi_{i,j+1} + \varphi_{i,j-1} - 2\varphi_{ij})$$

The discrete operator  $(Q_x^n + Q_y^n)$  corresponds to the differential operator  $\underline{u}^n \cdot \nabla - \nabla^2$

Discrete Projection Operator P

Introduce the discrete analog P of the operator  $\mathcal{P}$  as follows.

Let

$$(G\varphi)_{ij} = \left( \frac{1}{2h} (\varphi_{i+1,j} - \varphi_{i-1,j}), \frac{1}{2h} (\varphi_{i,j+1} - \varphi_{i,j-1}) \right) \quad (6-4)$$

$$(D\underline{u})_{ij} = \frac{1}{2h} (u_{1,i+1,j} - u_{1,i-1,j}) + \frac{1}{2h} (u_{2,i,j+1} - u_{2,i,j-1}) \quad (6-5)$$

The operators G and D correspond to grad and div. Then we can define a discrete operator P by the equations

$$P \underline{w} = \underline{w} - G \varphi \quad (6-6)$$



where  $\varphi$  is a scalar chosen in such a way that  $D(P\underline{w}) = 0$ . To accomplish this we must have

$$D G \varphi = D \underline{w} \quad (6-7)$$

From (6-4) and (6-5)

$$DG \varphi = \frac{1}{4h^2} (\varphi_{i+2, j} + \varphi_{i-2, j} + \varphi_{i, j+2} + \varphi_{i, j-2} - 4\varphi_{ij}) \quad (6-8)$$

so that (6-7) is a discrete Poisson equation for  $\varphi$ .

### Difference Equations

With the foregoing operators defined, consider the following system of equations

$$(I + \delta t Q_x^n) \underline{u}^* = \underline{u}^n + \delta t \underline{F}^n \quad (6-9)$$

$$(I + \delta t Q_y^n) \underline{u}^{**} = \underline{u}^* \quad (6-10)$$

$$\underline{u}^{n+1} = P \underline{u}^{**} \quad (6-11)$$

By direct substitution we have

$$(I + \delta t Q_x^n) (I + \delta t Q_y^n) \underline{u}^{**} = \underline{u}^n + \delta t \underline{F}^n \quad (6-12)$$

or neglecting terms in  $(\delta t)^2$  and rearranging

$$\underline{u}^{**} - \underline{u}^n = \delta t [ - (Q_x^n + Q_y^n) \underline{u}^{**} + \underline{F}^n ] \quad (6-13)$$

Applying  $P$  to both sides yields

$$\underline{u}^{n+1} - \underline{u}^n = \delta t P [ - (Q_x^n + Q_y^n) \underline{u}^{**} + \underline{F}^n ] \quad (6-14)$$

That the last equation is consistent with (6-1) follows from the correspondence of  $P$  with  $\bar{P}$ , and of  $-(Q_X^n + Q_Y^n)$  with  $-\underline{u}^n \cdot \nabla + \nabla^2$ , and from the fact that  $\underline{u}^{**} \rightarrow \underline{u}^n$  as  $\delta t \rightarrow 0$ .

#### Solution of the Local Difference Equations on a Periodic Domain

Each of the equations (6-9) and (6-10) has differences in only one space direction, and each of them can be reduced to the form

$$-A_k X_{k-1} + B_k X_k - C_k X_{k+1} = D_k \quad (6-15)$$

where

$$A_k = \frac{\delta t}{h^2} + \frac{u_k^n \delta t}{2h}$$

$$B_k = \frac{2\delta t}{h^2} + 1 \quad (6-16)$$

$$C_k = \frac{\delta t}{h^2} - \frac{u_k^n \delta t}{2h}$$

and where the second subscript, which plays the role of a parameter, has been dropped. The notation  $u_k^n$  indicates either  $u_{1,k,j}^n$  in equation (6-9) or  $u_{2,ik}^n$  in equation (6-10).

The following inequalities are important:

$$B_k > A_k + C_k \quad (6-17)$$

which holds for all  $u$ , and

$$A_k > 0 \quad (6-18)$$

$$C_k > 0$$

The latter pair can hold simultaneously only if

$$h \left| u_k^n \right| < 2 \quad (6-19)$$

To see what goes wrong when the last condition is violated, consider a uniform flow in an infinite fluid with velocity  $U$  in the  $x$  direction and imagine that a local force disturbance (external force) is applied at the point  $x = k_0$  for all  $y$ . In that case the equations to be solved are

$$-AX_{k-1} + BX_k - CX_{k+1} = \delta_{kk_0} \quad (6-20)$$

with

$$B = 1 + 2 \frac{\delta t}{h^2}$$

$$A = \frac{\delta t}{h^2} + \frac{U \delta t}{2h}$$

$$C = \frac{\delta t}{h^2} - \frac{U \delta t}{2h}$$

The homogeneous equation has solutions of the form

$$X_k = e^{\alpha k} \quad (6-21)$$

where

$$-Ae^{-\alpha} + B - Ce^{\alpha} = 0 \quad (6-22)$$

The function  $Ae^{-\alpha} + Ce^{\alpha}$  has the value  $A + C < B$  at  $\alpha = 0$ .

If  $A > 0$  and  $C > 0$  it rises toward  $+\infty$  for large  $|\alpha|$  independent of the sign of  $\alpha$ . Therefore (6-22) always has positive and negative roots which we designate  $\alpha_+$  and  $\alpha_-$ , see Fig. (6-1a).

Therefore, one can construct a solution of the form

$$X_k = c_0 e^{+\alpha_k (k-k_0)}$$

where

$$\alpha_k = \begin{cases} \alpha_- & k > k_0 \\ \alpha_+ & k < k_0 \end{cases} \quad (6-23)$$

The constant  $c_0$  is chosen to satisfy (6-20) at  $k = k_0$ . Thus  $X_k$  decays away from  $k_0$  on both sides as desired. On the other hand, if  $Uh > 2$  we have  $C < 0$  and the function  $Ae^{-\alpha} + Ce^{\alpha}$  is monotonic as shown in Fig. (6-1b). Therefore, only the root  $\alpha_-$  remains and it is not possible to construct a decaying solution to the left of  $k = k_0$ . If the inequalities (6-17) and (6-18) hold the matrix of (6-15) is said to be well conditioned.

We are interested in the solution of (6-15) on a periodic domain consisting of  $N$  points. The equations hold as written even at the end points if modulo  $N$  arithmetic is understood in the subscripts. Thus, when  $k = N$ ,  $k + 1 = 1$ ; when  $k = 1$ ,  $k - 1 = N$ .

The difficulty in solving such a system of equations comes from the cyclical nature of the coupling of the unknowns. The matrix of the system has the form indicated in Fig. (6-2). It is tridiagonal

Fig. (6-1)      The equation  $B = Ae^{-\alpha} + Ce^{\alpha}$   
has two solutions of opposite sign in (a) but  
only one solution in (b).

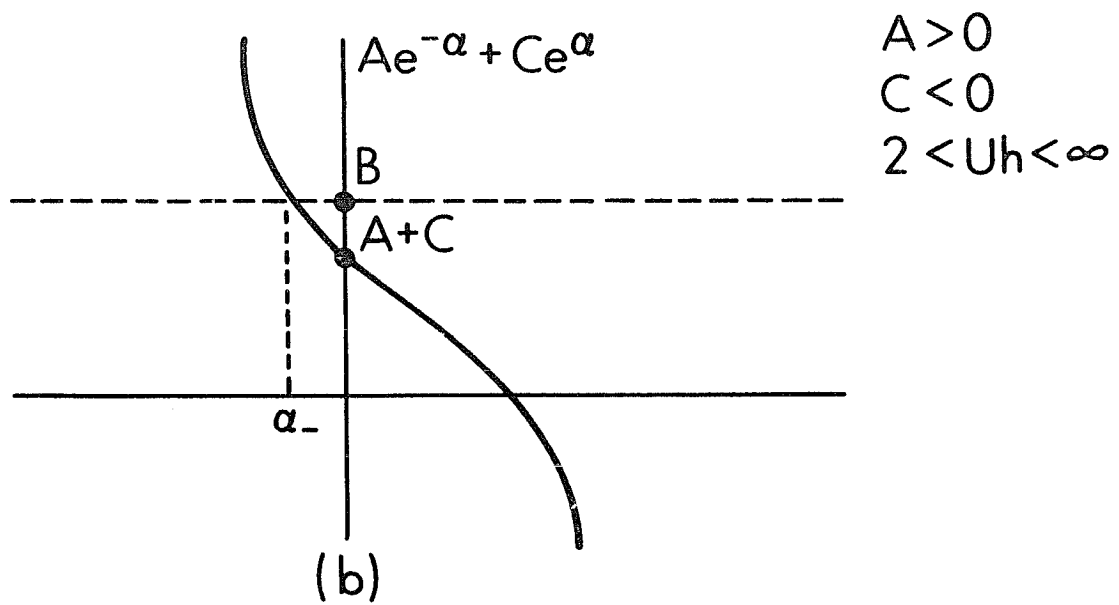
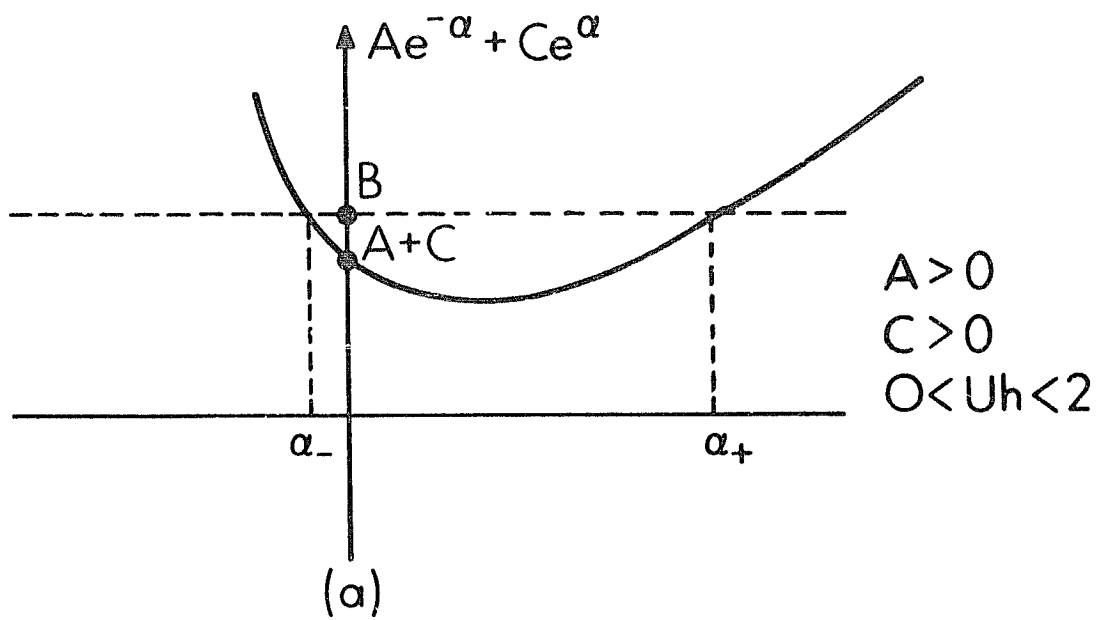
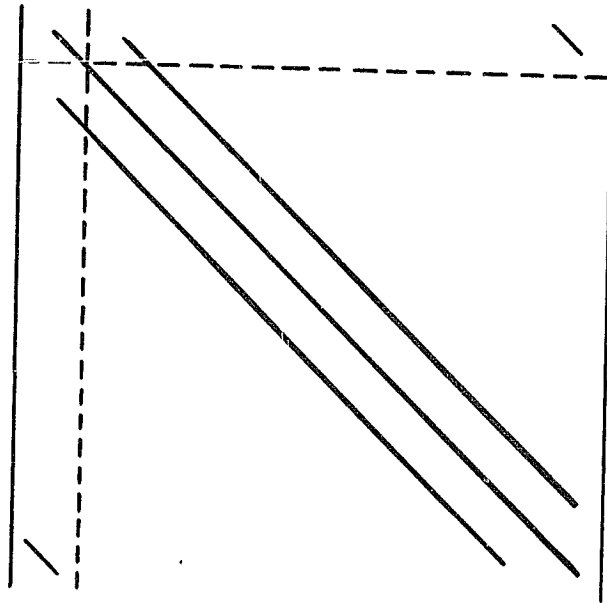


Fig. (6-2)      Structure of the local difference equations. The matrix is tri-diagonal except for two corner elements.





except for two corner elements.

Deletion of the first equation (1st row of the matrix) and the first unknown (1st column) results in an uncoupling of the cyclical structure and in a matrix which is strictly tridiagonal.

We take advantage of these facts as follows. Suppose we revert to ordinary subscript arithmetic, introduce an auxiliary point at  $k = N + 1$ , and solve the following problems, each of which has a strictly tridiagonal matrix.

$$-A_k X_{k-1}^{(1)} + B_k X_k^{(1)} - C_k X_{k+1}^{(1)} = 0 \quad (6-24)$$

$$-A_k X_{k-1}^{(0)} + B_k X_k^{(0)} - C_k X_{k+1}^{(0)} = D_k \quad (6-25)$$

$$k = 2, 3, \dots, N$$

$$X_1^{(1)} = X_{N+1}^{(1)} = 1$$

$$X_1^{(0)} = X_{N+1}^{(0)} = 0$$

Each of these problems has an easy method of solution which is given in Richtmeyer and Morton [32]. Now let

$$X_k = \lambda X_k^{(1)} + X_k^{(0)} \quad (6-26)$$

and note that  $X_k$  is a solution of (6-15) for  $k = 2, 3, \dots, N$ .

It remains to determine  $\lambda$ ; this is done by requiring that (6-15) be satisfied for  $k = 1$ . The result is

$$\lambda = \frac{D_1 + A_1 X_N^{(0)} + C_1 X_2^{(0)}}{-A_1 X_N^{(1)} + B_1 - C_1 X_2^{(1)}} \quad (6-27)$$

which completes the solution. This method of reducing the periodic case to the tridiagonal case was discovered independently by the

author; it is actually equivalent to previously existing techniques known as modification methods [33]. In this case we have rank one modification because one unknown is deleted.

### Solution of the Discrete Poisson Equation

The system of equations under consideration has the form

$$\varphi_{i+2,j} + \varphi_{i-2,j} + \varphi_{i,j+2} + \varphi_{i,j-2} - 4\varphi_{ij} = d_{ij} \quad (6-28)$$

where  $d_{ij}$  is given and the domain is periodic in each direction with period  $N$ .

The structure of these equations is important. There are actually four separate non-interacting subdomains called "chains". In equations (6-28) there is no coupling between points unless the parity (even or odd) of their  $x$  coordinates and also the parity of their  $y$  coordinates agree. Thus the four chains are the sets:

$$\{(i, j) : i \text{ even}, j \text{ even}\}$$

$$\{(i, j) : i \text{ even}, j \text{ odd}\}$$

$$\{(i, j) : i \text{ odd}, j \text{ even}\}$$

$$\{(i, j) : i \text{ odd}, j \text{ odd}\}$$

The importance of the separateness of these chains appears when one considers what happens when a local force is applied to the fluid, like the local forces applied along a boundary. To see what can go wrong here, imagine that a force field  $\underline{F} = (\delta_{ii_0}, 0)$  is applied to the fluid. Then the right hand side of the discrete Poisson equation is

$$\underline{DF} = \begin{cases} 1/2h & i = i_0 - 1 \\ -1/2h & i = i_0 + 1 \\ 0 & \text{otherwise} \end{cases} \quad (6-29)$$

Suppose, for example that  $i_0$  is even. Then  $\varphi$  is zero on all the points with even values of  $i$  and  $G\varphi$  is zero on all the points with odd values of  $i$ . Thus  $\underline{F}$  influences only half the points of the domain, namely those with an  $x$  coordinate which has the same parity as  $i_0$ . To prevent our boundaries from acting in this way it is essential that we distribute all of the boundary forces equally among all four chains. This is an important motivating consideration in the choice of a  $\delta$ -function analog as discussed in Section IX.

By summing over any chain and making use of the periodic nature of the domain one can easily show that equations (6-28) have no solution unless

$$\sum_{ij} d_{ij} = 0 \quad (6-30)$$

This condition is guaranteed by the fact that  $d_{ij}$  is the discrete divergence of some vector field on a periodic domain.

We turn now to the question of how to solve the discrete Poisson equation. Two general types of methods are available: iterative and direct. The advantage of the direct methods is that they solve the equations extremely accurately; the only error is due to the round-off error in the computer. At one time, the best iterative methods had the advantage that one could get the accuracy required in practice with less expenditure of computer time,

especially when the Poisson equation had to be solved many times with solutions that were only slightly different each time. Recently, direct methods have been improved to the point where they take only as much computer time as a few sweeps of the iterative methods. This subject is reviewed by Hockney [24] who discusses both types of methods and gives comparisons of the computer times. In the present work we are now using a direct method due to O. Widlund, G. Golub and O. Hald [25]. The programming was done by C. Leiva and D. Fischer.

## VII. REPRESENTATION OF VALVE AND MUSCLE: THE LINK FORMALISM

In this work all physical structures are represented by the forces they exert on the fluid, and these forces are determined by the configuration of the structures in space. In addition, in the case of muscle certain internal parameters (length of the contractile elements) enter into the calculation of the forces.

Each of the structures of interest is represented by a collection of points which move with the fluid and exert forces locally on the fluid. If the coordinates of the points are denoted by  $\underline{x}_k$ , then we call the set of numbers  $\{\underline{x}_k\}$  the spatial configuration of the valve, or muscle. This configuration determines the forces  $\underline{f}_k$  applied by point  $k$  to the fluid according to the following rules which we call the link formalism. It will be seen below that this formalism is sufficiently general to describe natural valves, artificial valves, and heart muscle.

All of the forces are assumed to act along straight lines which connect specified pairs of points. These lines, called links, are designated by the index  $\ell$ , with  $k_1(\ell)$ ,  $k_2(\ell)$  being the subscripts of the points connected by the link  $\ell$ . We adopt the convention  $k_1(\ell) < k_2(\ell)$ . The lists  $k_1(\ell)$ ,  $k_2(\ell)$  determine the topology of the immersed structure: these lists are fixed for all time as the motion evolves. Each link is under tension, and the tension depends on the length of the link.

Let

$$\underline{r}_\ell = \underline{x}_{k_2}(\ell) - \underline{x}_{k_1}(\ell) \quad (7-1)$$

$$r_\ell = |\underline{r}_\ell| \quad (7-2)$$

$$\hat{\underline{a}}_\ell = \underline{r}_\ell / r_\ell \quad (7-3)$$

$$T_\ell(r_\ell) = \text{Tension in link } \ell \quad (7-4)$$

$$e_{\ell k} = \begin{cases} 1 & k = k_1(\ell) \\ -1 & k = k_2(\ell) \\ 0 & \text{otherwise} \end{cases} \quad (7-5)$$

Then

$$\underline{f}_k = \sum_{\ell} e_{\ell k} \hat{\underline{a}}_\ell T_\ell(r_\ell) \quad (7-6)$$

For example, the links may act like linear springs in which case

$$T_\ell(r_\ell) = S_\ell (r_\ell - r_\ell^0) \quad (7-7)$$

where

$S_\ell$  = Stiffness of link  $\ell$

$r_\ell^0$  = Resting length of link  $\ell$

We now show that a variety of structures of physiologic interest can be represented in terms of the formalism outlined above.

### Natural Valve Leaflet

In the two-dimensional representation of the flow field, the natural valve leaflet appears as a flexible line resisting extension but not bending. Thus, we need a chain of links in which the tension is given by

$$T_\ell(r_\ell) = \begin{cases} S(r_\ell - r_\ell^0) & r_\ell > r_\ell^0 \\ 0 & r_\ell \leq r_\ell^0 \end{cases} \quad (7-8)$$

as shown in Fig. (7-1).

### Rigid Occluders for Artificial Valves

The links must resist compression as well as extension and be connected in such a way that the overall structure resists bending, as indicated in Fig. (7-2).

### Muscle

The Hill model [34], applied to heart muscle by Sonnenblick [35], can be accommodated by the link formalism. Briefly the model asserts that muscle can be represented as a passive elastic element connected in parallel with a series combination of another elastic element and a contractile element. To represent this we use a pair of links like those used in the representation of the natural valve leaflet (above). The link representing the passive element has fixed properties, while in the active link the quantity  $r^O$  represents the length of the contractile element. Thus  $r^O$  has a time variation described by the Hill hyperbola:

$$(v + v_O)(T + T_O) = K_O$$

$$\frac{dr^O}{dt} = -v \quad (7-9)$$

and  $v_O$ ,  $T_O$  and  $K_O$  are given functions of time whose time course determines the kinetics of active state in cardiac muscle. The constant volume feature of muscular contraction is automatically assured if the muscle is represented as having finite thickness, since the points that represent the muscle move in an incompressible

Fig. (7-1)      Representation of a flexible  
elastic structure like a natural valve leaflet.



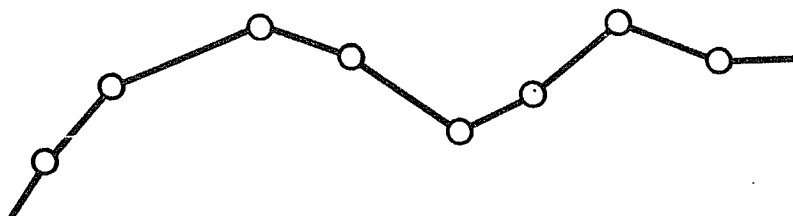
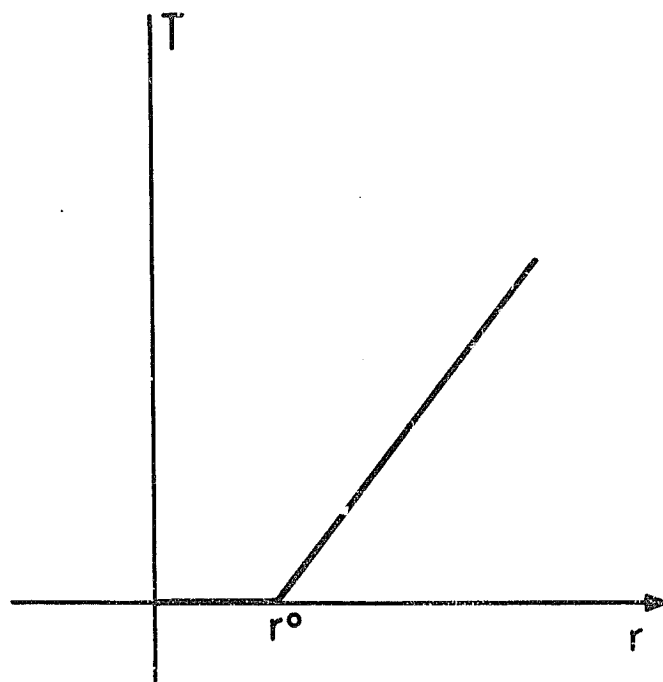
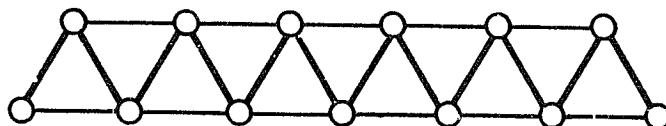
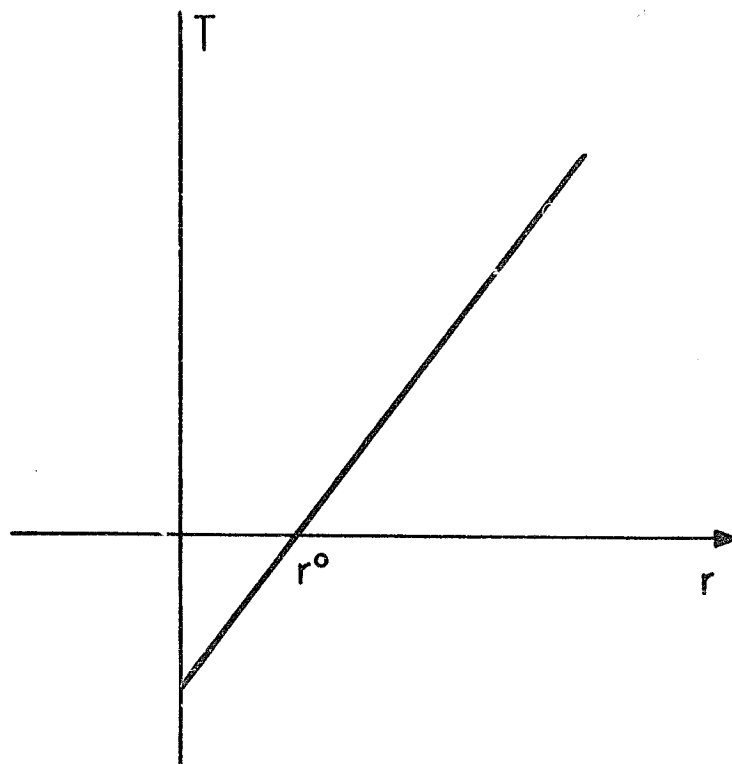


Fig. (7-2)      Representation of a disc  
type occluder for an artificial valve.



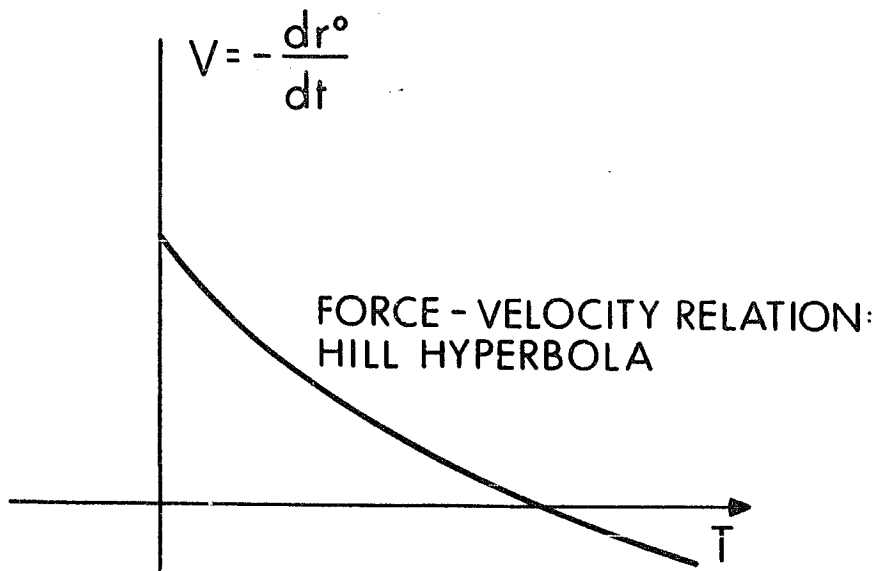
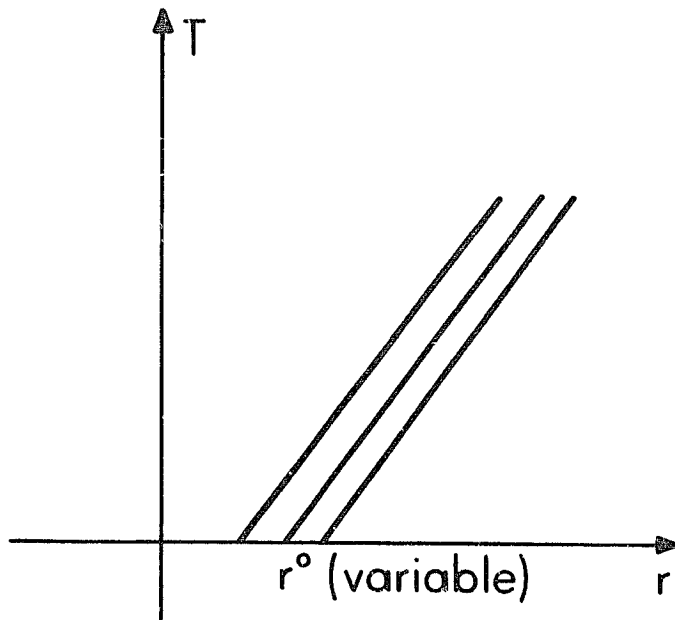
fluid.

The properties of the active link are summarized in Fig. (7-3).

The length dependence of cardiac muscle (Starling's law) can be brought into the picture by replacing  $T$  in (7-9) by the tension per cross-bridge and assuming that the number of cross-bridges is a definite function of the length of the link.

The foregoing description has been given to show that detailed muscle physiology can be accommodated by the link formalism. However, in the present work, where the main interest is in the flow pattern, simplified muscles have been used. That is, we have used only the active link, and we have prescribed the time course of contraction and relaxation of the contractile element.

Fig. (7-3)      Representation of muscle in terms of the link formalism. The parallel elastic element has to be added as an extra passive link.



### VIII. NUMERICAL STABILITY

As stated in Section VII there is a definite set of forces  $\{f_k\}$  associated with each configuration  $\{x_k\}$  of the valve. The simplest procedure, then, is to calculate the forces at each time step from the initial valve configuration for that time step. Unfortunately, such a procedure will lead to numerical instability unless the time step taken is exceedingly small compared to the time constants of interest of the problem. This situation is familiar in numerical analysis. For example, the numerical methods for the one dimensional wave equation (vibrating string) exhibit the same phenomena [32].

The usual difficulty is that when the time step taken is too large and when the initial forces for the time step are applied for the whole duration of the time step, they push the system past equilibrium and set up an oscillation which grows with successive time steps. This oscillation has nothing to do with the actual behavior of the physical system under study; it is simply an undesirable consequence of taking time steps which are too large. Unfortunately one cannot always avoid this difficulty by making the time step small enough; first, because it may take too much computer time, and second, because taking a large number of time steps leads to the accumulation of round-off errors.

The standard way out of this difficulty is to use the forces calculated from the final data for a time step, not from the initial data. Of course this involves solving an equation, since the final data are not known and depend on the forces applied. Such a procedure, called an implicit scheme, has the effect of damping out those frequencies which are larger than  $(\delta t)^{-1}$  where  $\delta t$  is

the time step. Thus  $\delta t$  can be chosen with the frequencies of interest in mind, without worrying about the highest frequency that can occur.

In fact, it may be adequate to use not the final data, but some approximate expression for the final data. The important point is that the expression must take account of the influence of the forces on the final data. It need not represent that influence exactly but it must take adequate account of it, at least in a qualitative way. In fact, a moderate overestimate of the influence of the forces on the final data is desirable.

Motivated by these considerations we pose the following problem. Let  $\underline{x}_k^n$  be the configuration of the valve at the beginning of the  $n^{\text{th}}$  time step and let  $\underline{u}_k^n$  be the velocity at the beginning of the  $n^{\text{th}}$  time step interpolated to the point  $\underline{x}_k^n$ .

The notation  $\underline{f}_k(\dots \underline{x}_{k'}, \dots)$  will be used to denote the functional dependence of the valve forces on the valve configuration. (Equations (7-1) through (7-7) give the explicit form of these functions.) Let

$$\underline{x}_k^0 = \underline{x}_k^n + \delta t \underline{u}_k^n \quad (8-1)$$

Then we define certain forces  $\underline{f}_k^*$  as the solution of the following system:

$$\underline{x}_k^* = \underline{x}_k^0 + (\delta t)^2 \frac{9}{64h^2} \beta \underline{f}_k^* \quad (8-2)$$

$$\underline{f}_k^* = \underline{f}_k(\dots \underline{x}_{k'}^*, \dots) \quad (8-3)$$



Where  $\beta$  is a parameter  $\approx 1$ . Substituting we find that

$$f_{-k}^* = f_{-k} (\cdots [x_{k'}^0 + (\delta t)^2 \frac{9}{64h^2} \beta f_{-k'}^*] \cdots) \quad (8-4)$$

Now if we let the symbol  $f^*$  stand for the whole list of components of  $f_{-k}^*$  we have

$$f^* = M(f^*) \quad (8-5)$$

where  $M(f^*)$  stands for the right hand side of (8-4).

Thus we have a non-linear multidimensional fixed point problem. If the number of points in the boundary is  $N$ , the number of components of  $f$  is  $2N$ , one component for each space direction at each point.

Such problems can be solved by Newton's method [36], which will be outlined here. Let  $f^m$  be a particular value of  $f$  and expand  $M(f)$  about  $f^m$ . To first order in  $(f - f^m)$  we have

$$M(f) \approx M(f^m) + A^m (f - f^m) \quad (8-5a)$$

where  $A^m$  is a matrix which depends on the vector  $f^m$ . It is the Jacobian matrix of the transformation  $M$ . That is, if we write  $M$  out in components

$$M_p(\cdots f_q \cdots) \quad p, q = 1, \dots, 2N$$

then

$$A_{pq}^m = \frac{\partial M_p}{\partial f_q} (\cdots f_q^m \cdots) \quad (8-6)$$

Using this family of matrices  $A^m$  (one for each choice of  $f^m$ ) we construct the iteration

$$f^{m+1} = f^m + (I - A^m)^{-1} (M(f^m) - f^m) \quad (8-7)$$

To see why this iteration is effective, consider the special case when  $A^m = A$ , independent of  $f^m$ , that is, when  $M$  is linear. In that case we have exactly

$$M(f) = M(f^m) + A(f - f^m) \quad (8-8)$$

In particular

$$f^* = M(f^*) = M(f^m) + A(f^* - f^m) \quad (8-9)$$

It follows that

$$M(f^m) - f^m = (I - A)(f^* - f^m) \quad (8-10)$$

and

$$f^{m+1} = f^m + (I - A)^{-1} (I - A)(f^* - f^m) = f^* \quad (8-11)$$

independent of  $f^m$ . Thus, for the special case of  $M$  linear the method converges to the solution in one step. For a discussion of the convergence in a non-trivial case see [36].

The implementation of Newton's method can be far from trivial when the number of dimensions is large. For example, we have applied this method to cases in which  $2N \approx 10^3$ . For such cases  $A$  contains  $10^6$  elements. Its inversion by standard matrix inversion techniques would require more than  $10^9$  operations. These numbers are unacceptably large. The key to the solution is the realization that most of the elements of  $A$  are zero. In fact the number of non-zero elements is of order  $2N$ . The problem is to find a method of inversion for which the number of non-zero elements involved remains of order  $2N$  throughout the process.

First we consider the structure of the matrix  $(I - A)$ . The construction of the elements of  $A$  proceeds as follows. Let

$$\underline{f}_k = (f_{k1}, f_{k2}) \quad (8-12)$$

$$\underline{x}_k = (x_{k1}, x_{k2}) \quad (8-13)$$

and similarly for other vectors.

It follows from equations (7-1) through (7-6) that

$$\begin{aligned} \frac{\partial f_{kp}}{\partial x_{k'p'}} &= \sum_{\ell} e_{\ell k} a_{\ell p} T'_{\ell}(r_{\ell}) \frac{\partial r_{\ell}}{\partial x_{k'p'}} \\ &+ \sum_{\ell} e_{\ell k} \frac{\partial a_{\ell p}}{\partial x_{k'p'}} T_{\ell}(r_{\ell}) \end{aligned} \quad (8-14)$$

The derivatives on the right are evaluated as follows:

$$2r_{\ell} \frac{\partial r_{\ell}}{\partial x_{k'p'}} = -2e_{\ell k'} (x_{k_2}(\ell), p' - x_{k_1}(\ell), p')$$

$$\frac{\partial r_{\ell}}{\partial x_{k'p'}} = -e_{\ell k'} \frac{x_{k_2}(\ell), p' - x_{k_1}(\ell), p'}{r_{\ell}} = -e_{\ell k'} a_{\ell p'} \quad (8-15)$$

$$\begin{aligned} \frac{\partial a_{\ell p}}{\partial x_{k'p'}} &= \frac{1}{r_{\ell}} \frac{\partial}{\partial x_{k'p'}} (x_{k_2}(\ell), p - x_{k_1}(\ell), p) - \frac{r_{\ell p}}{(r_{\ell})^2} \frac{\partial r_{\ell}}{\partial x_{k'p'}} \\ &= \frac{1}{r_{\ell}} \delta_{pp'} (-e_{\ell k'}) + \frac{r_{\ell p}}{(r_{\ell})^2} e_{\ell k'} a_{\ell p'} \\ &= \frac{1}{r_{\ell}} e_{\ell k'} (a_{\ell p} a_{\ell p'} - \delta_{pp'}) \end{aligned} \quad (8-16)$$

Combining these results we have

$$\frac{\partial f_{kp}}{\partial x_{k'p'}} = \sum_{\ell} e_{\ell k} e_{\ell k'} \{ (a_{\ell p} a_{\ell p'} - \delta_{pp'}) \frac{T_{\ell}(r_{\ell})}{r_{\ell}} - a_{\ell p} a_{\ell p'} T'_{\ell}(r_{\ell}) \} \quad (8-17)$$

If we write (8-2) out in components, we find

$$x_{kp}^* = x_{kp}^0 + (\delta t)^2 \frac{9}{64h^2} \beta f_{kp}^* \quad (8-18)$$

and hence

$$\frac{\partial x_{k'p'}^*}{\partial f_{k''p''}^*} = \gamma \delta_{k'k''} \delta_{p'p''} \quad (8-19)$$

where

$$\gamma = (\delta t)^2 \frac{9}{64h^2} \beta \quad (8-20)$$

Combining (8-17) and (8-19) we compute the derivative

$$\begin{aligned} \frac{\partial f_{kp}}{\partial f_{k''p''}^*} &= \sum_{k'p'} \frac{\partial f_{kp}}{\partial x_{k'p'}^*} \frac{\partial x_{k'p'}^*}{\partial f_{k''p''}^*} \\ &= \gamma \sum_{\ell} e_{\ell k} e_{\ell k''} \{ (a_{\ell p}^* a_{\ell p''}^* - \delta_{pp''}) \frac{T_{\ell}(r_{\ell}^*)}{r_{\ell}^*} - a_{\ell p}^* a_{\ell p''}^* T'_{\ell}(r_{\ell}^*) \} \end{aligned} \quad (8-21)$$

These are the elements of the matrix  $A$  evaluated at  $f^*$  (recall that  $A$  depends on  $f$ ). The meaning of the  $*$  on the right hand side of (8-21) is in each case that the variable in question is to be evaluated at the configuration  $\underline{x}_k^*$  determined from  $\underline{f}_k^*$  by equation (8-2). The form of  $A$  is the same for any other  $f$ , with the variables evaluated at the appropriate configuration  $\underline{x}_k$  connected with  $\underline{f}_k$  by an equation of the same form as (8-2).

The matrix  $A$  has some important properties:

(i) The matrix is sparse. That is, most of its elements are zero. To see this, note that the product  $e_{\ell k} e_{\ell k''}$  is non-zero only if the link  $\ell$  touches both point  $k$  and point  $k''$ . Thus if  $k \neq k''$  and there is no link joining  $k$  and  $k''$ , then  $e_{\ell k} e_{\ell k''} = 0$  for all  $\ell$ . It follows that

$$\frac{\partial f_{kp}}{\partial f_{k''}^* p''} = 0 \quad \text{for } k \neq k'' \quad (8-22)$$

unless there is a link joining  $k$  and  $k''$ . Let  $w_0$  be the maximum number of points joined by links to any given point. Then the number of non-zero elements of  $A$  is at most  $4N(w_0 + 1)$ , where  $N$  is the number of points. In the factor  $(w_0 + 1)$ , the 1 comes from the influence of a point on itself. The factor 4 comes from the 4 possible values of  $pp'' = 1, 2$ . Since the total number of elements in the matrix is  $4N^2$ , we have a great reduction if  $w_0 \ll N$ , which is always the case.

Remark: The graph of a matrix is a useful concept when the matrix is sparse. The graph consists of a collection of nodes, one representing

each variable. A line segment is drawn connecting nodes  $i$  and  $j$  only if the element  $a_{ij}$  is non-zero. If the matrix is symmetrical  $a_{ij} = a_{ji}$  there is no need to assign a direction to the line segment. Now suppose we remove the variables  $p, p''$  by agreeing that we will only put one node for each point  $k$ , and that we shall draw a line segment joining  $k$  to  $k''$  if any of the 4 elements

$$\frac{\partial f_{kp}}{\partial x_{k''p''}} \quad p, p'' = 1, 2$$

is non-zero. The graph that we construct in this way is actually a picture of the heart valve leaflet, or whatever other immersed structure we are representing, since each line segment in the graph is in fact a link (except for the self-loops representing the diagonal terms in the matrix).

From the foregoing considerations it is clear that the matrix  $A$  is not only sparse, but its topology is fixed since its graph is invariant as the valve leaflet moves about.

(ii) The matrix is symmetrical:

$$\frac{\partial f_{kp}}{\partial f_{k''p''}^*} = \frac{\partial f_{k''p}}{\partial f_{kp}^*} = \frac{\partial f_{k''p''}}{\partial f_{kp}^*} \quad (8-23)$$

(iii)

$$\sum_{k''} \frac{\partial f_{kp}}{\partial f_{k''p''}^*} = 0 \quad (8-24)$$

This property is evident since the form of (8-21) is

$$\frac{\partial f_{kp}}{\partial f_{k''p''}^*} = \sum_{\ell} e_{\ell k} e_{\ell k''} b_{\ell pp''} \quad (8-25)$$

Hence

$$\sum_{k''} \frac{\partial f_{kp}}{\partial f_{k''p''}^*} = \sum_{\ell} e_{\ell k} b_{\ell p p''} \sum_{k''} e_{\ell k''}$$

From the definition of  $e_{\ell k''}$ , equation (7-5), it is clear that

$$\sum_{k''} e_{\ell k''} = 0 + 1 - 1 = 0 \quad (8-26)$$

which completes the proof.

(iv) An immediate corollary of (iii) is the following:

$$\sum_{k''p''} \frac{\partial f_{kp}}{\partial f_{k''p''}^*} = 0 \quad (8-27)$$

and by symmetry the same statement holds for the sum over  $kp$ . Thus each row or column of  $A$  has sum zero.

(v) The eigenvalues of  $A$  are negative (or zero) or the link configuration is unstable.

Recall that the elements of  $A$  are simply  $\gamma$  times the elements of  $\partial f_{kp} / \partial x_{k'p'}$  where  $\gamma > 0$ . Then if  $A$  has a positive eigenvalue  $\lambda$ , the matrix  $\partial f_{kp} / \partial x_{k'p'}$  has a positive eigenvalue  $\lambda/\gamma$ , and hence there exists a perturbation  $\delta x_{k'p'}$  such that

$$\delta f_{kp} = \sum_{k'p'} \frac{\partial f_{kp}}{\partial x_{k'p'}} \delta x_{k'p'} = (\lambda/\gamma) \delta x_{kp} \quad (8-28)$$

Thus, the perturbation produces forces which tend to increase the perturbation. We shall assume that this case does not arise and that the eigenvalues of  $A$  are always negative.

Remark: If  $T_{\ell}(r) \geq 0$  and  $T'_{\ell}(r) \geq 0$ , then it can be shown directly from the form of (8-21) that the eigenvalues of  $A$  are all non-positive. That is, a link structure under tension is always stable provided that stretching the links can only increase the tension.

On the other hand, a link structure under compression may not be stable. For example a straight line of rigid links will tend to buckle under compression. (A toy train which is not on tracks can be pulled along smoothly but not pushed). However, with sufficient care it is possible to guarantee stability even when negative tension is allowed. For example, I would conjecture that in a plane, a network of triangles in which those triangles that share a vertex also share a side is always stable to small enough perturbations if  $T'(r) \geq 0$  for all links whether the links are under tension or compression.

(vi) If the link configuration is stable, the matrix  $(I-A)$  is positive definite. Let  $\lambda$  be an eigenvalue of  $(I-A)$ . Then there is a non-zero  $f$  such that

$$(I-A)f = \lambda f \quad (8-29)$$

then

$$Af = (1-\lambda)f \quad (8-30)$$

and  $(1-\lambda)$  is an eigenvalue of  $A$ . Then, from (v), if the link configuration is stable

$$\begin{aligned} 1 - \lambda &< 0 \\ \lambda &> 1 \end{aligned} \quad (8-31)$$

Thus, all eigenvalues of  $(I-A)$  are positive and  $(I-A)$  is positive definite.

Because the matrix  $(I-A)$  is symmetric and positive definite the Cholesky algorithm can be used to factor  $(I-A)$  and hence to compute  $(I-A)^{-1}f$ . [36]

We have adapted the Cholesky algorithm to the present problem in such a way that the number of non-zero elements remains small throughout the computation. To explain this method it is necessary



first to state the algorithm. The statement we shall use is taken from [36].

Let  $B$  with elements  $b_{ij}$  be a positive-definite symmetric matrix. We seek a matrix  $L$  with elements  $\ell_{ij}$  such that  $L$  is lower triangular ( $\ell_{ij} = 0$   $j > i$ ) and  $\tilde{L}L = B$ . The elements  $\ell_{ij}$  are defined recursively as follows:

$$\ell_{ij} = \begin{cases} \frac{1}{\ell_{jj}} (b_{ij} - \sum_{k=1}^{j-1} \ell_{ik} \ell_{jk}) & i \geq j \\ 0 & i < j \end{cases} \quad (8-32)$$

(when  $j = 1$  the sum is assumed to be zero)

Note that for  $i = j$  this implies

$$\ell_{jj}^2 = (b_{jj} - \sum_{k=1}^{j-1} \ell_{jk}^2) \quad (8-33)$$

so that a square root has to be evaluated to compute  $\ell_{jj}$ . The positive definiteness of  $B$  guarantees that the argument of this square root is never negative.

To see that (8-32) gives the desired elements  $\ell_{ij}$  let  $i \geq j$  and consider

$$(\tilde{L}L)_{ij} = \sum_{k=1}^n \ell_{ik} \ell_{jk} = \sum_{k=1}^j \ell_{ik} \ell_{jk} = \ell_{ij} \ell_{jj} + \sum_{k=1}^{j-1} \ell_{ik} \ell_{jk} = b_{ij} \quad (8-34)$$

Clearly, for  $i < j$  the same calculation gives

$$(\tilde{L}L)_{ij} = b_{ji} = b_{ij} \quad (8-35)$$

We now examine the question of how non-zero elements are generated during the course of the algorithm. The aim is to find a set of positions in the matrix, such that if all of the non-zero elements of B fall into this set, then all of the non-zero elements of L also fall into this set at every stage of the algorithm. We note that non-zero elements are generated by pairs of previously existing non-zero elements in the same column. That is, A non-zero pair  $(\ell_{ik}, \ell_{jk})$   $i \geq j > k$  generates a possible non-zero element at  $(i, j)$ . The situation is indicated in Fig. (8-1).

Now let

$$\begin{aligned} S_1 &= \{(i, k): 0 \leq i - k \leq w\} \\ S_2 &= \{(i, k): i \geq k \text{ and } i \geq n - m\} \end{aligned} \quad (8-36)$$

where  $n$  is the number of rows in the matrix and  $w$  and  $m$  are small integers. The two sets are indicated in Fig. (8-2). They overlap in the lower right hand corner of the matrix.

Now, if all the non-zero elements are initially in  $S_1 \cup S_2$  they remain confined to  $S_1 \cup S_2$  throughout the algorithm. The proof is simple. Consider any pair of non-zero elements with both members of the pair in the same column. Such a pair either has or has not its lower element in  $S_2$ . If it has, the non-zero element it generates is in  $S_2$ . If it has not, then both elements of the pair are in  $S_1$ , and hence the non-zero element generated is in  $S_1$ . These statements follow from the fact that the element generated is in the same row as the lower element of the pair, and to the right of the column containing the pair.

The algorithm used, then, is a Cholesky algorithm with all the




Fig. (8-1) In the Cholesky algorithm, a non-zero pair of elements in column k at rows j and i,  $j \leq i$ , generate a possible non zero element in row i column j.

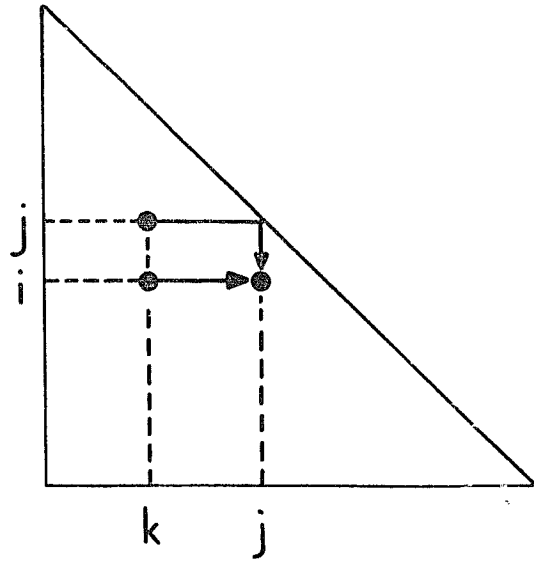
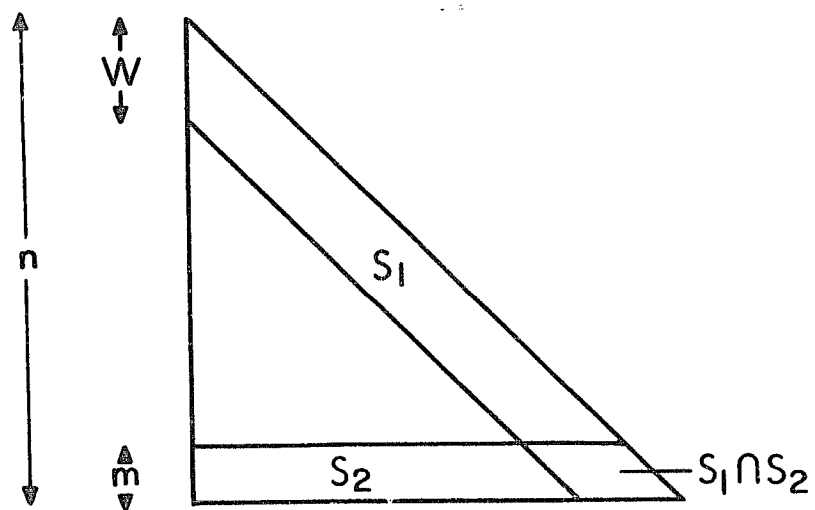


Fig. (8-2)      Location of the non-zero elements  
of the matrix. If the non-zero elements are  
initially confined to the indicated regions  
they remain confined there throughout the  
algorithm.



elements of the matrix which lie in neither  $S_1$  nor  $S_2$  ignored. The amount of storage required is  $n(m+w)$  and the number of operations for computing the factors is roughly  $n(m+w)^2$  multiplications, with an equal number of additions, plus  $n$  square roots. The crucial fact is that both the storage and the time go linearly with  $n$ .

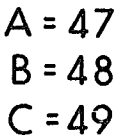
It remains to show that link structures of interest can be put in such a form that the matrices associated with them will look like the matrix of Fig. (8-2).

Given a link structure, the problem is to choose a numbering of the points, such that points are linked only to neighboring points or to one of a few special points which are numbered last. For example, in Fig. (8-3), which represents a mitral valve situated between atrium and ventricle, three points A, B, C are singled out to be numbered last, and the remaining points are numbered successively. The resulting matrix has the structure of Fig. (8-2) with  $n = 2 \times 48 = 96$ ,  $m = 2 \times 3 = 6$ ,  $w = 2 \times (1+1) = 4$ .

An important point is that we can refine the representation and include more points (increase  $n$ ) without changing  $m$  and  $w$ . Thus, as the representation is refined, the amount of computation varies only linearly with the fineness of the mesh. (This only holds for one-dimensional boundaries in a two-dimensional problem).

Fig. (8-3)      Numbering for a heart-like link structure. Three special points A, B, C are singled out to be numbered last. Every other point is linked ~~to~~ either <sup>to</sup> one of these or to a point whose number is very close to its own ( $\pm 1$ , in this case).





## IX. THE CONNECTION BETWEEN VALVE AND FLUID

The points  $\underline{x}_k$  which represent the heart valve leaflet interact with the fluid in two ways.

- (i) Each of these points is moved by the fluid at the local fluid velocity. Thus we have

$$\frac{d\underline{x}_k}{dt} = \underline{u}(\underline{x}_k) = \int_{\text{fluid}} \underline{u}(\underline{x}) \delta(\underline{x} - \underline{x}_k) d\underline{x} \quad (9-1)$$

- (ii) Each of these points exerts a force  $\underline{f}_k$  on the fluid locally. This force depends, of course, on the number of points used to represent the valve. Let this number be  $N$ . Then as  $N \rightarrow \infty$  the  $\underline{f}_k$  are of order  $1/N$ . With this understanding we can assert that the force density in the fluid is given by

$$\underline{F} = \lim_{N \rightarrow \infty} \sum_{k=1}^N \underline{f}_k \delta(\underline{x} - \underline{x}_k) \quad (9-2)$$

In the construction of the numerical scheme it is necessary to replace these equations by discrete equations of the form

$$\underline{x}_k^{n+1} = \underline{x}_k^n + \delta t \sum_{ij} h^2 \underline{u}_{ij}^n D_{ij}(\underline{x}_k^n) \quad (9-3)$$

$$\underline{F}_{ij}^n = \sum_k \underline{f}_k D_{ij}(\underline{x}_k^n) \quad (9-4)$$

where the function  $D_{ij}(\underline{x}_k)$  corresponds in some sense to  $\delta(\underline{x} - \underline{x}_k)$  with  $\underline{x} = (ih, jh)$ .

As explained in Section II, the points  $\underline{x}_k$  of the valve need not coincide with mesh-points  $ij$  but may lie anywhere in the fluid. Consequently, the function  $D_{ij}(\underline{x})$  plays the following double role:

- (i) Interpolation of the fluid velocity from the fluid mesh

to points of the valve.

(ii) Spreading the valve forces from the points of the valve  
to the mesh-points of the fluid.

We specify the function  $D_{ij}(\underline{x})$  as follows:

Let  $\underline{x} = (xh, yh)$  so that the mesh-points are given by integer values of  $x$  and  $y$ . ( $h$  is the mesh-width). Then let

$$D_{ij}(\underline{x}) = \frac{1}{h^2} \varphi(x - i) \varphi(y - j) \quad (9-5)$$

where

$$\varphi(r) = \begin{cases} \frac{1}{2} \cos^2 \frac{\pi r}{4} = \frac{1}{4} (1 + \cos \frac{\pi r}{2}) & |r| \leq 2 \\ 0 & |r| > 2 \end{cases} \quad (9-6)$$

as shown in Fig. (9-1).

The function  $\varphi(r)$  has the following properties:

(1)  $\varphi$  is continuous and once continuously differentiable (the 2nd derivative is discontinuous at  $r = \pm 2$ ). It is also an even function.

(2)

$$\int_{-\infty}^{\infty} \varphi(r) dr = 1 \quad \text{and} \quad \varphi(r) = 0 \quad \text{for} \quad |r| \geq 2 \quad (9-7)$$

(3)

$$\sum_{k \text{ even}} \varphi(r - k) = \sum_{k \text{ odd}} \varphi(r - k) = \frac{1}{2} \quad (9-8)$$

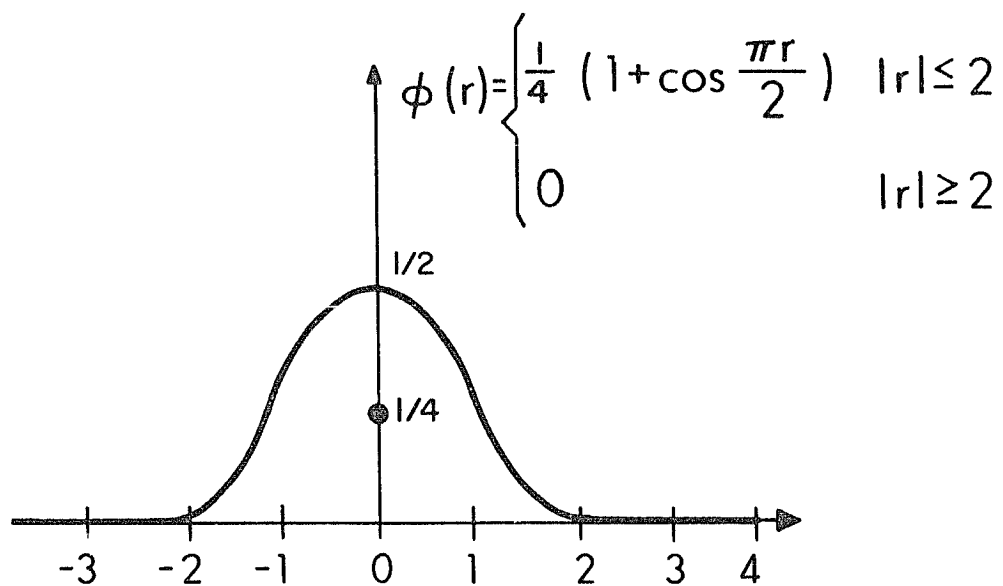
and therefore

$$\sum_k \varphi(r - k) = 1 \quad (9-9)$$

(4)

$$\sum_k \varphi^2(r - k) = \frac{3}{8} \quad (9-10)$$

Fig. (9-1)      A  $\delta$ -function analog for the  
numerical scheme.



independent of  $r$ , and therefore, from the Schwarz inequality

$$\sum_k \varphi(r-k) \varphi(s-k) \leq \sum_k \varphi^2(r-k) \quad (9-11)$$

for all  $r$  and  $s$ .

The importance of these properties is discussed below:

Because of (1) the coefficients  $D_{ij}(\underline{x})$  that link any particular mesh-point with any particular valve point vary continuously as the valve point moves.

The importance of (2) is that it connects  $D_{ij}$  with the  $\delta$ -function. To see this, let

$$f_h(z) = \frac{1}{h} \varphi\left(\frac{z}{h}\right) \quad (9-12)$$

Then

$$f_h(z) = 0 \quad \text{for } |z| \geq 2h \quad (9-13)$$

and

$$\int_{-\infty}^{\infty} f_h(z) dz = \frac{1}{h} \int_{-\infty}^{\infty} \varphi\left(\frac{z}{h}\right) dz = \frac{1}{h} \int_{-\infty}^{\infty} \varphi\left(\frac{z}{h}\right) d\left(\frac{z}{h}\right) h = 1 \quad (9-14)$$

Thus  $f_h(z)$  is a  $\delta$ -sequence. That is

$$\lim_{h \rightarrow 0} \int_{-\infty}^{\infty} f_h(z) g(z) dz = g(0) \quad \text{all } g \quad (9-15)$$

Property (3) guarantees that  $D_{ij}$  is a sensible interpolation formula in that if  $\underline{u}_{ij}$  is constant in the neighborhood of  $\underline{x}_k$  we expect the interpolation of  $\underline{u}_{ij}$  to  $\underline{x}_k$  to recover this constant value. Actually, this much is guaranteed by

$$\sum_k \varphi(r-k) = 1 \quad (9-16)$$

The reason for imposing the stronger condition that the sums over  $k$  even and  $k$  odd should separately be  $1/2$  has to do with the separate "chains" that are involved in the solution of Poisson's equation. (see Section VI) It should be recalled that the force applied to the fluid at one point influences distant points instantaneously only through the pressure field, which is computed by the solution of Poisson's equation. Moreover, in the difference equations used here, Poisson's equation breaks up into 4 separate systems, one over each of the chains defined in Section VI. The property (3), then guarantees that the total linkage of a valve point with one chain is the same as its total linkage with any other chain.

Property (4) is derived from consideration of the influence of the force due to a valve point on the motion of that same valve point. One would like that influence to be independent of the relationship of that valve point to the mesh. That is, one would like it to be the same whether the valve point coincides with a mesh point or lies at any position between mesh points.

Consider a time step for which the fluid velocity is initially zero. A force  $\underline{f}_k$  is applied to the fluid at the valve point  $\underline{x}_k$ . We want to find the displacement produced by this force at some other point  $\underline{x}_\ell$  after one time step. (Assume there are no forces other than the single force applied at  $\underline{x}_k$ . If there were others, we could use superposition, since the equations for one time step are linear.)

We have

$$\underline{F}_{ij} = D_{ij}(\underline{x}_k) \underline{f}_k \quad (9-17)$$

Now the force  $\underline{F}_{ij}$  produces, after one time step, a velocity field  $\underline{u}_{pq}$  which depends linearly on  $\underline{F}_{ij}$ . Thus there must be some

2 x 2 matrix  $G$  associated with every pair of points  $(pq, ij)$  of the domain such that

$$\underline{u}_{pq} = \sum_{ij} G(pq, ij) \underline{E}_{ij} \quad (9-18)$$

Moreover, because of the periodic nature of the domain and because all of our difference equations have constant coefficients (we are considering here the case  $\underline{u}^n = 0$ ),  $G$  depends only on  $(p-i, q-j)$ .

Thus we write

$$\underline{u}_{pq} = \sum_{ij} G(p-i, q-j) D_{ij}(\underline{x}_k) \underline{f}_k \quad (9-19)$$

Finally, if we interpolate  $\underline{u}_{pq}$  to the point  $\underline{x}_\ell$  we have

$$\underline{u}(\underline{x}_\ell) = \left[ \sum_{pq} h^2 \sum_{ij} D_{pq}(\underline{x}_\ell) G(p-i, q-j) D_{ij}(\underline{x}_k) \right] \underline{f}_k \quad (9-20)$$

Where  $\underline{x}_\ell$  is another point of the valve. (If  $k = \ell$  it is the same point.) The expression in square brackets is a 2 x 2 matrix which depends on  $\underline{x}_\ell, \underline{x}_k$ ; since it is derived from  $G$  we designate it by  $\tilde{G}$ . Thus

$$\tilde{G}(\underline{x}_\ell, \underline{x}_k) = h^2 \sum_{pq} \sum_{ij} D_{pq}(\underline{x}_\ell) G(p-i, q-j) D_{ij}(\underline{x}_k) \quad (9-21)$$

Now, if we rewrite  $D_{ij}$  in terms of  $\varphi$  with  $\underline{x}_\ell = (x_\ell h, y_\ell h)$  and  $\underline{x}_k = (x_k h, y_k h)$  we get

$$\tilde{G}(\underline{x}_\ell, \underline{x}_k) = \frac{1}{h^2} \sum_{pq} \sum_{ij} \varphi(x_\ell - p) \varphi(y_\ell - q) G(p-i, q-j) \varphi(x_k - i) \varphi(y_k - j) \quad (9-22)$$

One can rewrite the sums in terms of  $\delta i, \delta j$  where

$$\begin{aligned} \delta i &= p - i \\ \delta j &= q - j \end{aligned} \quad (9-23)$$



$$\tilde{G}(\underline{x}_\ell, \underline{x}_k) = \frac{1}{h^2} \sum_{\delta i, \delta j} \left[ G(\delta i, \delta j) \cdot \left( \sum_i \varphi(x_\ell - \delta i - i) \varphi(x_k - i) \right) \cdot \left( \sum_j \varphi(y_\ell - \delta j - j) \varphi(y_k - j) \right) \right] \quad (9-24)$$

Now consider a fixed term in the sum over  $\delta i, \delta j$  and ask the question how does this term vary as  $\underline{x}_\ell$  and  $\underline{x}_k$  vary. Because of property (4) we can assert that this term is maximal when

$$x_\ell - \delta i = x_k \quad (9-25)$$

$$y_\ell - \delta j = y_k$$

and moreover this maximal value is

$$\frac{9}{64h^2} G(\delta i, \delta j)$$

The important point is that the constant which multiplies  $G(\delta i, \delta j)$  is constant, independent of  $x_\ell, x_k, y_\ell, y_k$ , provided only that their differences obey Eqs. (9-25).

Actually, one would like to impose an even stronger condition than (4), namely (4'):

$$\sum_k \varphi(x_1 - k) \varphi(x_2 - k) = \varphi(x_1 - x_2) \quad (9-26)$$

a condition which is motivated by the  $\delta$ -function identity

$$\int_{-\infty}^{\infty} \delta(x_1 - x) \delta(x_2 - x) dx = \delta(x_1 - x_2) \quad (9-27)$$

If (4') held, one could simplify (9-24) to read

$$\tilde{G}(\underline{x}_\ell, \underline{x}_k) = \frac{1}{h^2} \sum_{\delta i, \delta j} G(\delta i, \delta j) \varphi(\underline{x}_\ell - \underline{x}_k - \delta i) \varphi(\underline{y}_\ell - \underline{r}_k - \delta j) \quad (9-28)$$

so that  $\tilde{G}$  would depend only on the difference  $\underline{x}_\ell - \underline{x}_k$ . Unfortunately (4') cannot hold if  $\varphi = 0$  outside a finite region, so that it is an impractical constraint to apply (if every point of the valve interacts with every point of the fluid through  $D_{ij}$  the computations become astronomical!) What we have done in formulating condition (4) is to extract an important consequence of (4'), namely the fact that  $\sum_i \varphi^2(x - i)$  is independent of  $x$  and to use that as our condition (4).

It is interesting to note that the properties (1) - (4) almost determine the function  $\varphi$ . To see this consider  $0 \leq r \leq 1$ . Then  $\varphi(r - i)$  is non-zero at only the four values  $i = -1, 0, 1, 2$  because of the part of (2) which asserts that  $\varphi(r) = 0$  for  $|r| \geq 2$ . The values of  $\varphi$  that enter into the sums in (3) and (4) are

$$\varphi(r - 2) = \varphi(2 - r)$$

$$\varphi(r - 1) = \varphi(1 - r)$$

$$\varphi(r)$$

$$\varphi(r + 1)$$

where we have used the fact that  $\varphi$  is even. Because of (2)

$$\varphi(2 - r) = \frac{1}{2} - \varphi(r) \quad (9-29)$$

$$\varphi(1 + r) = \frac{1}{2} - \varphi(1 - r) \quad (9-30)$$

Using these equations, (4) becomes

$$\left[ \frac{1}{2} - \varphi(r) \right]^2 + [\varphi(r)]^2 + \left[ \frac{1}{2} - \varphi(1-r) \right]^2 + [\varphi(1-r)]^2 = \frac{3}{8} \quad (9-31)$$

Actually, the constant  $3/8$  is not arbitrary. It can be found by putting  $r = 1$  and noting that continuity requires that  $\varphi(2) = 0$ . From conditions (2) we find  $\varphi(1) = \frac{1}{2}$  and  $\varphi(0) = 1/2$ . Substituting these in (9-31) with  $r = 1$  we find that the constant must be  $3/8$ .

Thus

$$\frac{1}{4} - \varphi(r) + 2[\varphi(r)]^2 + \frac{1}{4} - \varphi(1-r) + 2[\varphi(1-r)]^2 = \frac{3}{8} \quad (9-32)$$

Rearranging:

$$[4\varphi(r) - 1]^2 + [4\varphi(1-r) - 1]^2 = 1 \quad (9-33)$$

It follows that

$$4\varphi(r) - 1 = \cos \theta(r) \quad (9-34)$$

$$4\varphi(1-r) - 1 = \sin \theta(r) \quad (9-35)$$

where

$$\theta(1-r) = \frac{\pi}{2} - \theta(r) \quad (9-36)$$

If (9-36) does not hold, (9-34) and (9-35) are inconsistent. As shown above,  $\varphi(0) = 1/2$  so that  $\theta(0) = 0$ . From (9-36),  $\theta(1/2) = \frac{\pi}{4}$ .

Actually, any  $\theta(r)$  can be chosen on  $0 \leq r \leq 1/2$  which satisfies these conditions, but the simplest choice is clearly  $\theta(r) = \frac{\pi r}{2}$  which leads to the function  $\varphi$  that we have used throughout this section.

# X. SUMMARY OF THE NUMERICAL METHOD

The setting for the calculation is a  $1 \times 1$  periodic domain covered by a mesh which is rectangular with mesh width  $h$ . Immersed in the domain is a link structure representing the heart apparatus. Its points, labeled by the index  $k$ , need not coincide with points of the rectangular mesh. The configuration<sup>†</sup> of the heart apparatus is written  $\{\underline{x}_k\}$  and a system of forces  $\{f_k(\dots \underline{x}_k, \dots)\}$  corresponds to each possible configuration.

At the beginning of the  $n^{\text{th}}$  time step the given data are the velocity field  $\underline{u}_{ij}^n$  and the configuration  $\underline{x}_k^n$  of the heart apparatus. The process of finding  $\underline{u}_{ij}^{n+1}$  and  $\underline{x}_k^{n+1}$  is summarized here. (The notation is defined in the foregoing sections.)

1. Using Newton's method, solve the non-linear system of equations

$$\underline{x}_k^* = \underline{x}_k^n + \delta t \underline{u}^n(\underline{x}_k^n) + \frac{9}{64h^2} \beta \underline{f}_k^* (\delta t)^2 \quad (10-1)$$

$$\underline{f}_k^* = \underline{f}_k(\dots \underline{x}_k^*, \dots) \quad (10-2)$$

2. Apply the forces  $\underline{f}_k^*$  to the fluid by computing

$$\underline{F}_{ij} = \sum_k D_{ij}(\underline{x}_k^n) \underline{f}_k^* \quad (10-3)$$

<sup>†</sup>To accommodate active boundaries the concept of configuration is generalized, so that its specification requires more than just data about the position of the heart apparatus in space.

3. Solve successively the following systems of equations

$$(I + \delta t Q_x^n) \underline{u}^* = \underline{u}^n + \delta t \underline{F} \quad (10-4)$$

$$(I + \delta t Q_y^n) \underline{u}^{**} = \underline{u}^* \quad (10-5)$$

$$\underline{u}^{n+1} = P \underline{u}^{**} \quad (10-6)$$

4. Move the heart apparatus according to the formula

$$\underline{x}_k^{n+1} = \underline{x}_k^n + \delta t \sum_{i,j} h^2 D_{i,j} (\underline{x}_k^n) \underline{u}_{i,j}^{n+1} \quad (10-7)$$

This completes the time step. Return to 1.

## COMPUTER EXPERIMENTS ON THE PHYSIOLOGY OF THE NATURAL MITRAL VALVE

In this section we apply our techniques to the physiology of the natural mitral valve. The mitral valve was chosen for several reasons: first, because it has been the object of intense study (using other methods) by a group of workers headed by Frater and Yellin with whom the present author has had close contact throughout this research, and also because the mitral valve with its bicuspid anatomy seems most likely to lend itself to an adequate two dimensional representation. A further advantage of the mitral valve is that during diastole when the valve is open, the atrium and ventricle together form almost a closed system, the qualification being the inflow from the pulmonary veins to the atrium. Because these inlets are multiple (4 in man) and small, it is not likely that their presence will significantly disturb the flow pattern at the valve. On the other hand, the pulmonary venous inflow during diastole certainly does increase the volume available for filling the ventricle. One can account for this volume effect by postulating a larger than normal atrium at the beginning of diastole, instead of continuous inflow throughout. In this way, we can study the mitral valve in a setting which is closed and consists of simply an atrial and a ventricular chamber. The atrium empties into the ventricle through the valve; the ventricle contracts and the valve closes. Although we have to stop the calculation at this point, since our ventricle has no outflow tract, we have nevertheless covered that part of the cardiac cycle that is of interest from the point of view of the normal dynamic physiology of the mitral valve. A stress analysis of the mitral valve during systole would also be of interest, but that is primarily a

statics problem in which the role of the fluid is simply to provide the pressure load that holds the valve closed.

In the computer experiments reported here we have taken no account of the prominent asymmetry between the sizes of the mitral leaflets. The methods certainly can accommodate such an asymmetry but it was simplest to start without it. In this work, we shall report on the physiology that the mitral valve would have if its leaflets were of equal size, while a significant question for future work will be how much difference it makes that the leaflets are not in fact equal. This manner of proceeding illustrates what some will see as a weakness and others will see as a strength of this technique: the user is free to design the heart and valve he wishes to study. How close that heart and valve will come to reality depends on the user's knowledge of the anatomy and physiology of real hearts, and on how close to reality he wants the simulated heart to come. One may impose differences between the actual heart and the heart under study to see how much difference they make. Such an approach is analogous to the production of experimental lesions, but in the computer there is far greater flexibility and control over the "lesions" that one can produce. For example, one could "cut" one of the chordae tendineae at a precise time in the cardiac cycle and observe the effect.

Simplifications were also made when it was considered how to represent the atrial and ventricular wall. Wall thickness was not taken into account and each wall was represented as an initially circular arc composed of links of the type discussed in Section VII. The tension in these links tends to keep the arcs circular at

equilibrium, though the circular shape is distorted by the flow and sometimes by the papillary muscle tension. The geometry is thus incorrect: a more accurate ventricular shape could be maintained by having muscular links which go across the ventricle from one side to the other. Such links would be the best that one could do in two dimensions toward representing the circular muscle of the ventricular wall; they have not been included here. The physiology of the muscular links was also simplified, even more than in the Hill model [34] which is itself a simplification for cardiac muscle. Our muscle can be described in the language of the Hill model by stating that we have ignored the parallel elasticity and that we have made the length of the contractile element a given function of time. (In the Hill model the rate of shortening of the contractile element depends on the load). The rationale for all of these liberties that we have taken with the walls is that we are primarily interested in the physiology of the valve and its flow pattern. The walls that we have designed are perfectly adequate to get the fluid moving which is also what the walls of the heart do. The present method could incorporate a more accurate representation of the muscle physiology and wall geometry.

One of the most difficult and important questions we have to face is how to represent the anatomy of the valve, chordae, and papillary muscles. A description of this anatomy will be given here to motivate the subsequent paragraph in which our simplified representation of this apparatus will be described. When the ventricle is viewed from the base of the heart through the open mitral valve (see Netter [41], p. 11) the papillary muscles and chordae are seen to lie roughly below the commissures on either side. Each papillary muscle



is thus situated between the leaflets, and each gives chordae to both leaflets in the region near the commissure. Now let a plane be constructed perpendicular to the plane of the valve ring and bisecting both the anterior and the posterior leaflets. This plane intersects each leaflet along a curve which adequately describes the configuration of that leaflet; the plane also intersects the apex of the heart and the outflow tract from the ventricle to the aorta. If a single plane must be chosen for studying the flow pattern around the mitral valve, this is the plane of choice. However, this plane passes between the two papillary muscles; it contains neither papillary muscle nor chordae. If the projections of the papillary muscles onto this plane are taken they lie superimposed on one another and they appear to originate from the apex of the heart (actually from a point in the fluid just above the apex). The projections of the chordae on this plane appear to insert at the tip of each valve leaflet, and also further back along the ventricular surface of the leaflet.

These remarks justify, insofar as it can be justified, our simple two dimensional representation of the papillary muscles and their elegant webs of chordae tendineae: A single link from the apex of the ventricle to the tip of each valve leaflet is used. The links are part muscle and part chordae. The part representing the chordae is passive (fixed resting length) while the muscular part is assumed to have the same kinetics as the rest of the ventricular muscle, contracting and relaxing simultaneously with the rest of the ventricle. An important experimental variable is how much of the distance between valve tip and ventricular apex should be assigned to the muscles and how much to the chordae, as this determines whether the chordae go

slack during diastole or remain under tension.

The dynamics of our typical experiment are completely determined when the functions of time are given for the lengths of the contractile elements of the atrial and ventricular muscle. A convenient reference time to call  $t = 0$  is the instant when the atrial and ventricular pressures are in equilibrium at the beginning of diastole.

To start the experiment smoothly, we set the initial conditions in such a way that at  $t = 0$  the tensions in the atrial and ventricular walls will be in the same ratio as their radii. By Laplace's law, this guarantees equality of the pressures. The tensions in the valve, chordae, and papillary muscles are all zero at this initial instant. The fluid is at rest.

It would also be possible to begin the experiment at a slightly earlier time, during the isovolumetric relaxation of the ventricle, before ventricular pressure has fallen as low as atrial pressure. Beginning at this earlier time would allow study of the unloading of the valve that occurs just prior to diastole. By comparing this earlier starting point with the equilibrium starting point, it would be possible to study the consequences of this unloading to subsequent valve dynamics.

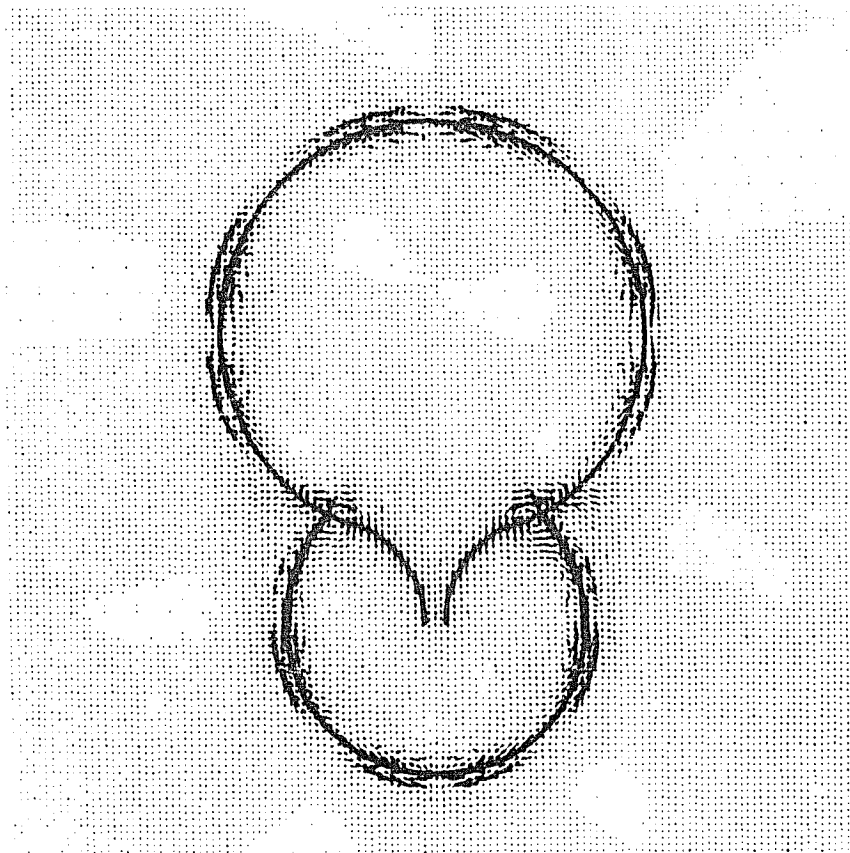
Figure(11-1) presents individual frames of a cine' film of the valve, heart, and fluid motions. The film was produced directly by the computer. Each frame shows the instantaneous configuration of valve, atrium and ventricle, and also the instantaneous fluid velocity vectors. In this computer experiment the calculation starts at  $t = 0$  with the distance from valve tip to ventricular apex apportioned as follows: 20% papillary muscles, 80% chordae tendineae. (The ratio changes during diastole as the papillary muscles relax). With this

proportion the relaxation of the papillary muscle is not sufficient to make the cords entirely slack. An index of the tension is the very slight indentation that occurs at the apex of the ventricle.

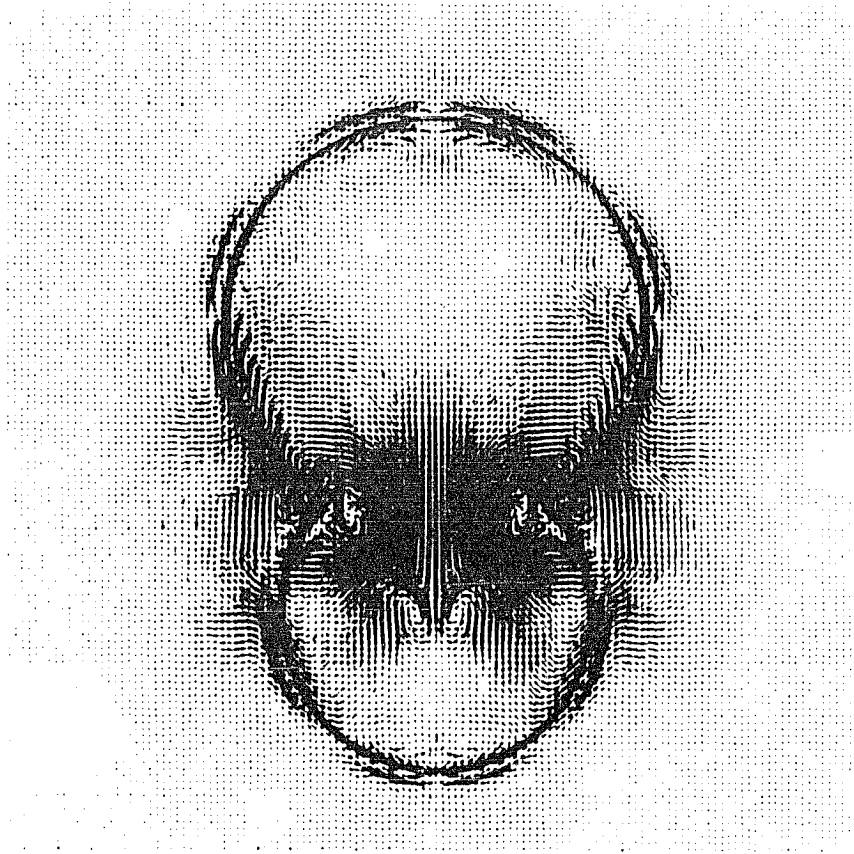
Some points of interest about the flow pattern will be discussed here. See also the legends of Fig. (11-1) and the discussion of valve physiology in Section XII.

During valve opening, the requirement that fluid move outward to open the valve appears to prevent initially the formation of a well defined jet. When the valve is fully open a jet appears with a typical vena contracta near the valve ring. However, the valve leaflets do not appear to follow the contraction of the jet. In the real mammalian heart it is possible that the continuity of the tissue around the valve ring forces the valve to follow this contraction. We could simulate such an effect with a link joining the two valve leaflets near the valve ring, but we have not yet done so. Though a jet is apparent near the valve ring it diffuses outward at the edges of the cusps (as described by Taylor and Wade - see Section III). It does not appear to strike the ventricular apex until later in diastole. When the valve leaflets have stopped their outward motion, vortex formation begins. The vortex is formed at the tip of the valve leaflet, rather than behind the cusp, and in our studies its center never moves far from this site of formation, though subsequent closure movements of the leaflet leave the vortex in a position somewhat behind the cusp. If the valve were in a pipe rather than in a ventricle, the vortex would be swept off downstream. Here it remains essentially in place while its streamlines move the valve in the direction of closure. Significant diastolic movements toward closure are produced by this

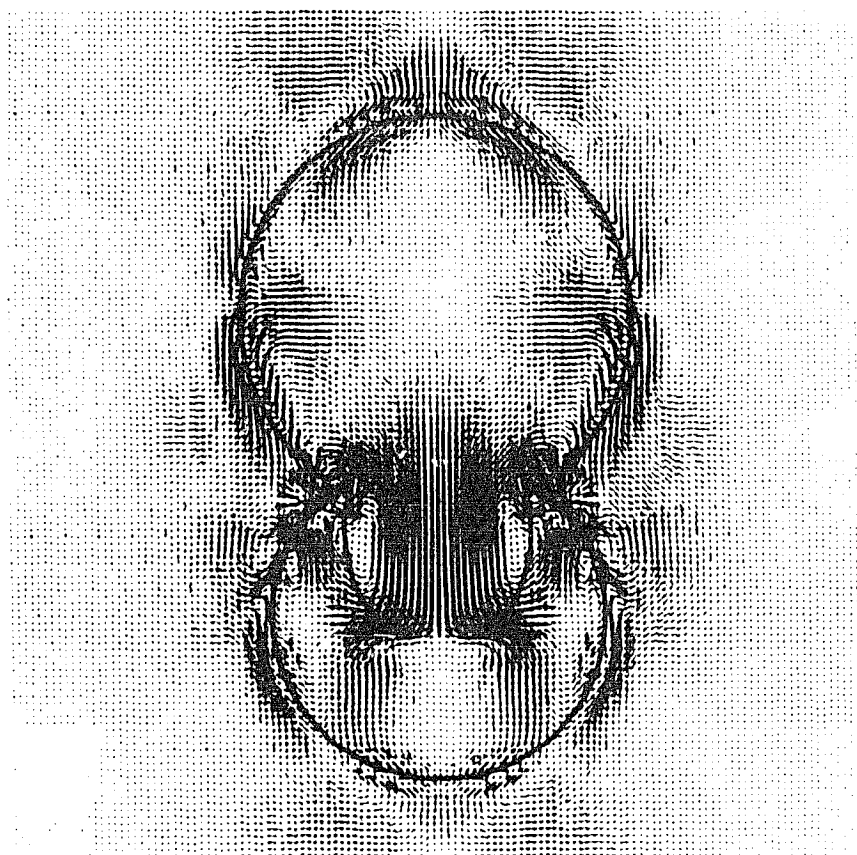
Fig. (11-1)      Computer generated diastolic  
flow pattern for our representation of the  
mitral valve. The frames (a) - (p) were selected  
from 640 time steps generated by the computer.



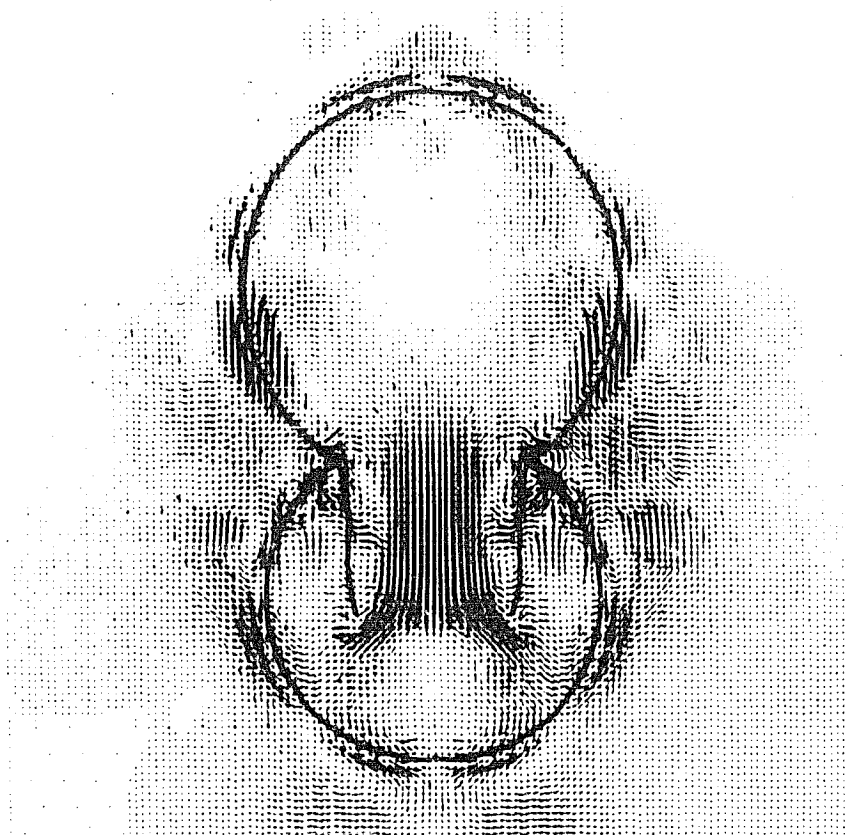
(a) The initial configuration of the simulated atrium, ventricle, and mitral valve. The chordae, not shown, connect the valve tips to the ventricular apex. They are under tension throughout diastole in this computer experiment.



(b) As the ventricle relaxes the valve opens.

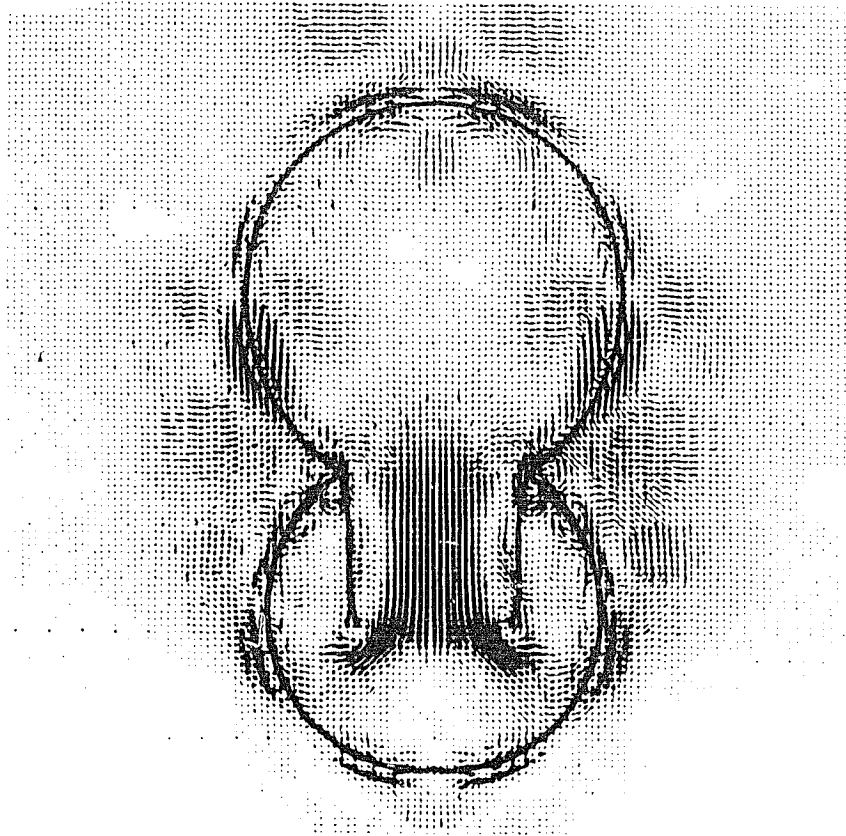


(c) A jet is formed with a typical vena contracta; the jet diffuses outward near the cusp margins.

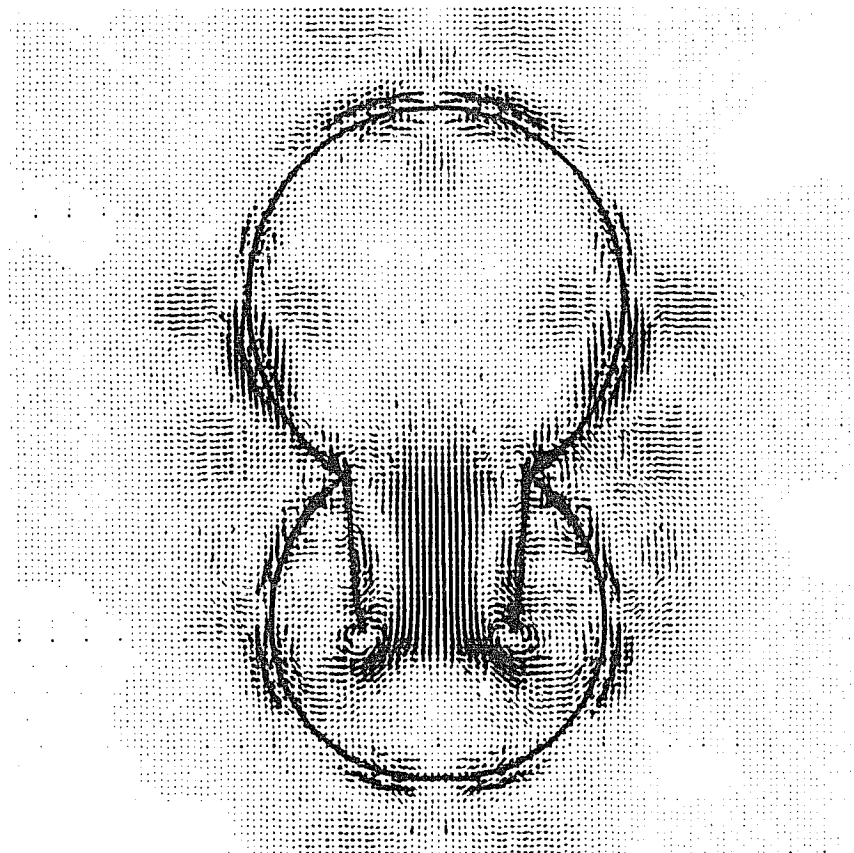


(d) A very early stage of vortex formation. There is a small vortex about  $2/3$  of the way down each cusp on the atrial side.

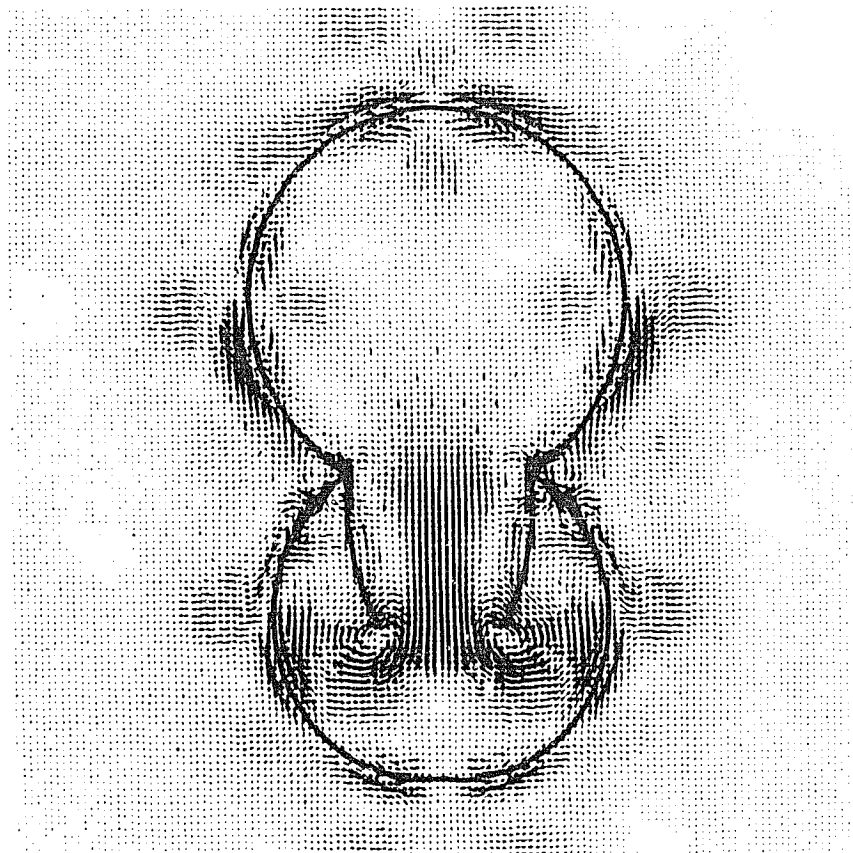




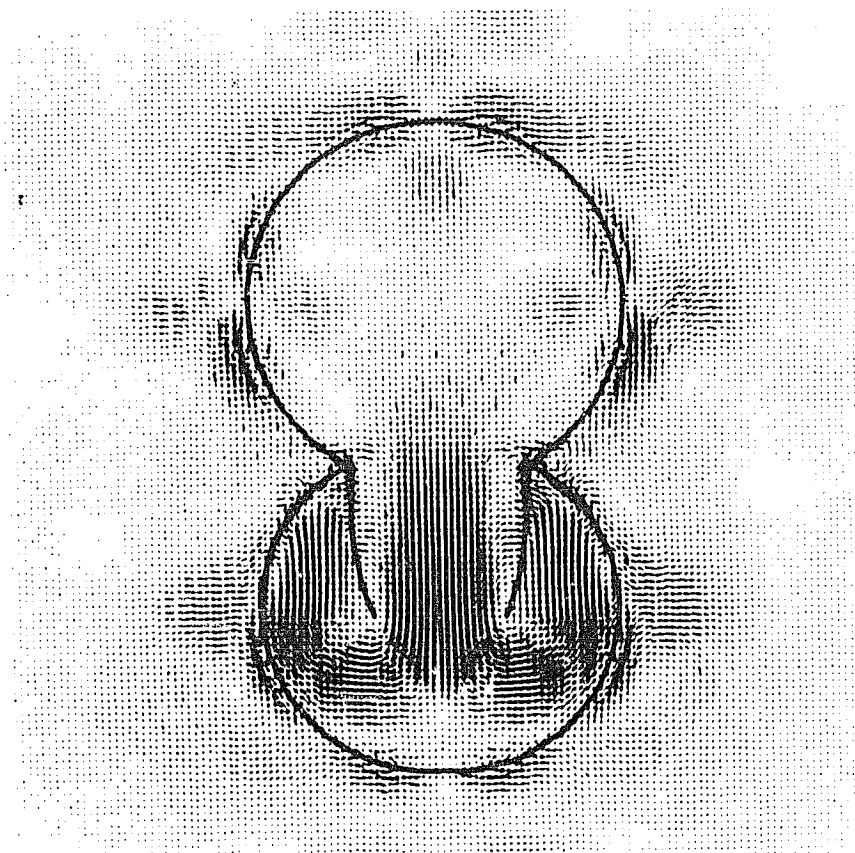
(e) The vortex moves to the tip of the cusp. The valve is now fully open.



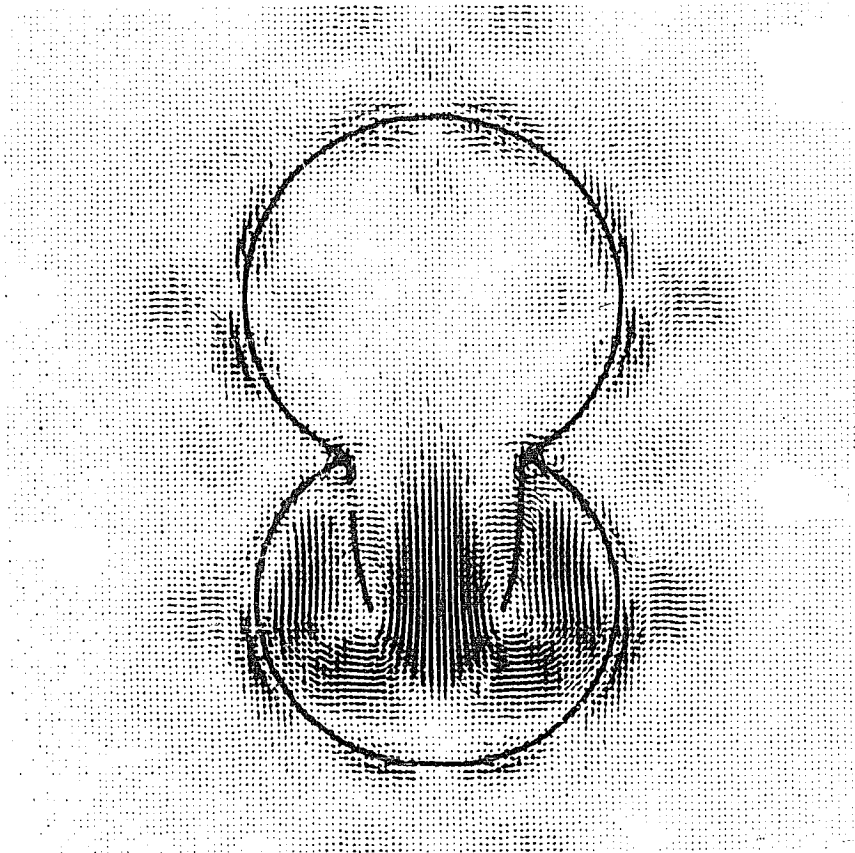
(f) A **strong, well-defined vortex** appears.



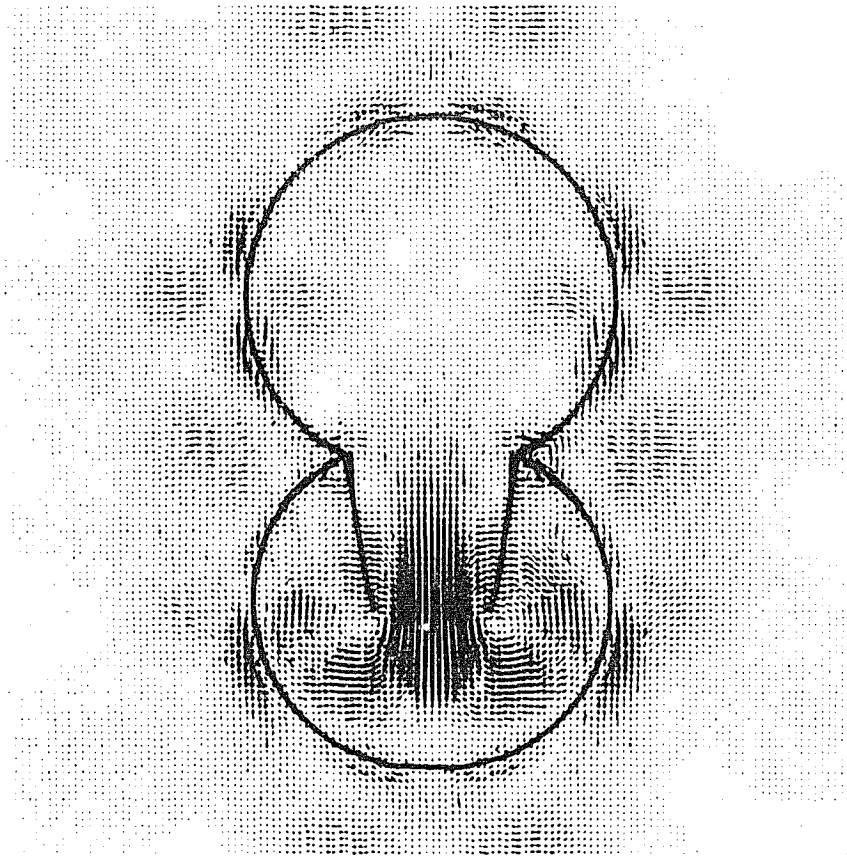
(g) The vortex grows in size, and the valve leaflets begin to move together under the influence of its streamlines.



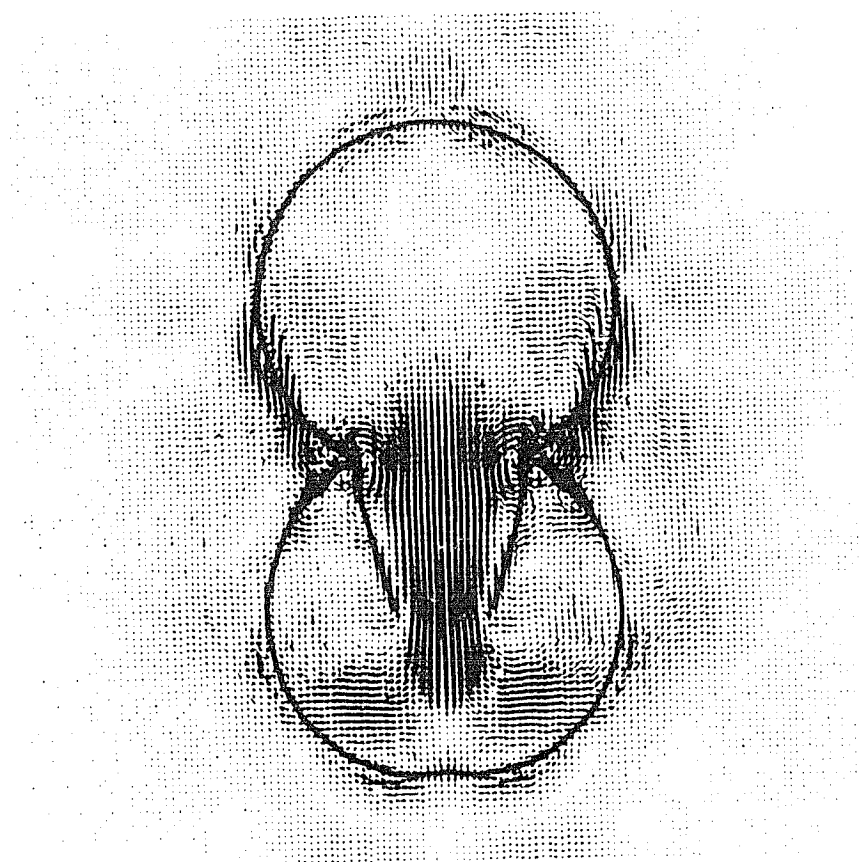
(h) A smooth flow pattern is established in which flow from the atrium merges with a diffuse vortex centered at the valve tip.



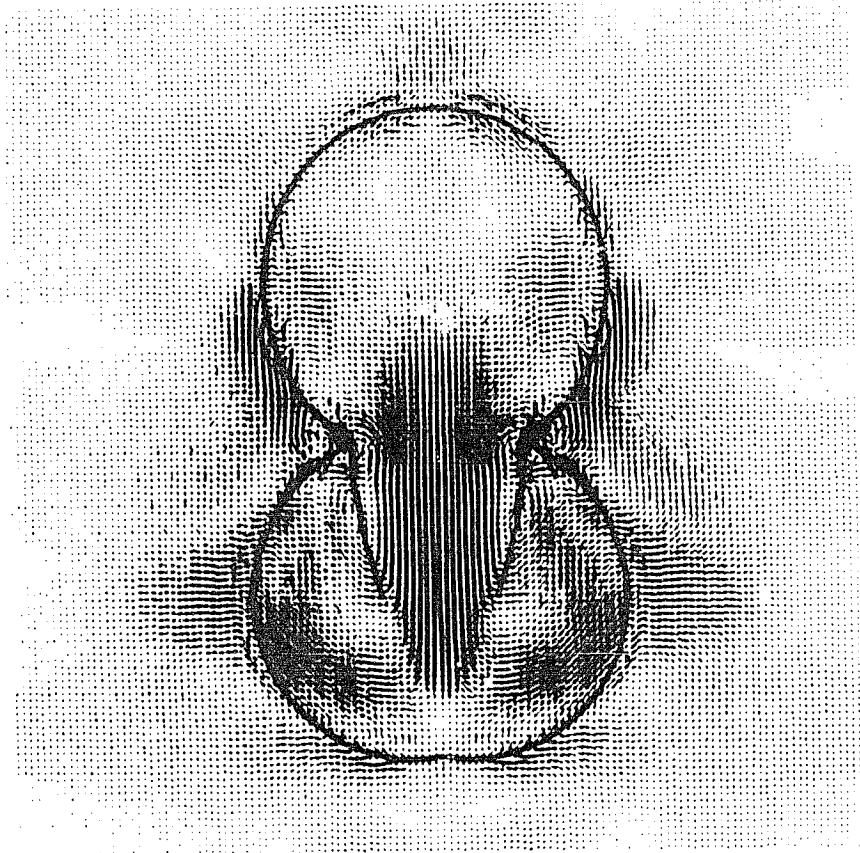
(i) As the inflow from the atrium is reduced the vortex becomes much more prominent and the valve leaflets move rapidly toward closure.



(j) Inflow from the atrium becomes even smaller and the vortices dominate the flow pattern. The broken jet lies between the two vortices.

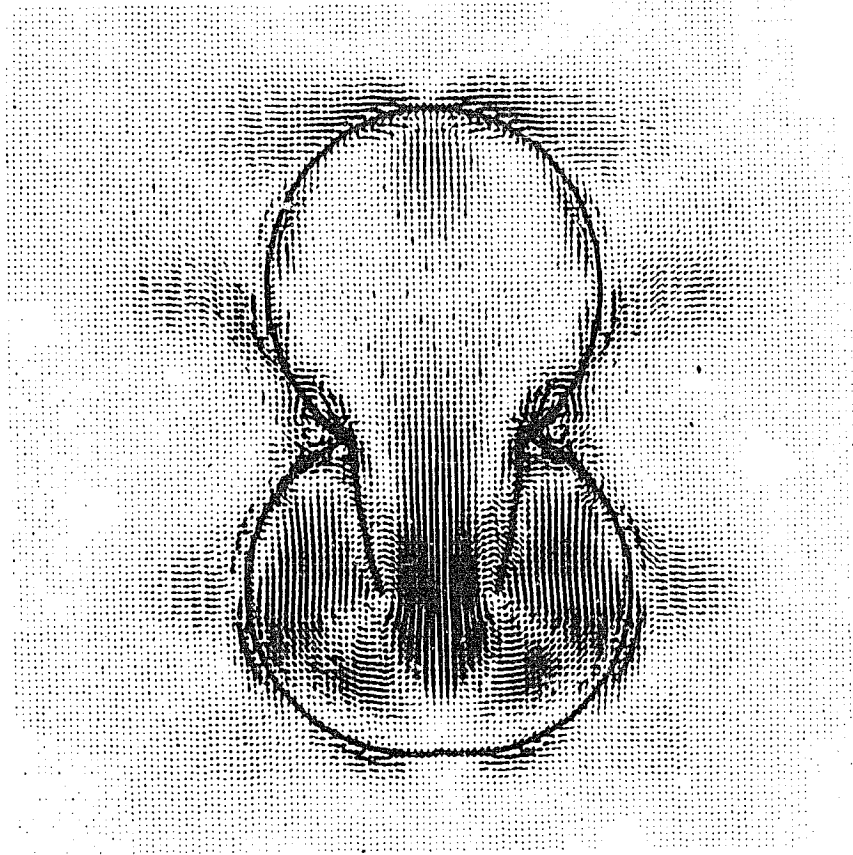


(k) The onset of atrial systole connects the jet with the atrium again.  
The remains of the vortices can barely be seen.

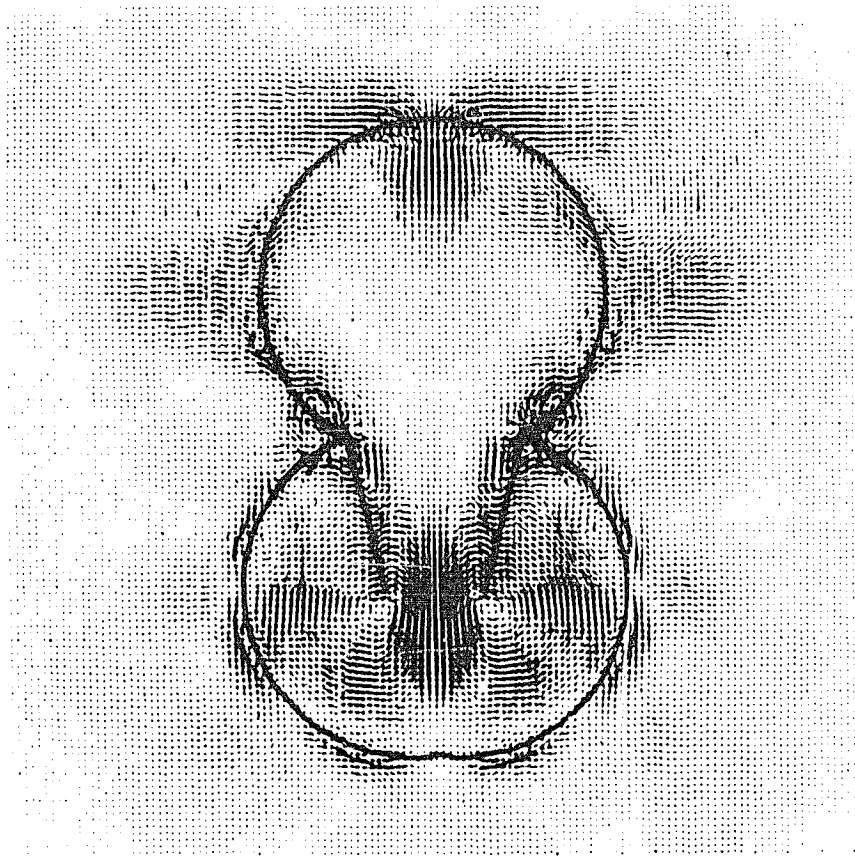


(1) Atrial systole pushes the valve open slightly. The tension on the chordae is now evident in the indentation at the ventricular apex.

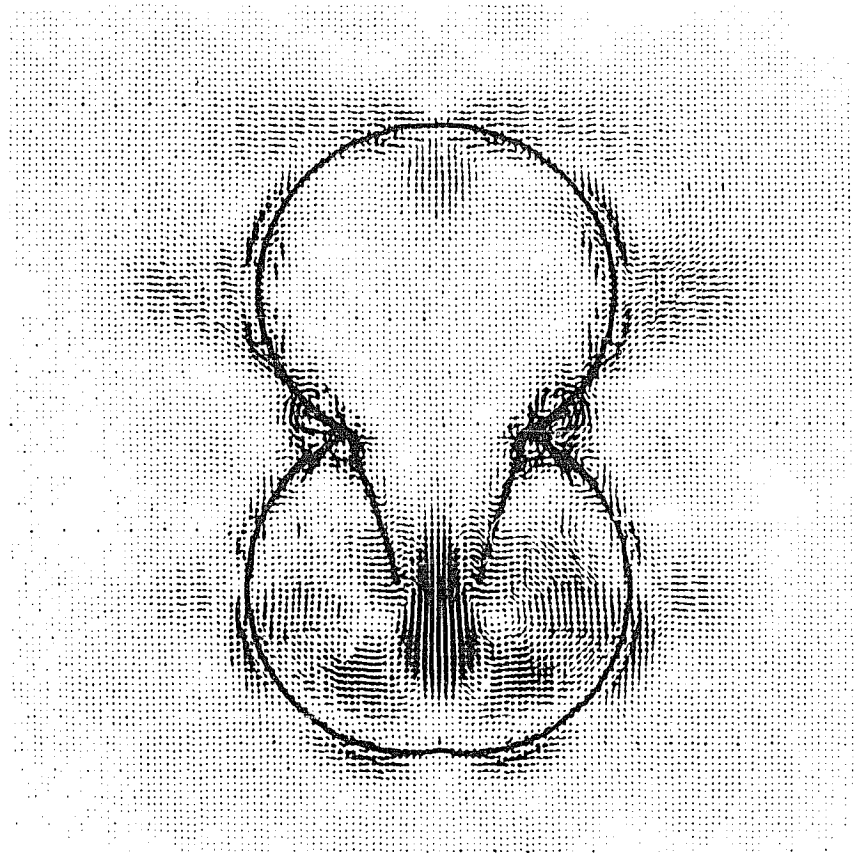




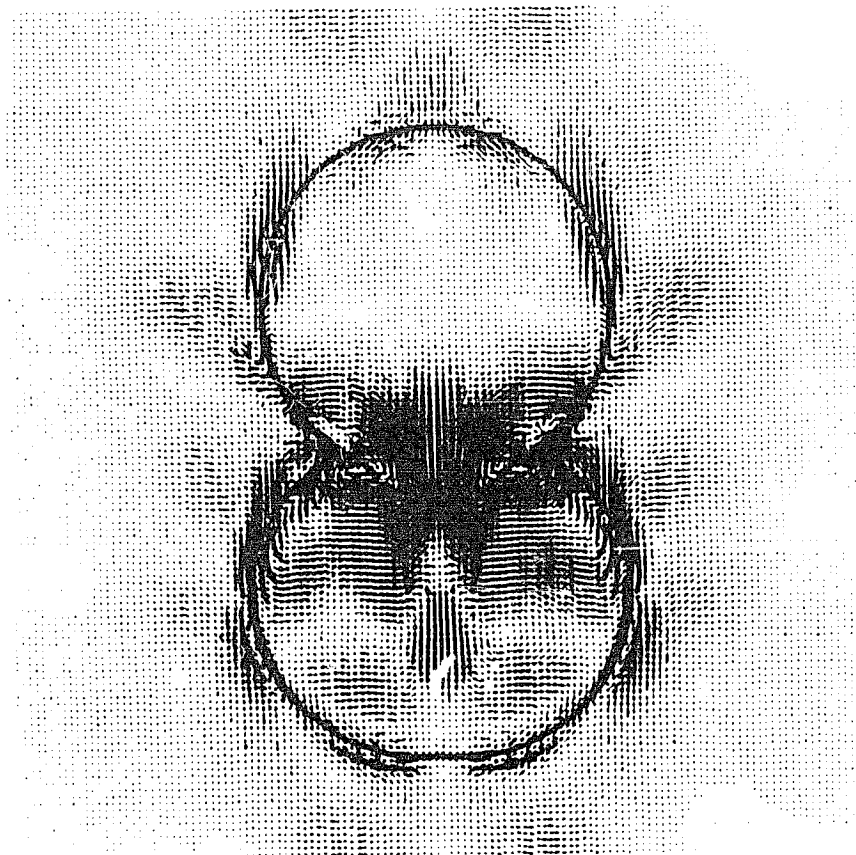
(m) Vortices form again at the valve tips, as they did during rapid filling prior to atrial systole. The valve is moved toward closure and the jet begins to break.



(n) The jet is broken, vortices dominate the flow pattern, and the valve is swept toward closure.



(o) In this frame the vortices lie somewhat behind the line of the valve leaflets, while previously they were at the valve tips. The change is due to the motion of the leaflets. The vortex remains essentially at its site of formation.



(p) Ventricular systole completes the closure by generating streamlines from ventricle to atrium. These intersect the cusps and carry them closed. There is a stagnation point between the valve leaflets near the tips. Fluid on the ventricular side of the stagnation point is still moving into the ventricle, while fluid on the atrial side is being squeezed out into the atrium. The flow meter records this as a spurt of backflow, but no fluid is actually escaping between the valve cusps.

mechanism only when the inflow slows down. At this time the vortex appears to expand tremendously in size and its streamlines uniformly intercept the valve and carry it toward closure. Vortex formation also influences the shape of the jet of fluid entering the ventricle. With the formation of vortices the jet becomes longer; it passes between the two vortices like a piece of metal being pressed out between two rollers. As the flow decelerates fewer and fewer of the streamlines of the jet connect with the atrium and more of them circulate around the vortices and help close the valve. This supports the contention made in Section III that the "broken jet" theory is essentially equivalent to the vortex theory. With atrial systole the phenomena described above repeat themselves. The valve is opened again to some extent, more vortices are formed, and further closure movements occur immediately before ventricular systole. Finally, with the onset of ventricular systole, the first streamlines from ventricle to atrium appear. These streamlines assist in the final closure of the valve.

We have also run a computer experiment in which the chordae were slack during diastole. In that experiment the leaflets were opened wide and remained open wide until the onset of ventricular systole. There was little vortex formation, apparently because the leaflets were thrown out of the main stream and the necessary interaction between the leaflets and the main stream was missing.

The absence of vortex formation when the valve is thrown out of the main stream and the site of vortex formation as the tip of the valve leaflet both emphasize the role of the leaflet itself in vortex formation, as well as the importance of the chordae in restraining

the leaflet so that it interacts with the main stream. These results are contrary to those of the Bellhouse group, as will be discussed in Section XII.

## XII. CONCLUSIONS

### The Physiology of Mitral Valve Closure

In this section we introduce a classification of the streamline types which may be associated with the closure of the mitral valve. We discuss the time sequence of the appearance of these streamline types during a single diastole, and we evaluate the influence of the different streamlines on valve performance. We begin with a definition of the term "streamline" and a discussion of the significance of streamlines in a fluid bounded by moving walls.

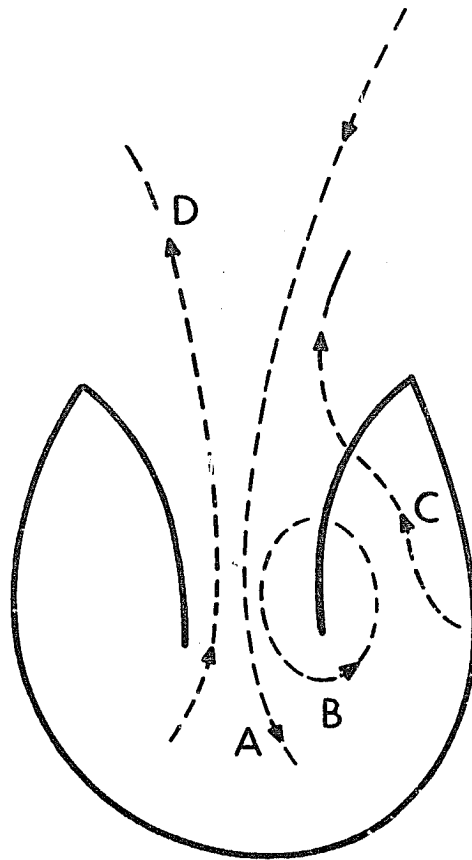
A streamline is a curve in space associated with the instantaneous velocity field of a fluid. The association is that the streamline is parallel at each of its points to the local fluid velocity vector. If a streamline crosses an immersed boundary, this implies that the boundary has a non-zero component of velocity normal to itself. If no streamlines cross an immersed boundary, then the boundary is either at rest or moving parallel to itself everywhere. In particular, the filling of the ventricle requires streamlines that intersect the ventricular wall, and the opening and closing of heart valves require streamlines that cross the valve leaflets. In neither case is it implied that fluid is penetrating the boundary, but simply that the boundary itself is in motion.

With these considerations in mind we introduce the classification of streamlines which is listed here and illustrated in Fig. (12-1):

- A. Streamline from atrium to ventricle which passes between the valve leaflets.

Fig. (12-1)      Four streamline types that may be associated with valve closure. A and D influence ventricular volume without moving the valve. B and C close the valve, but C reduces ventricular volume while B does not.





- B. Circulating streamline which crosses the valve, moves the valve in the direction of closure, and completes its circuit within the ventricle.
- C. Streamline from ventricle to atrium which intersects the valve and moves it toward closure.
- D. Streamline from ventricle to atrium which passes between the valve leaflets.

A given instantaneous flow pattern can be characterized qualitatively by stating which of these streamline types is most prominent or quantitatively by giving the total amount of flow associated with each of the streamline types. Let these flows be called  $F_A$ ,  $F_B$ ,  $F_C$ ,  $F_D$ . Then a flow meter mounted at the valve ring measures  $F_A - F_C - F_D$ . From a cine record of cusp motion it is possible to estimate the rate at which volume is displaced by the cusps. This is  $F_B + F_C$ . Clearly the two measurements are not enough to determine the four flows separately. This illustrates the point that knowledge of the flow pattern permits a more detailed characterization of valve dynamics than can be obtained from combined flow meter measurements and cine records of cusp motion. On the other hand, once the flow pattern is known quantitatively, the results of these measurements can be predicted.

In terms of this streamline classification it is possible to discuss the evolution in time of the flow pattern during a single diastole. When the valve is maximally open, all of the streamlines are of type A, passing between the valve leaflets from atrium to ventricle. As vorticity is added to the fluid, circulating type B streamlines appear and may begin to close the valve early in

diastole. † When an adverse pressure difference does appear, for example at the onset of ventricular systole, it slows down fluid which is moving toward the ventricle and speeds up fluid which is moving toward the atrium. Fluid at rest is set in motion in the direction of the atrium. Consequently the fluid behind the valve cusps begins to move in the direction of the atrium, while the fluid in midstream continues to flow toward the ventricle though at a decreasing rate. Thus the introduction of an adverse pressure difference causes type C streamlines to appear and type A streamlines to disappear. These changes take time, however, because of the inertia of the fluid. The adverse pressure difference has no direct effect on the circulating type B streamlines ( $\text{curl grad } p = 0$ ). Consequently at this phase the valve is moved toward closure under the combined influence of the B and C streamlines. If the valve is not yet closed by the time the midstream fluid has been stopped, then that fluid is turned around by the adverse pressure difference and type D regurgitant streamlines are formed. In summary, the natural order of appearance in time of the streamline types, is A, B, C, D. The functional significance of this will be shown below.

We now discuss the role of each of the streamline types in valve performance. Type A streamlines are the most desirable in the sense that they fill the ventricle. But it is not possible

† Two complications in discussing the type B streamlines are the following: First, not all circulating streamlines need intersect the valve. Second, one can have vorticity in the fluid without having closed streamlines, though one cannot have closed streamlines without vorticity (in a simply connected region). Thus vorticity is a necessary but not a sufficient condition for the existence of type B streamlines.

to have a valve with only type A streamlines, since these streamlines do not move the valve and thus cannot bring about closure. Type B streamlines are unique in that they close the valve without reducing the ventricular volume. Type C streamlines also close the valve. They reduce the ventricular volume if the border of the ventricle is taken to be the plane of the valve ring, but there is an upper limit to the amount of volume which can be lost in this way. This limit is the volume of fluid which lies between the cusps at the time when type C streamlines are first formed. At worst this is the volume of fluid between the cusps at maximal opening, but it can be smaller if a significant amount of closure was produced by the type B streamlines before the appearance of type C. Type D streamlines also reduce the ventricular volume but they do not participate in the closure of the valve. Thus there is no similar upper limit to the amount of volume which can be lost by the ventricle via type D streamlines. In fact when regurgitation continues throughout ventricular systole, as for example when the valve leaflets are immobilized by calcification, the regurgitant streamlines are of type D.

The following table summarizes the functional significance of the streamline types:

	EFFECT ON VENTRICULAR VOLUME	EFFECT ON VALVE CLOSURE
A	+	0
B	0	+
C	-	+
D	-	0

Thus, the rank order of desirability of the streamline types is A, B, C, D with the understanding that it is not possible to design a valve with only type A streamlines. In principle it would be best to produce all of the closure with type B streamlines, but this is not quite achieved even by healthy natural valves, for one always sees in the flow meter record at least a small spurt of backflow associated with closure. Our computer results indicate that this is associated with streamlines of type C, and that type D streamlines are definitely pathological. Such pathological streamlines do appear, however, if the valve is wide open at the onset of ventricular systole, for in that case they are formed before the C streamlines have time to complete the closure.

The natural order of appearance in time of the streamline types coincides with their rank order of desirability. The functional significance of this is that with a properly performing valve the early streamline types will have time to fill the ventricle and accomplish most of the closure before the appearance of the later and less desirable streamlines.

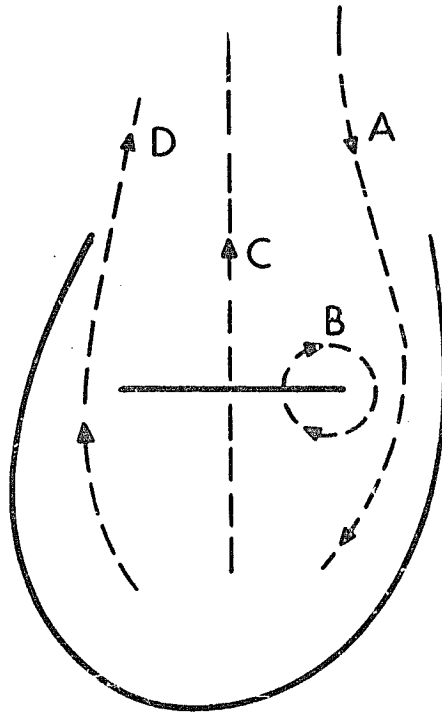
This description of the streamlines, their evolution in time, and their functional significance is in part a synthesis of the ideas of other workers as outlined in the historical section of this thesis, Section III. For example, the importance of the circulating streamlines is prominent in the work of Leonardo and the Bellhouse group, while the role of inertia has been emphasized by Yellin and Frater. The experiments of Henderson and Johnson are especially interesting in this regard since they illustrate the conversion of one streamline type into another. The jet of Henderson and Johnson consists of type A streamlines. When this jet is disconnected from

the atrium ("broken") the fluid in the ventricular part of the jet continues to move forward but the streamlines change to type B. They circulate through the ventricular part of the broken jet and they close the valve from the sides.

Our classification of the streamline types is especially useful because it is also applicable to flow patterns around artificial valves. The four representative streamlines are shown in Fig. (12-2) for a caged disc valve. It is important to have a mode of description that applies to both natural and prosthetic valves so that the flow pattern of the former can be used as a standard. We have not yet performed the computer calculations, but we anticipate that most prosthetic valves will be closed primarily by the type C streamlines. This would explain the relatively fixed backflow that is associated with the closure of most artificial valves. The prosthetic valve designer should seek to achieve the persistence of type A and the production of type B streamlines. We have offered a solution to this problem in Figs. (3-6) and (3-7) in which an artificial valve motivated by the experiments of Henderson and Johnson is introduced. Our computer methods are useful both because they lead to the formulation of such goals, and because they provide a means of determining how well a particular valve design actually achieves the goals that have been laid down.

We have shown how instantaneous flow patterns can be characterized in terms of a streamline classification. A more difficult problem is to isolate certain features of valve design and explain how these features contribute to the formation of the different streamline types. One such feature has already emerged from our work:

Fig. (12-2)        The same streamline types as  
in Fig. (12-1) for an artificial valve.





the diastolic role of the chordae tendineae in restraining the open valve. Such a role is explicitly denied by Bellhouse [8] who has mounted his model valve in such a way that its inextensible chordae are definitely slack during diastole. In the model, Bellhouse finds that vortices form and diastolic movements occur without the intervention of the chordae. On the other hand, Wieting [37] has mounted a human mitral valve in a pulse duplicator system and supported the papillary muscles on springs in such a way that the papillary muscle tension can be controlled. The method is not capable of controlling systolic and diastolic tension separately, but it is apparent from the records that they vary together. Wieting noted the appearance of a vortex behind the anterior leaflet in his experiments when the papillary muscle tension was optimal, and the absence of this vortex when the tension was 10% optimal. Rushmer [38] has noted that in the shrunken heart of the thoracotomized animal the chordae are slack and the valve opens widely, while in the closed chest animal the opening is much narrower presumably because the chordae are under tension during diastole.

In our work, in the absence of diastolic tension on the chordae, the valve is flung open wide early in diastole, so much so that it fails to interact strongly with the incoming fluid. As a result vortices fail to form, diastolic movement toward closure does not occur, atrial systole only opens the valve more widely, and the valve is closed with a large loss in ventricular volume by ventricular systole. When diastolic tension is provided by the chordae we find that distinct vortices are shed from the valve leaflets, that type B streamlines are formed with consequent early and significant diastolic closure movements, that atrial systole partially reopens the valve

out that this is followed at once by more vortex formation and more closure, and that only a few type C streamlines are needed to complete the closure when ventricular systole occurs. In short we are able to produce in the computer the same general pattern of flow and cusp motion as obtained by Bellhouse, but only in the presence of diastolic tension on the chordae. Such tension was definitely absent in the Bellhouse studies. Our results are entirely consistent with those of Wieting and Rushmer, cited above.

Clearly there is a need for further work in this area. First, it does not appear to be known from a direct measurement whether the chordae are under tension during diastole in vivo. Even if they are it does not prove that such tension is necessary for vortex formation. The role of the upstream and downstream chambers also needs to be considered. In the Bellhouse model the atrium is a rigid tube of the same diameter as the valve ring, while the ventricle is distensible. In Wieting's work both atrium and ventricle are rigid, but their diameters are larger than that of the valve ring. Rushmer's chamber was the heart itself, but his observations were necessarily indirect for that very reason. In the present work both the atrium and ventricle are distensible and larger than the valve ring. Finally, if one accepts the idea that restraints on the valve are important, it becomes important to ask if the three dimensional shape of the valve itself is a significant restraint on its opening independent of any role of the chordae.

If our results concerning the diastolic role of the chordae are accepted, they illustrate beautifully the kind of dynamic interaction between valve and fluid that our mathematical method was

designed to elucidate. If the chordae are under tension the valve always has an equilibrium position under their influence, but when it is flung open beyond this equilibrium it presses against the incoming stream and shears it to form vortices that participate in its return toward equilibrium. It is not meaningful to say that the diastolic closure movements are caused only by the chordae pulling the valve closed or only by the fluid flow pattern moving it in that direction. In fact, the forces set up the flow pattern which moves the valve toward closure.

### Future Applications

The methods of this thesis can be used to investigate natural valve physiology or prosthetic valve performance. The following studies are examples of those which can be performed with these methods in their current state of development.

#### Mitral valve physiology:

1. The influence of valve and ventricular asymmetry. The anterior leaflet is larger than the posterior, and the space behind the anterior leaflet, the ventricular outflow tract, is larger than the space behind the posterior leaflet.
2. The contraction of the mitral valve ring. Such a contraction occurs at the time of atrial systole and presumably has an influence on the form of the jet. We could easily include this effect by making the single link that supports the valve ring have the same properties as the atrial muscle.

### Prosthetic valve design:

1. A survey of two dimensional representations of different mitral valve types to compare their flow patterns with each other and with the natural valve.
2. For a particular valve type, systematic variation in the parameters of valve design. For example, the eccentric monocusp valve is a design which mimics in some respects the anterior leaflet of the natural mitral valve. The rigid cusp is capable of tilting open out of the way of the main stream. In addition the cusp is free to translate away from the valve ring until it hits a stop. The normal opening motion is a translation until the stop is reached followed by the tilting motion. The two parameters of interest for this valve are the limits on these two motions: the distance of the stop from the valve ring and the maximum angle of opening. To investigate the role of these parameters one can vary them in the computer and observe the influence on the flow pattern, on the amount of pressure drop across the valve, and on the nature and amount of backflow associated with closure. In addition it will be important to vary the size and shape of the ventricular chamber, for the optimum choice of the design parameters will probably depend on these factors. Two especially interesting questions about this valve have emerged from the experimental work. These questions can probably be answered by our technique. First, Frater [39] noted that the pressure drop across the valve was consistently different depending on whether the valve was placed in the position normally occupied by the anterior or the posterior cusp of the natural valve. One would like to understand the reason for this difference.

Second, from the measurements shown in Fig. (3-15) it can be deduced that the volume of backflow associated with the closure of this valve is slightly less than the volume displaced by the cusp during its closure movement. This implies either that type A streamlines are continuing while C streamlines close the valve, or that type B streamlines also participate in closure, or both. In either case such an effect is desirable, but one would like to understand it.

#### Further Development of the Methods

Experience with this technique suggests a number of areas in which research of a primarily mathematical nature could be expected to extend the range and power of this work.

First, the physiologist needs an efficient language for specifying to the computer the physical and geometric properties of the heart apparatus he wishes to study. One would like to be able to describe a heart type or valve type to the computer as a function of some small number of easily varied parameters whose influence one wishes to study. Then the computer should be able to generate a link structure corresponding to each choice of the parameters.

Second, it would be desirable to remove the restriction on the Reynolds number that is implicit in the present methods. A technique recently developed by A. J. Chorin [40] accomplishes this by taking explicit account of vortices and vortex shedding. Since vortices also appear to be an important aspect of valve physiology it will be especially interesting to apply this new method to heart valve problems.

Third, the methods of Section VIII, Numerical Stability, are heuristic in motivation. They were arrived at by consideration of analogies with simpler (linear) problems, and they are justified by the fact that they yield smooth results where simpler methods break down. A mathematical theory of numerical stability is needed for problems involving configuration dependent boundary forces when the boundary moves about in space.

#### Concluding remarks

The flow pattern of blood in the heart has a structure which, in a way, is an integral part of the heart anatomy. Re-created during each heart beat by the simplest physical laws, the flow pattern is also a product of natural selection. As a physical entity the flow pattern has equations of motion; as a biological entity it has a function. This function appears to be intimately connected with the performance of heart valves.

The evolution of the flow pattern was not accomplished by making changes in the equations of motion. Instead, the physiology and geometry of the heart apparatus evolved, and consequent changes in the flow pattern appeared. In this work we have tried to follow the example of Nature by providing a mathematical tool which can predict the flow pattern of the blood given any design for the heart and valves. We then perform a kind of unnatural selection process by modifying our design according to what we see in the flow pattern and how it compares with what we expect or want to see. It is up to the experimenter to determine what the facts actually are. The present technique is aimed at understanding their significance.

## LITERATURE CITED

- [1] Frater, R. W. M., Wexler, H., Halpern, I., Yellin E.,  
"Factors in the Hemodynamic Performance of Mitral Valve  
Prostheses", (Abstract) Bull. N. Y. Academy of Medicine  
45:971, 1969.
- [2] O'Malley, C. D., Saunders, J. B. de C. M., Leonardo da Vinci  
on the Human Body, New York: Henry Schuman, 1952, pp. 216-326.
- [3] Henderson, Y., Johnson, F. E., "Two Modes of Closure of the  
Heart Valves", Heart 4:69-82, 1912.
- [4] Landau, L. D., Lifshitz, E. M., Fluid Mechanics, (Translators:  
Sykes, J. B. and Reid, W. H.), London: Pergamon Press, 1959,  
p. 150.
- [5] Taylor, D. E. M., Wade, J. D., "Flow Through the Mitral Valve  
During Diastolic Filling of the Left Ventricle", J. Physiol.  
200:73P, 1969.
- [6] Taylor, D. E. M., Wade, J. D., "The Pattern of Flow Around the  
Atrio-Ventricular Valves During Diastolic Ventricular Filling",  
J. Physiol. 207:71P, 1970.
- [7] Bellhouse, B. J., Talbot L., "The Fluid Mechanics of the Aortic  
Valve", J. Fluid Mech. 35:721-735, 1969.
- [8] Bellhouse, B. J., Bellhouse, F. H., "The Fluid Mechanics of a  
Model Mitral Valve and Left Ventricle", University of Oxford,  
Dept. of Engineering Science Report 1013/71.  
  
Bellhouse, B. J., "Fluid Mechanics of a Model Mitral Valve and  
Left Ventricle", Cardiovascular Research 6:199-210, 1972.
- [9] Winsberg, F., Gabor, G. E., Hernberg, J. G., Weiss, B., "Fluttering  
of the Mitral Valve in Aortic Insufficiency", Circulation 41:225,  
1970.

- [10] Wieting, D., Dynamic Flow Characteristics of Heart Valves,  
(Thesis) University of Texas at Austin, 1969.
- [11] Ledley, R. S., Use of Computers in Biology and Medicine,  
New York: McGraw Hill, 1965, pp. 248-255.
- [12] Spencer, M. P., Greiss, F. C., "Dynamics of Ventricular  
Ejection", *Circulation Research* 10:274-279, 1962.
- [13] Nolan, S. P., Dixon, S. H., Fisher, R. D., Morrow, A. G.,  
"The Influence of Atrial Contraction and Mitral Valve  
Mechanics on Ventricular Filling", *American Heart Journal*  
77:784-791, 1969.
- [14] Yellin, E. L., Silverstein, M., Peskin, C. S., Frater, R. W. M.,  
"Pulsatile Flow Dynamics Across the Natural and Prosthetic  
Mitral Valve", *Proc. 23rd Annual Conference on Engineering in  
Medicine and Biology*, 1970, p. 96.
- [15] Yellin, E. L., Frater, R. W. M., Peskin, C. S., Epstein, W. H.,  
"Dynamics of Flow Across the Natural Mitral Valve", ASME  
preprint 71-WA/BHF-2.
- [16] Yellin, E. L., Frater, R. W. M., Mayer, D., "The Gorlin Equation  
Revisited: The Dynamics of Pulsatile Flow Across a Stenosis",  
*Proc. 8th International Conference on Medical and Biological  
Engineering*, 1969, p. 33-9.
- [17] Frater, R. W. M., Peskin, C., Yellin, E., "Comparison of  
Natural and Prosthetic Mitral Valves by Simultaneous Study  
of Pressure, Flow and Movement with Additional Computer  
Simulation", (Abstract) 6th Congress: European Society for  
Experimental Surgery, 1971, p. 86.
- [18] Harlow, F. H., Welch, J. E., "Numerical Calculation of Time -



- Dependent Viscous Incompressible Flow of Fluid with a Free Surface", *Phys. Fluids* 8:2182, 1965.
- [19] Chorin, A. J., "Numerical Solution of the Navier-Stokes Equations", *Mathematics of Computation* 22:745-762, 1968.
  - [20] Chorin, A. J., "On the Convergence of Discrete Approximations to the Navier-Stokes Equations", *Mathematics of Computation* 23:341-353, 1969.
  - [21] Vieceilli, J. A., "A Method for Including Arbitrary External Boundaries in the MAC Incompressible Fluid Computing Technique", *Journal of Computational Physics* 4:543-551, 1969.
  - [22] Vieceilli, J. A., "A Computing Method for Incompressible Flows Bounded by Moving Walls", *Journal of Computational Physics* 8:119-143, 1971.
  - [23] Peskin, C. S., "Flow Patterns Around Heart Valves: A Numerical Method", *Journal of Computational Physics*, to appear.
  - [24] Hockney, R. W., "The Potential Calculation and Some Applications", *Methods in Computational Physics* 9:135-211, 1970.
  - [25] Widlund, O., "On the Use of Fast Methods for Separable Finite Difference Equations for the Solution of General Elliptic Problems", in Sparse Matrices and Their Applications (Ed: Rose, D., Willoughby, R.) New York: Plenum, 1972, pp. 121-134.
  - [26] Hung, T. K., "A Computational Model of Blood Flow Past Artificial Heart Valves", *Proc. 21st Annual Conference on Engineering in Medicine and Biology*, 1968, p. 16.2.
  - [27] Greenfield, H., Kolff, W., "The Prosthetic Heart Valve and Computer Graphics", *JAMA* 219:69-74, 1972.
  - [28] Clark, A. J., Comparative Physiology of the Heart, Cambridge: University Press, 1927, p. 83.

- [29] Altman, P. L. (Compiler) Handbook of Circulation (National Academy of Sciences. National Research Council) W. B. Saunders Co., 1959, p. 25, 81.
- [30] Hirt, C. W., Cook, J. L., Butler, T. D., "A Lagrangian Method for Calculating the Dynamics of an Incompressible Fluid with Free Surface", Journal of Computational Physics 5:103-124, 1970.
- [32] Richtmeyer, R. D., Morton, K. W. Difference Methods for Initial-Value Problems, 2nd ed., New York: Wiley, 1967, p. 198-201.
- [33] Householder, A. S., The Theory of Matrices in Numerical Analysis, New York: Baisdell Publishing Co., 1965, p. 123-124.
- [34] Hill, A. V., First and Last Experiments in Muscle Mechanics, Cambridge: University Press, 1970, pp. 23-55.
- [35] Braunwald, E., Ross, J., Sonnenblick, E. H., Mechanisms of Contraction of the Normal and Failing Heart, Boston: Little Brown, 1968, pp. 31-48.
- [36] Isaacson, E., Keller, H. B., Analysis of Numerical Methods, New York: John Wiley and Sons, 1966, pp. 52-55, 97-98, 115.
- [37] Wieting, D. W., Hwang, N. H. C., Kennedy, J. H., Ruark, B. S., "Engineering Evaluation of Chordae Tendineae Tension and Mitral Valve Function", ASME preprint 71-WA/BHF-4.
- [38] Rushmer, R. F., Finlayson, B. L., Nash, A. A., "Movements of the Mitral Valve", Circulation Research 4:337-342, 1956.
- [39] Frater, R. W. M., Wexler, H. R., Yellin, E. L., "The In Vivo Comparison of Hemodynamic Function of Ball, Disk, and Eccentric Monocusp Artificial Mitral Valve", in Prosthetic Heart Valves (Ed. Brewer, L.) Springfield: Charles C. Thomas, 1969, pp. 262-277.

- [40] Chorin, A. J. "A Point-Vortex Method for the Study of Rapid Flow", Proceedings: Third International Conference on Numerical Methods in Fluid Dynamics. Springer, 1972.
- [41] Netter, F. H., Heart (v. 5, The Ciba Collection of Medical Illustrations) 1969, p. 11.